

STORAGE RING BASED STEADY STATE MICROBUNCHING

Alex Chao*, Tsinghua University, Beijing, China

Abstract

Powerful light sources are highly desired tools for scientific research and for industrial applications. Electrons are the objects that most readily and easily radiate photons. A natural conclusion follows that one should pursue electron accelerators as the choice tools towards powerful light sources. How to manipulate the electron beam in the accelerator so that it radiates light most efficiently, however, remains to be studied and its physical principle and technical limits be explored and optimized for the purpose. One such proposed concepts is based on the steady state microbunching (SSMB) mechanism in an electron storage ring. We make a brief introduction of the SSMB mechanism and its recent status in this presentation.

INTRODUCTION

As we have observed in the past few decades, modern physics has evolved out of the more traditional regime of nuclei and quarks, and now has backtracked to the regime of atoms and molecules. This means the prime research means has evolved out of particles of ever higher energies and into photons of various wavelengths, and the tools have evolved out of colliders and into light sources. This trend has been a major evolution expected to continue in the next decades.

At present, there are two main approaches in advanced light sources, the third- (and fourth-) generation storage ring synchrotron radiation sources, and free electron lasers.

In a third-generation synchrotron radiation light source, with an RF focusing, the electron bunches are separated by perhaps ~ 1 m, while each bunch has a length of the order of ~ 10 mm. With the electrons circulating around the storage ring in steady state, the radiation has a high repetition rate. However, with a bunch much longer than the wavelength of radiation, the radiation from the electrons is incoherent. The radiation peak power is low, proportional to N , the number of electrons in the bunch.

In a free electron laser light source, on the other hand, the electrons are provided by a linac. A single electron bunch is cleverly manipulated in such a way that it gets microbunched by the time it is about to exit a long undulator and therefore radiates coherently, with a very high peak power proportional to N^2 . However, using a linac in a pulsed mode, the repetition rate is low.

The present situation is therefore that, towards the goal of high power light sources, one of our main approaches has a high repetition rate but low peak power, the other has a high peak power but low repetition rate. Since the net radiation power is the product of repetition rate and peak power, we naturally come to an idea of a somehow combined device. This device aims to have both the high repetition rate of a

storage ring and a high peak power of a microbunched beam like in an FEL.

It must be quickly pointed out that a straightforward insertion of a long undulator in a storage ring will destroy the microbunches of the electron beam — FELs always use linacs for a good reason. If an FEL linac is simply inserted into a storage ring, the storage ring will have to be operated in a pulsed mode; every time the electron beam traverses the FEL, it has to wait in the storage ring for a long time to cool down before a next passage can be made, effectively making this device a pulsed operation and the benefit of high repetition rate of the storage ring does not apply.

Such a combined device must be done while keeping the integrity of the microbunched structure of the electron beam. The way being proposed to accomplish this is named steady state microbunching (SSMB). Once accomplished, an SSMB device aims for simultaneously a high repetition rate and a high peak power. Since N is a very large number, an SSMB ring potentially gains a large factor in the desired radiation power compared to a third-generation storage ring facility.

In terms of its operation principle, this conceived storage ring-based SSMB functions very closely to that of a conventional storage ring, except that the microwave RF is replaced by an IR laser modulator. The equilibrium beam distribution becomes microbunched with the bunch spacing given by the modulation laser wavelength λ_m instead of a conventional RF wavelength. This represents an extrapolation of six orders of magnitude in bunch spacing but the mechanism of the steady state is the same, i.e., a balance between radiation damping and quantum excitation. No FEL mechanism is invoked. To demonstrate the applicability of our recent understanding of storage rings to this six orders of magnitude extrapolation, a critical proof-of-principle test has been launched.

SSMB SCENARIOS

Before we discuss its technical design, we first need to know that there are a variety of SSMBs that one can aim for, ranging from simple to sophisticated ones. Depending on the applications, particularly depending on the targeted wavelength of the SSMB radiation, there are several different SSMB scenarios with different levels of sophistication.

To illustrate the various scenarios, we start with a conventional third-generation storage ring source. The electron beam is bunched with a Gaussian distribution with bunch length ~ 10 mm. The radiation is incoherent, as mentioned. If the targeted wavelength is long enough, e.g., in the THz range, then by some conventional techniques, one may try to compress the bunch length toward the desired wavelength and accomplish some enhancement of the radiation. This source however remains basically a conventional design.

* achao@slac.stanford.edu

REVIEW OF HARMONIC CAVITIES IN FOURTH-GENERATION STORAGE RINGS

F. J. Cullinan*, Å. Andersson, P. F. Tavares, MAX IV Laboratory, Lund, Sweden

Abstract

Several third generation light-source storage rings have used harmonic cavities to lengthen the electron bunches. With the advent of the fourth generation however, they have become an almost universal feature as the small transverse electron beam sizes make long bunches essential for increasing Touschek lifetime and reducing emittance blow-up from intrabeam scattering. Multiple technological solutions exist for the implementation of harmonic cavities and which to use and how to implement it are questions that many facilities have to tackle. This is therefore a very active area of study in which there is strong collaboration within the community. In this proceeding, the approaches taken, as determined from a survey of different projects, are summarised. Avoiding coherent collective beam instabilities is of particular concern and those that are driven by the impedance of the harmonic-cavity fundamental mode are outlined with reference to the relevant theories. Where appropriate, the discussion is complemented by a description of the observations made at the MAX IV 3 GeV ring, the first fourth generation storage ring which was commissioned with normal-conducting passive harmonic cavities already installed.

INTRODUCTION

Harmonic cavities (HCs) are used in storage rings to alter the slope of the RF voltage over the duration of the charged particle bunches. In electron storage rings used as synchrotron light sources, by far the most common aim is to lengthen the bunches in order to increase the Touschek lifetime¹. For this reason, several third-generation light-source storage rings had harmonic cavities installed [2–6]. Now, the fourth-generation of storage rings are coming online and lengthened electron bunches are even more desirable due to the smaller transverse beam sizes, which lead to shorter Touschek lifetimes. Without bunch lengthening, fourth-generation storage rings also suffer from significant emittance blow-up due to intrabeam scattering [7]. For these reasons, harmonic cavities have become critical components in almost all fourth-generation storage rings and are included in their baseline designs. A significant amount of research has therefore been conducted to develop these harmonic cavities, better understand the beam dynamics and to decide which type and design of HC is best suited to a particular storage ring. Successful collaborations such as the recent one between HZB, DESY and ALBA [8] play a key role in how facilities overcome the technical and theoretical challenges and workshops, such as the dedicated HarmonLIP

series in Europe, provide a crucial platform for advances to be shared.

The goal of this proceeding is to present a review of this latest wave of research and the environment and context in which it is being carried out. This is done from a beam dynamics perspective so will leave out the important work that is going into the technical designs, which interested readers may find elsewhere: [8–11] and others. A survey of the world's light-source facilities that have fourth-generation storage-ring projects has been conducted and in the first part of this proceeding, the results of this survey are presented. It is hoped that the results provide a helpful guide to future projects that will be faced with the same considerations.

Of particular interest in the survey were the fill patterns to be used in the storage ring since it is well established that an uneven fill pattern can negatively impact the bunch lengthening that can be achieved and lead to a distribution of different bunch lengths over the bunch train. This aspect in particular been the subject of a lot of research. Byrd and Georgsson [4] used single-particle tracking to predict the effects of this before Bassi et al. [12] took advantage of more powerful computing techniques and employed macroparticle tracking. More recently, a semi-analytical approach was taken by Yamamoto et al [13] and Olsson et al. [14] used a matrix equation and the Newton method to iterate towards a self-consistent solution that showed good agreement with tracking using a fraction of the computational resources. Since then, other approaches have emerged [15, 16] showing improved performance and the potential to include the effects of short-range wakefields.

HARMONLIP

In October 2022, a workshop called HarmonLIP was convened at MAX IV Laboratory in Lund, Sweden [17]. This was the first in a series that is an internal project supported by the League of European Accelerator-based Photon Sources (LEAPS) Working Group 2 [18]. The hybrid workshop had delegates from eleven different synchrotron light-source facilities in Europe come in person or join remotely and was also joined remotely from South America and from Asia. The workshop photo is shown in Fig. 1. Facilities gave an update on the status of their respective harmonic-cavity systems before more general topics were discussed. These discussions included short comment talks briefly presenting the perspective of one facility or one participant. The next edition of the HarmonLIP workshop series is planned for March 2024 and will be hosted by the ESRF in Grenoble.

In preparation for the workshop, a survey was carried out of the technical specifications of the HC systems at each

* francis.cullinan@maxiv.lu.se

¹ Bunch shortening is also sometimes the aim [1]

BEAM DYNAMICS USING SUPERCONDUCTING PASSIVE HARMONIC CAVITIES WITH HIGH CURRENT PER BUNCH

A. Gamelin*, V. Gubaidulin, A. Loulergue, P. Marchand, L. S. Nadolski, R. Nagaoka
 Synchrotron SOLEIL, Gif-sur-Yvette, France
 N. Yamamoto, KEK, Ibaraki, Japan

Abstract

In 4th generation synchrotron light sources, harmonic cavities (HCs) are critical components needed to achieve the required performance. They provide longer bunches, which helps to reduce statistical effects (intra-beam scattering and Touschek effect). In "timing" modes, where the bunch spacing is larger than in conventional modes and the number of particles per bunch is higher, this need is even greater. In this article, we present the beam dynamics in the high current per bunch regime and how it interacts with the single bunch collective effects. In particular, a dipole-quadrupole instability is observed above the microwave threshold and a coupling between the dipole and cavity modes is shown to limit bunch lengthening at low current. The effective gain from the use of HCs in terms of lifetime, emittance, and energy spread is also discussed.

INTRODUCTION

In this paper, we explore the beam dynamics of a double RF system with harmonic cavities (HCs) in the context of high currents per bunch. The parameters of the SOLEIL II project [1–3], which aims to replace the existing SOLEIL storage ring by a 4th generation synchrotron light source are used throughout the article.

Double RF System

For a passive unloaded cavity at the k^{th} harmonic of the RF frequency f_{RF} , the only knob is the cavity tuning angle ψ or equivalently the cavity detuning Δf :

$$\Delta f = f_r - k f_{RF}, \quad (1)$$

$$\tan \psi = Q \left(\frac{f_r}{k f_{RF}} - \frac{k f_{RF}}{f_r} \right) \approx 2Q \frac{\Delta f}{f_r}, \quad (2)$$

where f_r is the cavity resonance frequency and Q is the cavity quality factor (equal to the unloaded quality factor Q_0 in that case). The beam-induced voltage V_2 in the harmonic cavity (neglecting form factors) is given by [4]:

$$V_2 = 2I_0 R_s \cos \psi \approx I_0 \frac{R_s}{Q} \frac{k f_{RF}}{\Delta f} \sin \psi, \quad (3)$$

where I_0 is the total current, R_s is the cavity shunt impedance (using the circuit ohm definition). For a main cavity voltage V_1 , an approximate voltage of $V_2 \approx V_1/k$ is needed to get close to the near flat potential (NFP) conditions [5] and longer bunches. Using the beam voltage induced at

resonance, one can set a lower limit on the needed shunt impedance:

$$R_s \gg \frac{V_1}{2kI_0}. \quad (4)$$

For $V_1 = 1.8$ MV, a 4th HC and the lowest beam current of 20 mA, the total shunt impedance of the HCs should be much larger than 11.25 M Ω . As the system should also be stable at higher currents, the total R_s/Q should not exceed 100 Ω to avoid instabilities [5, 6]. Both conditions are only possible with superconducting (SC) cavities, which typically have Q_0 around 10^8 , while normal conducting (NC) cavities typically have Q_0 of a few 10^4 . For these reasons, we consider in this article a double RF system using SC HCs as detailed in Table 1 and for such a SC passive system there is $\psi \approx \pi/2$ and thus $\sin \psi \approx 1$ in Eq. (3).

Table 1: RF Cavity Parameters

Parameter	NC MC	SC HC
Harmonic number k	1	3 or 4
Shunt impedance R_s (per cavity)	5 M Ω	4.5 G Ω
Unloaded quality factor Q	35 700	10^8
R_s/Q (per cavity)	140 Ω	45 Ω
Loaded quality factor	6 000	10^8
Cavity number	4	2

BEAM DYNAMICS

In this part, the beam dynamics in 8-bunch mode at 100 mA and in single bunch mode at 20 mA is studied by tracking using mtrack2 [7]. Results for SOLEIL II main operation mode, uniform filling at 500 mA, using the same RF system but without short-range wake, were already discussed in Ref. [5].

Short Range Wake

To be able to estimate accurately the beam dynamics at a high charge per bunch, a preliminary impedance model including the most important features of SOLEIL II (resistive wall with NEG coating, tapers, BPMs, ...) is included in the simulations [8]. Figure 1 shows the relative variation of the bunch length and energy spread when the single bunch current is varied from 0 mA to 20 mA. It can be observed that the micro-wave instability (MWI) threshold, characterized by an energy spread increase, is reached at 3 mA.

Even in uniform filling mode, where the current per bunch is limited to 1.2 mA, the short-range wake effect is important

* alexis.gamelin@synchrotron-soleil.fr

BUNCH-LENGTHENING RF SYSTEM USING ACTIVE NORMAL-CONDUCTING CAVITIES

N. Yamamoto*, D. Naito, S. Sakanaka, T. Yamaguchi, Accelerator Laboratory, KEK, Tsukuba, Japan
A. Gamelin, P. Marchand, Synchrotron SOLEIL, Gif-sur-Yvette, France

Abstract

A normal conducting (NC) harmonic cavity (HC) bunch-lengthening system, powered with an external rf generator, is attractive for future generation synchrotron light rings. This system is expected to improve the bunch lengthening performance even at low stored currents. As a result of recent particle tracking simulations, a proper control of the external rf generator is also expected to be a countermeasure for reduction in bunch lengthening efficiency due to the transient beam loading (TBL) and for unstable beam motions in the vicinity of the "flat-potential" condition. In order to realize such a system, a low R/Q 1.5GHz-TM020 HC and a broadband kicker cavity with a bunch phase monitor integrated in the digital rf control for the TBL compensation, are being developed.

INTRODUCTION

Bunch lengthening using a double RF system with fundamental and harmonic cavities (FC and HC) [1] is essential in preserving the extremely low emittance in fourth and future generation synchrotron light rings. For these rings, the relatively low required rf voltage makes the use of normal conducting (NC) cavities quite attractive.

For more than 20 years, double rf systems with passive HCs have been used in a number of third-generation light sources to lengthen the electron bunches for improving the beam lifetime and stability [2–5]. These previous works have revealed that the transient beam loading (TBL) reduces the bunch lengthening efficiency when bunch gaps are introduced in the fill pattern, especially for systems consisting of HCs having their resonant frequency higher than 1 GHz. It has also been reported that reducing the total R/Q of the HCs is essential in mitigating such transient effects [6].

In addition, recent studies have shown that in many cases, unstable beam motions, such as the so-called "mode-0" [7, 8] and the "periodic transient beam loading (PTBL)" [9–11] instabilities, prevent one from reaching the optimum bunch lengthening condition at low and high beam current, respectively, even with symmetric filling patterns. While reducing the R/Q will help the latter, it will worsen the former.

To realize an efficient bunch lengthening system, the KEK team proposed a promising solution relying on a powered TM020 HC with RF feedbacks (RF-FBs) [12], as reported at FLS2018. Based on this concept, we are developing a HC using the TM020 resonant mode [13], a kicker cavity with a bandwidth > 5 MHz [14], a bunch phase monitor (BPhM)

and RF-FBs. In this paper, we describe our complete bunch lengthening system including the cavity and BPhM designs.

ACTIVE NC DOUBLE RF SYSTEM

A feature of our proposed system is the use of powered TM020 HCs, also called "active HCs". The use of the higher frequency TM020 resonant mode instead of the lowest TM010 mode allows to reduce the R/Q by about 40% [13] and active HCs have some advantages over the more commonly used passive HCs:

- The external generator of an active HC can provide sufficient voltage to lengthen the bunches even at a low stored current (operation with a single or few bunches) [15]
- A proper control of the external generator by using advanced low-level rf (LLRF) techniques can mitigate the voltage fluctuations due to the TBL effect and circumvent unstable beam motions.

The first point is important to maintain a wide use of the synchrotron radiation in the future light sources by preserving all the operating modes available in third-generation light sources. New concepts of synchrotron radiation sources that emphasize flexibility are proposed by KEK [16] and SOLEIL [17].

As shown in Ref. [12], transient rf voltage compensation can be achieved by using the generators of both FC and HC or by using a separate broadband kicker cavity. Besides, particle tracking simulations, performed with the mtrack2 code [18], have shown that an advanced feedback, such as a direct RF-FB (DRFB) loop can help to push back the PTBL instability threshold in the vicinity of the "flat-potential" condition [19].

In the following section, the development progress of hardware components, needed to realize our active NC double RF system is reviewed.

HARDWARE DEVELOPMENT STATUS

1.5GHz-TM020 Harmonic Cavity

The 508MHz-TM020 cavity was originally developed as a HOM-damped accelerating cavity for the SPring-8 II project [20], and four such cavities have already been installed as fundamental accelerating cavities at the new 3-GeV synchrotron radiation facility NanoTerasu in Japan [21].

In their design, two shallow coaxial slots are located on both end plates of the cavity, where the magnetic field of the accelerating mode vanishes (i.e., at its magnetic field node). By placing microwave absorbers on these slots, most of the harmful parasitic modes can be strongly damped without

* naotoy@post.kek.jp

GENERATING HIGH REPETITION RATE X-RAY ATTOSECOND PULSES IN SAPS

Weihang Liu¹, Yi Jiao*, Yu Zhao¹, Xingguang Liu¹, Xiao Li¹, Sheng Wang^{1,†}
Institute of High Energy Physics, Chinese Academy of Sciences, Beijing, China
University of Chinese Academy of Sciences, Beijing, China
¹also at Spallation Neutron Source Science Center, Dongguan, China

Abstract

Attosecond, which refers to 10^{-18} seconds, is the timescale of electron motion within an atom. Accurate observation of electron motion helps deepen the understanding of microscopic quantum processes such as charge transfer in molecules, wave packet dynamics, and charge transfer in organic photovoltaic materials. To meet the needs of relevant research, the South Advanced Photon Source (SAPS), currently in the design phase, is considering the construction of an attosecond beamline. This paper presents relevant research on achieving high-repetition-rate coherent attosecond pulses on the fourth-generation storage ring at SAPS. Realizing attosecond pulses in a storage ring requires femtosecond to sub-femtosecond-level longitudinal modulation of the beam, and the modulation scheme needs to consider multiple factors to avoid a significant impact on other users. The study shows that with high-power, few-cycle lasers, and advanced beam modulation techniques, the photon flux of attosecond pulses can be significantly enhanced with a minimal impact on the brightness of synchrotron radiation. Adopting high-repetition-rate lasers and precise time delay control, the repetition rate of attosecond pulses at SAPS can reach the megahertz level. To separate the attosecond pulse from the background synchrotron radiation, a pulse separation method was proposed. This method improves the signal-to-noise ratio of attosecond pulses by more than an order of magnitude. Currently, the design wavelength range for attosecond pulses covers the water window (2.3-4.4 nm), which is “transparent” to water but strongly absorbed by elements constituting living organisms. This wavelength range has significant application value in fields such as biology and chemistry.

INTRODUCTION

Attosecond, which represents the natural time scale of electron motion in atomic and molecular systems, holds significant implications for several cutting-edge fields, such as quantum physics, biology, chemistry, and medicine. To advance scientific research in these fields, it is considered crucial to develop high-flux and high-repetition-rate Attosecond light sources [1].

The storage ring based light source is a stable, high-repetition-rate, and multi-user tool for light generation, which has been at the forefront of high-brilliance experiments. Currently, it has evolved from the third generation to

the fourth generation, also known as the diffraction-limited storage ring (DLSR), resulting in an increase in Brilliance by more than two orders of magnitude. The ability to achieve attosecond pulses in DLSR would make it highly attractive due to the aforementioned advantages. During the design phase, the Southern Advanced Photon Source (SAPS) [2], aims to provide this new attosecond tool for attosecond science study. By pursuing high Brilliance and providing high flux and high repetition rate attosecond pulses, SAPS hopes to contribute to the development of attosecond science.

The natural pulse duration of light in storage rings typically ranges from 10 to 100 ps. To effectively reduce pulse duration while maintaining a high pulse flux, various laser-based beam modulation techniques have been proposed and applied to storage rings, such as echo-enabled harmonic generation (EEHG) and angular dispersion-induced microbunching (ADM) [3]. Recently, we propose a method by combine ADM with a few-cycle laser for the generation of attosecond pulses in a DLSR [4].

In this paper, we adopt this method for SAPS to generate attosecond pulses. Potential problems related to the ADM section were discussed, such as vertical dispersion bump-induced vertical emittance growth, and DA and MA reduction. And to increase the signal-to-noise ratio of the attosecond pulse, we propose a pulse separation method. This method improves the signal-to-noise ratio of attosecond pulses by more than an order of magnitude.

PARAMETERS OPTIMIZATION OF THE ADM

The ADM structure, located within one of the straight sections of SAPS as illustrated in Fig. 1, initially couples the electron beam in both transverse and longitudinal directions using a vertical dipole. Subsequently, the beam undergoes energy modulation through interaction with a short wiggler (known as a modular) and a few-cycle laser. Finally, a dog-leg consisting of two vertical dipoles with equal strength but opposite deflection angles imparts transverse and longitudinal dispersion, which converts the energy modulation into density modulation, resulting in microbunching or a large local peak current in the electron beam. The modulated beam then passes through an undulator (known as a radiator) to generate coherent attosecond pulses. After this process, the radiated electron beam passes through four dipole magnets, which have been designed specifically in position and strength to eliminate the vertical dispersion and allow the beam to return to the ring. The design of the ADM

* jiaoyi@ihep.ac.cn

† wangs@ihep.ac.cn

STATUS AND PERSPECTIVES FOR THE SWISS FREE-ELECTRON LASER (SwissFEL)

T. Schietinger* on behalf of the SwissFEL team
Paul Scherrer Institut, Villigen, Switzerland

Abstract

We summarize the status of SwissFEL, the X-ray free-electron laser at the Paul Scherrer Institute. Apart from some key operational performance figures the contribution covers the state of the experimental stations, the evolution of user demand and gives a brief overview of the use of advanced operation modes beyond SASE at our facility. Furthermore we report on progress of our seeding upgrade program on the soft X-ray line. Lastly we mention our long-term upgrade plans for a third undulator beamline in the tender and hard X-ray regime.

INTRODUCTION

SwissFEL is a free-electron laser (FEL) facility at the Paul Scherrer Institute in Switzerland featuring two beamlines, Aramis for the hard X-ray regime (1.8–12.4 keV) and Athos covering the soft X-ray spectrum (0.26–1.9 keV) [1]. The accelerator consists of an S-band photoinjector gun followed by an S-band booster radiofrequency (rf) linac, which accelerates electron bunches to an energy of 300 MeV. Main acceleration to the final beam energy of up to 6.2 GeV (Aramis) is accomplished through a series of C-band rf linacs.

A schematic view of the SwissFEL facility is given in Fig. 1. The electron gun generates two bunches, separated by 28 ns, at a repetition rate of 100 Hz. The first bunch goes straight to the Aramis undulator line, while the second bunch is extracted at a beam energy of 3.17 GeV into a dogleg beamline leading to the Athos undulator. A short tuning linac in the Athos branch allows for energy adjustments in the range ± 250 MeV. The electron bunches are compressed longitudinally in two magnetic chicanes (BC1 and BC2). In the Aramis branch they may be further compressed in an energy collimator chicane before the undulator, in Athos in the dogleg and in additional chicanes present in that beamline. The Aramis undulator line consists of 13 planar in-vacuum undulator modules of 4 m length each with 15 mm period. Athos features 2×8 highly flexible APPLE-X type undulator modules, which are 2 m long and have 38 mm period. The Athos undulator modules are interspersed with small magnetic delaying chicanes. Between the two undulator halves there is a larger chicane used for tuning the delay (up to 500 fs) between two-color pulses generated individually in the two undulator halves. All undulators have adjustable deflecting parameters K through variable gaps (up to a maximum value of 1.8 in Aramis, 3.8 in Athos). For more details we refer to the “first-lasing” publications for Aramis [2] and Athos [3] and references therein.

Several deflecting rf cavities at different locations along the accelerator are used for measurements of the bunch profile or longitudinal phase space. An S-band deflecting cavity after BC1 performs such measurements with a temporal resolution of about 10 fs, whereas two C-band deflecting cavities at the end of linac-3 provide subfemtosecond resolution [4]. In 2022, a set of two X-band rf deflecting cavities for postundulator measurements in the Athos line was installed and commissioned, marking the completion of the SwissFEL baseline design. The cavities are based on the PolariX design, which arose from a collaboration between DESY, CERN and PSI [5]. The system gives time-resolved information on the lasing process with subfemtosecond resolution [6] and is indispensable for the clean setup of the many advanced operation modes available in Athos. Longitudinal phase space measurements of similar quality can also be obtained by streaking the beam passively with the wakefields from metallic corrugated structures [7].

SwissFEL ENDSTATIONS

Each of the SwissFEL undulator lines is designed to deliver FEL pulses to one out of three endstations associated with that line. Pairs of offset mirrors are set to ensure transport of the X-rays to the desired endstations. The endstations are named after Swiss mountain passes: Alvra, Bernina and Cristallina at the Aramis line, Maloja, Furka and Diavolezza at the Athos line.

At the Aramis line, Alvra and Bernina have been in operation since the beginning of FEL operation, with pilot runs in 2018 followed by the start of regular user operation in 2019. Alvra focuses on ultrafast dynamics of photochemical and photobiological systems while Bernina primarily measures ultrafast phenomena in condensed matter systems. The third endstation, Cristallina, designed for quantum science and structural biology, is currently in its pilot phase and will switch to user operation at the beginning of 2024.

The Athos undulator line was completed in the course of 2020. The first endstation, Maloja, started its pilot run at the end of that year and moved on to regular user operation in the beginning of 2022. Its focus lies on atomic, molecular and nonlinear X-ray physics and chemical dynamics. The second endstation, Furka, addresses ultrafast dynamics in quantum matter. Its pilot phase began in early 2023 and is planned to last for about one year. Finally, a third endstation, to be called Diavolezza and dealing with attosecond and nonlinear X-ray science, is in a conceptual phase and expected to become operational in a few years.

* thomas.schietinger@psi.ch

FLASH: STATUS AND UPGRADE

M. Vogt*, S. Schreiber, J. Zemella

Deutsches Elektronen-Synchrotron DESY, Germany

Abstract

FLASH, the Soft X-Ray and Extreme-UV Free Electron Laser at DESY, is undergoing a substantial upgrade and refurbishment project, called FLASH2020+. The project will finally enable external seeded and SASE FEL operation for a wavelength range down to 4 nm with the EEHG method. This is achieved in two long shutdowns from November 2021 to August 2022 and from June 2024 to August 2025. Key ingredient of the upgrade were installation of a laser heater, replacing two early TTF-type L-band SRF accelerating modules by modern, high-gradient XFEL-type modules, redesign of the 2nd bunch compressor, and complete redesign of the FLASH1 beam line for HGHG/EEHG seeding.

This talk will report on the project and the status of FLASH after the first shutdown with emphasis on beam dynamics aspects.

FLASH

This contribution is a modified version of a contribution [1] to the 21st International Conference on Radio-Frequency Superconductivity, held this June in Grand Rapids, MI, USA. There the emphasis was on the energy upgrade, while this contribution emphasizes certain beam dynamics aspects of the FLASH2020+ Upgrade.

FLASH [2–8] is a superconducting high-gain vacuum-ultraviolet (VUV) / soft X-ray free-electron laser (FEL), operated mainly as a photon user facility with up to two beamlines operated simultaneously. FLASH is segmented into three functional beamlines: the common injector and linac FLASH0, preparing and accelerating bunch trains suitable for the FEL process, and the two FEL beamlines FLASH1 and FLASH2 which finalize and diagnose the bunch preparation, accommodate the FEL process each in their own internal undulator beamline, and finally dispose of the spent beam in a beam dump. The FLASH3 beamline is used by the plasma wake field acceleration experiment FLASHForward [9] which can be activated *alternatively* to FLASH2 by powering a DC dipole. The FLASH accelerating RF consists of 7 L-band (1.3 GHz) superconducting modules of 8 9-cell Tesla-type cavities.

At the moment FLASH is undergoing a substantial upgrade and refurbishment project, called FLASH2020+ (see next section). The first of two shutdowns started November 2021 and ended August 2022 successfully and the second scheduled to start June 2024 and to end August 2025, is being prepared now.

The original FLASH injector (before the upgrade) consisted of a normal-conducting photo-cathode 1.6-cell RF-

gun (1.3 GHz), an accelerating L-band module (ACC1), a third harmonic linearizer (ACC39) operated at 3.9 GHz, a BACCA longitudinal feedback cavity [10], the first bunch compression chicane, two more L-band accelerating modules (ACC2, ACC3), and the second bunch compression chicane — at that time an S-type 6-dipole chicane.

The bunches are produced in up to three trains mapped to the three injector lasers.

In its standard setting, the RF-gun is operated with approximately 5 MW and produces a 600 μs flat top. The bunch at the exit of the gun then has a momentum of 5.6 MeV/ c ” FLASH0 can therefore provide up to 6000 bunches per second (in 10 trains) at 1 MHz bunch repetition frequency and 10 Hz pulse repetition frequency. If the RF pulse is split between two sub-trains (for FLASH1 and FLASH2), a minimum of 70 μs has to be subtracted for transient effect of the extraction kicker and for interpolating between the RF parameters of the two flat tops which are otherwise within certain ranges independent.

The third harmonic linearizer ACC39 is typically operated in decelerating mode with a nominal set point is 19.5 MeV.

The first bunch compression chicane is a 4-dipole C-chicane designed for bending angles from 15° (longitudinal dispersion $M_{56} = 120$ mm) to 15° ($M_{56} = 255$ mm). Prior to the upgrade it used to be operated at a typical deflection angle of 18° ($M_{56} = 181$ mm). Downstream of the chicane used to be a comfortably equipped transverse diagnostics and matching section.

Before the upgrade, the second (ACC2) and third (ACC3) L-band Module were among the weakest in FLASH. Well tuned they were capable of (together) providing an E -gain of 304 MeV at an off-crest angle of up to 30°, i.e. an effective total amplitude of at most 350 MeV

In addition prior to the first shutdown, the second bunch compression chicane was a 6-dipole (S-type) chicane blocking the space for proper a proper second beam re-match upstream of the “main-linac”.

The FLASH0 “main-linac” consists of four L-band modules (ACC4/5/6/7). The maximum attainable energy gain of the main linac is about 800 MeV so that the maximum e^- -beam energy of FLASH was ~ 1250 MeV

Downstream of the last module the combined collimation and switch-yard section starts. Switching between FLASH1 and FLASH2 is achieved via a kicker-septum scheme with two vertically deflecting flat top kickers, deflecting the FLASH2 sub-train into the horizontally deflecting channel of a DC Lambertson septum. In order to achieve the required stability for the kicked bunches, the gap between the bunch trains needs to be >70 μs to cover the kicker rise-time and the damping of the initial ringing.

* vogtm@mail.desy.de

DEVELOPMENT OF A PULSED INJECTION STRIPLINE FOR DIAMOND-II

R. Fielder*, A. Lueangaramwong, A. Morgan, Diamond Light Source, Oxfordshire, UK

Abstract

Diamond-II will use a single bunch aperture sharing injection scheme. This applies a strong kick to both the injected and the targeted stored bunch with a very short duration (ideally <3 ns, if disturbance to the adjacent bunches is to be avoided). We have developed a design for the stripline kickers that can meet these requirements while minimising internal reflections and beam impedance. We show an analysis of the electric and magnetic fields produced by the stripline and simulations of the effects on injected and stored beam, and analysis of the wakefields and impedance of the structure.

INTRODUCTION

Diamond Light Source is a third generation light source which uses a standard four kicker bump injection method. The kickers have a pulse length of 6 μ s, giving some kick to the target bunch both the turn before and after injection, and affecting the entire bunch train even during single bunch injection. In theory this could have zero impact on the stored beam, but difficulty in precisely matching the full length of the four kicker pulses, plus other effects due to non-uniformity in the coating on the ceramic vessels make this difficult. Efforts have been made to reduce the measurable effects of injection on beamlines at Diamond [1,2], but there can still be some significant impact.

The Diamond-II upgrade [3] will have greatly reduced dynamic aperture compared to Diamond, making injection even more challenging. At the same time, reduced beam size and more advanced beamline detectors and optics greatly reduce the acceptable levels of beam disturbance. Diamond-II will therefore use stripline kickers which can provide pulse lengths on the order of nanoseconds to allow true single bunch injection without disturbing the bulk of the stored beam. This allows an aperture sharing injection scheme, as described in [4,5].

STRIPLINE DESIGN

The injection stripline design was initially based on the multibunch feedback stripline kickers and influenced by the SLS 2.0 design [6]. This has since been greatly modified to meet the requirements. A large vacuum chamber is used, with a smaller pipe with pumping grills to provide RF continuity and match radius to the incoming and outgoing beam pipe, shown in Fig. 1 with the outer vacuum chamber hidden. The stripline profile is a mix of circular arc with a flat central section to provide better field quality, but with a notch cut out to avoid synchrotron radiation (Fig. 2); a notch is

also included on the inboard side for symmetry. The gaps between the charged and grounded elements have been kept as large as possible to reduce the chance of arcing. All edges are rounded for the same reason.

There will be four stripline modules in total, at the downstream end of the mid-straight following the injection straight. The striplines are 150 mm long, with a module length of 180 mm including the surrounding structure. The curved portion of the stripline has a radius of 7 mm, while the flat part is 6.2 mm from the beam horizontally, however, the notch and hybrid shape means there is not a clearly defined gap between the striplines. The striplines are made of copper, while the rest of the chamber will be stainless steel, with ceramic spacers in the input feeds. The striplines will likely be supported inside the chamber by additional ceramic posts, but the mechanical design is not finalised yet. The total required kick of 175 μ rad can be provided by a peak voltage of 12.8 kV in each module. The rise time requirement of 0.6 ns leads to a bandwidth requirement of >0.8 GHz. The voltage requirement is 20 kV, driven by the desire to be resilient against a single module failure.

The ends of the striplines are designed to minimise longitudinal field roll off and also to minimise reflections and wake impedance. Alongside tuning of the conical coaxial transitions to the ports, the best overall solution has been found with no overall tapering of the curved section combined with strong tapering of the central flat section.

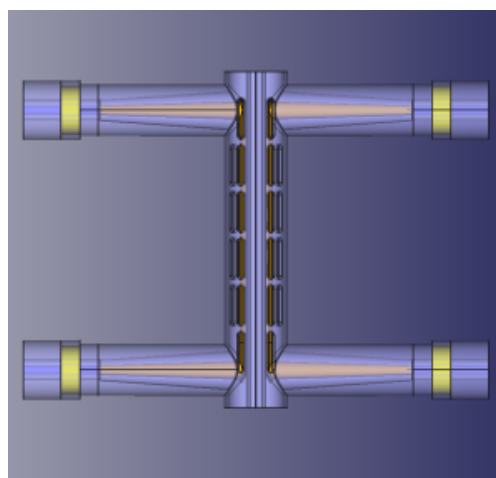


Figure 1: Top down view of stripline with vacuum vessel hidden.

Wakefield and Impedance Simulations

Wakefield and impedance simulations for the stripline were carried out using GdfidL [7] and CST Studio [8]. Impedance simulated with a 0.5 mm drive bunch is shown

* richard.fielder@diamond.ac.uk

DEVELOPMENT OF A COMPACT LIGHT SOURCE USING A TWO-BEAM-ACCELERATION TECHNIQUE *

P. Piot¹, C. Chen, X. Lu¹, J. G. Power, E. E. Wisniewski,
 Argonne National Laboratory, Lemont, IL, USA
 C. Jing, S. Kuzikov, Euclid TechLabs, Solon, OH, USA
 E. Frame, Northern Illinois University, DeKalb, IL, USA
¹also at Northern Illinois University, DeKalb, IL, USA

Abstract

The recent demonstration of sub-GV/m accelerating fields at X-band frequencies offers an alternative pathway to designing compact light sources. The high fields were enabled by powering the accelerating structures using short (< 10 ns) X-band RF pulses produced via a two-beam-accelerator (TBA) scheme. In this contribution, we discuss a conceptual roadmap to scale the concept to a ~ 0.5 GeV accelerator. We present the optimization of a photoinjector and preliminary beam-dynamics modeling of the accelerator. Finally, we discuss ongoing and planned experiments toward developing an integrated proof-of-principle experiment at Argonne National Laboratory employing the a 0.5 GeV TBA-driven accelerator to drive a free-electron laser.

INTRODUCTION

Low-emittance bunches are critical to reducing the footprint of the XFEL: for a given energy the gain length of a single-pass FEL scales with the electron-beam brightness [1]. Consequently, higher brightness translates into shorter undulator lengths. The beam emittance can only degrade between the electron source and the undulator, therefore the source "intrinsic" emittance sets the minimum emittance that can be ultimately attained in the accelerator. A pathway to producing low-emittance bunches is to subject the photocathode to an extremely high electric field as it mitigates the space-charge effect during the emission process and low-energy transport [2]. Currently, most normal-conducting RF guns operate at cathode fields $E_0 \in [80, 140]$ MV/m [3]. Operation at higher fields (~ 200 MV/m) is currently under investigation using high-frequency [4] or cryogenically-cooled C-band [5] RF guns.

Since 2020, our group has concentrated on the development of an X-band RF (XRF) photoemission gun powered by short (nanosecond) RF pulses and operating at 11.7 GHz; see Fig. 1(a,b) [6, 7] using a two-beam acceleration (TBA) scheme [8]. This operational choice is motivated by the empirical dependence of the breakdown rate (BDR) on the applied surface field E_0 and the RF-pulse duration τ given by $BDR \propto E_0^{30} \tau^5$ [9]. Such a scaling suggests that for a given BDR, reducing the pulse duration significantly enhances the attainable electric field; see Fig. 1(c). The RF

pulse (peak forward power $P_{FWD} \sim 200$ MW) was generated by passing a train of 8 high-charge (total charge of $Q \sim 8 \times 40 = 320$ nC) relativistic (~ 60 MeV) electron bunches in a power-extraction and transfer structure (PETS) [10]. The high-charge bunches are produced in the Argonne Wakefield Accelerator (AWA) drive-beam accelerator with a time separation of 769 ps corresponding to 1.3 GHz. The developed XRF gun enabled the generation of E-field on the photocathode surface of ~ 0.4 GV/m with a low BDR and insignificant dark current [7].

The ongoing R&D program leverages this recent accomplishment to focus on forming bright electron bunches and characterizing the associated beam parameters. We are also exploring the building blocks necessary to generate bright ultra-relativistic electron beams for linear collider and light-source applications. This paper summarizes our research program and the latest results.

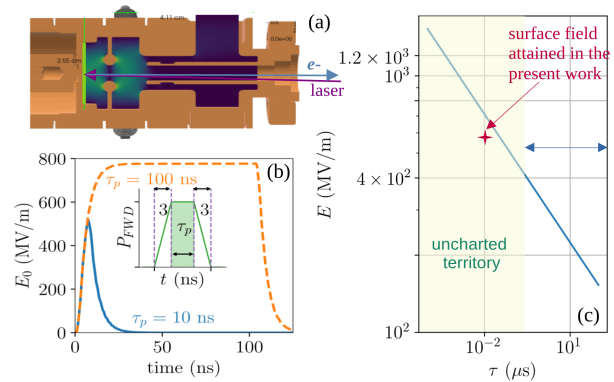


Figure 1: Schematics of the XRF gun with photocathode plane shown in green and electric-field amplitude appearing as a false-color map (a), RF-pulse envelope for short (blue) and (long) RF pulse excitation (b), and example of electric-field scaling with RF pulse duration for a given BDR constant (c). In plot (b), the inset shows the shape of the RF pulse produced from the PETS which yields the blue-trace pulse envelope.

PHOTOEMISSION IN EXTREME FIELDS

Ideally, the beam 4D brightness scales as $B \propto E_0^y / MTE$, the mean transverse energy (MTE) is related to the photocathode physical and chemical properties [2]. The brightness scaling suggests that a low-MTE photocathode combined

* This research is based on work supported by Laboratory Directed Research and Development (LDRD) funding from Argonne National Laboratory, provided by the Director, Office of Science, of the U.S. DOE under Contract No. DE-AC02-06CH11357.

AN EFFICIENT OPTIMISATION OF A BURST MODE-OPERATED FABRY-PEROT CAVITY FOR COMPTON LIGHT SOURCES

V. Muşat^{1,*}, A. Latina, E. Granados, CERN, Meyrin, Switzerland
 E. Cormier, G. Santarelli, LP2N, Talence, France
¹also at The University of Oxford, Oxford, UK

Abstract

The burst mode operation of a Fabry-Perot cavity (FPC) allows for the generation of a high-intensity photon beam in inverse Compton scattering (ICS) sources. The geometry and burst mode parameters of the FPC can be optimised to maximise the scattered photon flux. A novel optimisation method is presented, significantly improving processing speed and accuracy. The FPC's dimensions, mirror requirements, and effective energy can be obtained from the electron beam parameters at the interaction point. A multi-objective optimization algorithm was used to derive the geometrical parameters of the FPC; this brought orders of magnitude increase in computation speed if compared to the nominal Monte Carlo-based approaches. The burst mode parameters of the FPC were obtained by maximizing the effective energy of the laser pulse in the FPC. The impact of optical losses and thermal lensing on the FPC parameters is addressed. Preliminary parameters of an ICS source implementing this novel optimisation are presented. The source could reach high-performance photon beams for high-energy applications.

INTRODUCTION

Fabry-Pérot cavities are widely used to generate high-intensity photons from inverse Compton scattering [1]. FPCs are operated in one of two regimes: permanent or pulsed. Most ICS setups use the first option, which matches the high repetition rate requirements for storage ring sources.

More recently, FPCs operated in the pulsed regime have been considered for linac-based ICS sources [2], since both require a lower repetition rate than storage ring or energy-recovery linac designs. In burst mode, FPCs can achieve an effective gain 2 or 3 orders of magnitude larger than for the permanent mode.

This paper addresses the optimisation of an FPC's geometry and burst-mode parameters from [3]. Significant improvements were made relating to the runtime and efficiency of the optimisation.

THEORY

The mechanism of optical enhancement in FPCs can be described in terms of the temporal patterns of the electron and laser pulses in the cavity. N_p laser pulses are stacked in the FPC and interact with N_e electron bunches. Prior to the interaction, N_0 laser pulses are injected to provide an initial circulating laser power. A schematic of the interaction

between the electron train and the laser pulses stored in the FPC is shown in Fig. 1.

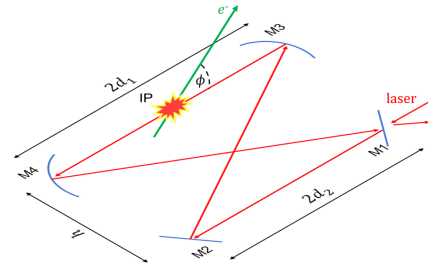


Figure 1: Layout of the ICS interaction of the input electron train with the laser pulses stored in the four-mirror planar Fabry-Pérot cavity. The electron beam enters the cavity plane with a crossing angle ϕ .

Given a small electron recoil, identical time separation between the electron and the laser pulses and no change in both the laser's pulse energy, \mathcal{E}_0 , and the bunch charge, Q , the total scattered photon flux from ICS, \mathcal{F} , can be determined from

$$\mathcal{F} = \sigma_C \frac{f_{\text{rep}} Q N_b \mathcal{E}_{\text{tot}}}{2\pi (ehc/\lambda) \sigma_{\gamma,y} \sqrt{\sigma_{\gamma,x}^2 + \sigma_{\gamma,z}^2} \tan^2(\phi/2)}, \quad (1)$$

where σ_C is the Compton cross section, e the elementary charge, h Planck's constant, c the speed of light in vacuum, λ the laser wavelength, ϕ the crossing angle between the electron and laser beam, \mathcal{E}_{tot} the laser effective energy, and σ_{γ} the source *rms* spot size at the interaction point (IP) [3]. To maximise the total flux, the FPC should provide the maximum \mathcal{E}_{tot} and the smallest laser waist size at the IP. The first condition depends mainly on the optimisation of the burst mode parameters provided by the input laser, while the second depends on the optimisation of the cavity geometry.

The circulating laser-beam energy determines \mathcal{E}_{tot} . It is a function of \mathcal{E}_0 , N_0 , N_p , N_e , and the cavity finesse, F ,

$$\mathcal{E}_{\text{tot}} = \epsilon (N_p, N_0, N_e, F) N_p \mathcal{E}_0, \quad (2)$$

where ϵ is the effective gain, and $N_p \mathcal{E}_0$ is the laser macropulse energy delivered to the FPC, in the following called U . The effective gain is a cavity-dependent parameter. Its linear dependence to \mathcal{E}_{tot} makes it relevant for the maximisation of the scattered photon flux. The optimum value for N_0 can be derived from $\partial\epsilon/\partial N_0 = 0$.

Given a high optical power, thermal lensing effects in the cavity mirrors must be considered, as they change their focal length, which can prevent the FPC from reaching a small

* vlad.musat@cern.ch

EVOLUTION OF THE INVERSE COMPTON SCATTERING X-RAY SOURCE OF THE ELSA ACCELERATOR*

A. Pires¹, V. Le Flanchec^{1,†}, R. Rosch, J. Touguet, CEA DAM DIF, Arpajon, France
 N. Delerue, Université Paris-Saclay, CNRS/IN2P3, IJCLab, Orsay, France
¹also at Université Paris-Saclay, CEA, LMCE, Bruyères-le-Châtel, France

Abstract

The Inverse Compton Scattering (ICS) X-ray source of ELSA accelerator at CEA-DAM, presents an efficient approach for generating X-rays with a compact linac. The source consists of a 30 MeV, 15 ps rms, up to 3 nC electron beam and a table-top Nd:YAG laser. X-rays are produced in the 10-80 keV range, higher X-ray energies achieved with frequency doubling of the laser. The yield is increased by a factor of 8 thanks to an optical mirror system developed at CEA, folding the laser beam path and accumulating successive laser pulses. We present a new version of the device, with improvement of mechanical constraints management, adjunction of motorized mirrors, and a new imaging system. A Chirped Pulse Amplification (CPA) system was also designed, enabling higher amplification levels without exceeding laser damage threshold. The uniqueness of this CPA system lies in its use of a short wavelength bandwidth, ± 250 pm after Self-Phase Modulation (SPM) broadening, and a line density of 1850 lines/mm for the gratings of the compressor. The pulse will be stretched with a chirped fiber Bragg grating (CFBG) before amplification in Nd:YAG amplifiers, and compressed by a double pass grating compressor.

ELSA X-RAY SOURCE

ELSA Accelerator

ELSA produces X-rays for studies of detectors used in facilities like the Laser Megajoule at CEA CESTA. The ICS source will be used to produce high flux in both single-shot and recurrent modes in the 10-80 keV range. The main goal is to produce 20 ps X-ray pulses in single-shot mode, with a flux of 10^{18} ph/s/cm². First experimental results have

been published in 2010 and 2016 [1, 2], still far from the ultimate goal, but showcasing potential for scaling up the X-ray flux. The accelerator (Fig. 1) is an electron linac featuring a 144 MHz photoinjector, 433 MHz accelerating cavities to reach 17 MeV, and a 1.3 GHz to reach 30 MeV, delivering 0.1 to 3 nC bunch trains typically at 1 Hz [3]. Double alpha magnets compress bunches from 80 to 28 ps before the final acceleration stage and the Inverse Compton Scattering (ICS) interaction point (IP). The accelerator can currently supply 10^4 bunches per train at 17 MeV, or 300 bunches per train at 30 MeV, and can also deliver single bunches.

Compton Laser

The laser dedicated to the ICS emits laser pulses at the same rate as the electron bunches, with similar temporal shape. It consists of a 144 MHz mode-locked Nd:YVO₄ oscillator at 1064 nm, a pulse selector, three Nd:YAG amplifiers, and eventually a KTP or LBO crystal for frequency doubling to 532 nm. Quadrupling can be achieved by the addition of a BBO crystal but is not implemented yet. The laser system can presently deliver up to 150 mJ per train at 1 Hz at 532 nm.

SMILE Device

At the interaction point (Fig. 2), our SMILE system (System Multipass Interaction Laser Electrons) focuses and superimposes 8 successive laser pulses going back and forth between two planes, reflecting on a series of spherical mirrors separated by a distance allowing a round trip time equal to the emission period of the laser pulses (Fig. 3). Thus eight successive pulses can interact with one electron bunch at the same time.

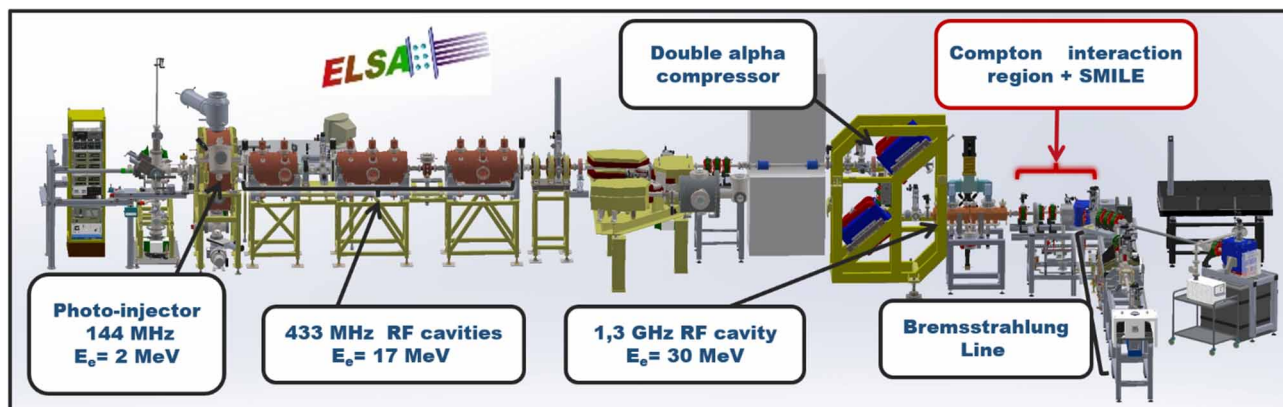


Figure 1: Layout of the ELSA Accelerator.

[†] Vincent.le-flanchec@cea.fr

THE CXFEL PROJECT AT ARIZONA STATE UNIVERSITY

W. S. Graves* on behalf of the CXFEL collaboration[†], Arizona State University, Tempe, AZ, USA

Abstract

The CXFEL Project encompasses the Compact X-ray Light Source (CXLS) that is now commissioning in the hard x-ray energy range 2-20 keV, and the Compact X-ray Free-Electron Laser (CXFEL) designed to lase in the soft x-ray range 250 - 2500 eV. CXFEL has recently completed a 3-year design phase and just received NSF funding for construction over the next 5 years. These instruments are housed in separate purpose-built laboratories and rely on inverse Compton scattering of bright electron beams on powerful lasers to produce femtosecond pulses of x-rays from very compact linacs approximately 1 m in length. Both instruments use recently developed X-band distributed-coupling, room-temperature, standing-wave linacs and photoinjectors operating at 1 kHz repetition rates and 9300 MHz RF frequency. They rely on recently developed Yb-based lasers operating at high peak and average power to produce fs pulses of 1030 nm light at 1 kHz repetition rate with pulse energy up to 400 mJ. We present the current commissioning performance of CXLS, and review the design of the fully coherent CXFEL.

INTRODUCTION

Future light sources aim to improve performance, cost, and accessibility over today's instruments. The CXFEL project is developing femtosecond x-ray light sources at a cost and size that makes the novel time-resolved molecular science they provide accessible to many institutions including universities, medical facilities, and industrial labs. The first instrument produced and now commissioning is the CXLS that produces partially coherent synchrotron-like x-ray pulses at few hundred fs duration in the hard x-ray range. The second instrument, CXFEL, has completed design and is now under construction. It is a further development of CXLS technology that adds novel nanometer-scale electron bunching to produce fully coherent x-rays in the soft x-ray spectrum. These instruments differ from the major XFEL and synchrotron facilities as well as current laboratory scale sources, thus require development of new experimental techniques, sample delivery, detector properties, controls and data analysis methods that are matched to their novel properties. These properties include lower flux than the major facilities as well as improvements in stability and precision of beam properties, and the ability to tailor integrated accelerator, laser, and x-ray beamline operations to optimize particular experiments. We first describe the labs that house the instruments and then the 2 instruments. For illustrations of the various equipment and laboratories discussed here please see oral presentation TU1C4 in the proceedings of the 2023 FLS workshop.

* wsg@asu.edu

[†] see Annex A

LABORATORY ENVIRONMENT

Environmental factors have a large impact on the stability and performance of experiments at molecular length and time scales. In 2018 we constructed a new laboratory building on campus, Biodesign C, with 2 essentially identical groups of labs that are purpose-built for the accelerators, RF systems, lasers, and x-ray endstations used by CXFEL and CXLS. The laser, accelerator, and x-ray labs are in separate rooms each with their own safety and air-handling systems but the 3 rooms share a single 2m thick reinforced concrete foundation that is physically separated from the adjoining building spaces to provide a common stable platform for the beams. These rooms are verified to meet VC-E vibration standards similar to an electron microscope lab. The air temperature stability in the laser labs is $\pm 0.25^\circ\text{C}$, and is $\pm 0.5^\circ\text{C}$ in the accelerator lab and x-ray hutch. Air humidity is at $40\% \pm 5\%$.

To mitigate electromagnetic interference we installed the RF systems including the klystrons in a Faraday cage preventing external pickup and suppressing any effects of the high power klystron pulses on sensitive x-ray experiments. The majority of equipment is water-cooled for temperature stability of high power systems. We designed and built a precision processed cooling water system that is tunable and stable to $\pm 0.05^\circ\text{C}$ with a future goal to achieve $\pm 0.01^\circ\text{C}$.

CXLS

The CXLS is constructed and now commissioning having produced first x-rays in February 2023. The technical components of CXLS including RF and accelerator sections, magnets, lasers, and diagnostics all serve as prototypes for the CXFEL equipment. CXLS will continue commissioning through 2023, transitioning to early science phase in 2024.

CXLS X-ray Performance

The CXLS design performance is given in Table 1. So far for commissioning we are running at lower electron bunch charge (10 - 20 pC) and laser ICS laser power (80 W) resulting in x-ray flux of 3×10^5 photons/shot at 1 kHz repetition rate. The charge is limited by damage to UV photoinjector optics that are currently being replaced with reflective optics. We are being conservative with the ICS laser power while developing automated steering software. In coming months we expect to increase UV and ICS laser powers to their full design specs. Simulations indicate that current x-ray performance (flux, emission angle, energy) is consistent with measured values. We anticipate meeting the full x-ray performance specifications as the power from both lasers is increased.

A HIGHLY COMPETITIVE NON-STANDARD LATTICE FOR A 4th GENERATION LIGHT SOURCE WITH METROLOGY AND TIMING CAPABILITIES

P. Goslawski*, M. Abo-Bakr, J. Bengtsson, K. Holldack, Z. Hüsches, A. Jankowiak, K. Kiefer, B. Kuske, A. Meseck, R. Müller, M. Sauerborn, O. Schwarzkopf, J. Viefhaus, J. Völker
 Helmholtz-Zentrum Berlin, BESSY, Berlin, Germany

Abstract

The PTB, Germany's national institute for standards & metrology, has relied on synchrotron radiation for metrology purposes for over 40 years and the most prominent customers are lithography systems from ASML/ZEISS. HZB is now working on a concept for a BESSY II successor, based on a 4th generation light source with an emittance of 100 pm rad @ 2.5 GeV. It is essential, that this new facility continues to serve the PTB for metrology purposes. This sets clear boundary conditions for the lattice design, in particular, the need for homogeneous bends as metrological radiation sources. Different Higher-Order-Multi-Bend-Achromat lattices have been developed, based on combined function gradient bends and homogeneous bends in a systematic lattice design approach. All lattices are linearly equivalent with the same emittance and maximum field strength. However, they differ significantly in their non-linear behavior. Based on this analysis, the choice of the BESSY III lattice type is motivated. A special focus is set also on TRIBs (Transverse Resonance Island Buckets) to operate with two orbits as a bunch separation scheme in MBAs, for different repetition rates or for the separation of short and long bunches.

HZB's AND BESSY's NEAR FUTURE

HZB is preparing for its future light source with two main projects [1]: the BESSY II+ project and BESSY III. BESSY II+ is a refurbishment and modernization project of BESSY II, to enable state-of-the-art operation for the next decade. The greenfield BESSY III project aims to establish a storage ring-based light source of the 4th generation based on a Multi-Bend-Achromat (MBA) lattice. A first sketch of the facility was recently published in a pre-CDR [2]. The initial operation of a greenfield project is not expected earlier than 2035, so a modernization of BESSY II, which has been running for 25 years, is mandatory and requested with the BESSY II+ project. It will pave the way towards BESSY III. The time schedule for BESSY II+/III is shown in Fig. 1.



Figure 1: Time schedule for BESSY II+/III project.

* paul.goslawski@helmholtz-berlin.de

VIA BESSY II+ TOWARDS BESSY III

The strategic focus points of the BESSY II+ project are *operando capabilities, modernization, and sustainability*. Overall it is a 100 M€ project, where nearly 25% will be covered by HZB, another 25% by strategic partners or third-party projects and 50% has been requested from the funding bodies. About 50% of the BESSY II+ project scope will be invested in new beamlines and endstations (25%), sample environment (12.5%), and digitalization (12.5%) to strengthen the *operando* capabilities of BESSY II and HZB. 35% will be used for the modernization of the accelerator complex (30%) and beamline instruments (5%), and 15% is foreseen to improve the sustainability of BESSY II.

The modernization scope for the accelerator complex will not only cover general preservation and modernization measures, but also includes technology development towards BESSY III.

A project already advanced is the development of an active normal conducting 1.5 GHz higher harmonic cavity (HHC) with HOM damper within a European collaboration between ALBA, DESY, and HZB. The prototype, designed and purchased by ALBA and RF tested at HZB, is installed in the BESSY II storage ring. Since autumn 2022, it is tested with beam and conditioned for user operation. Based on this experience, a new HHC system will be developed for BESSY II also including the option for a 1.75 GHz cavity system to generate a beating in the bunch focusing, allowing for simultaneously storing of short and long bunches.

Another important work package is the development of a BESSY II+/III digital twin as a natural interface for the efficient implementation of digitalization measures. This framework and methods are mandatory for the startup, commissioning, and efficient operation of BESSY III and already for the design process, e.g., in order to check for lattice robustness.

The work package *Permanent Magnets for Energy Efficiency* within the BESSY II+ is mainly motivated by BESSY III. In order to improve sustainability and to reduce the power consumption of BESSY III, it is discussed to replace the well-established classical iron yoke electromagnet technology with permanent magnets wherever possible, i.e., at dipoles and quadrupoles. Therefore conceptual designs, prototyping, and testing under real operating conditions are necessary. Within BESSY II+, it is foreseen to replace a very power-hungry bending electromagnet in the transferline between booster and storage ring with a permanent magnet

Content from this work may be used under the terms of the CC-BY-4.0 licence (© 2023). All distribution of this work must maintain attribution to the author(s), title of the work, publisher, and DOI

NONLINEAR OPTICS FROM HYBRID DISPERSIVE ORBITS*

Yongjun Li[†], Derong Xu, Victor Smaluk, Robert Rainer
Brookhaven National Laboratory, Upton, NY, USA

Abstract

In this paper we present an expansion of the technique of characterizing nonlinear optics from off-energy orbits (NOECO) [Olsson et al., Phys. Rev. Accel. Beams, vol. 23, p. 102803] to cover harmonic sextupoles in storage rings. The existing NOECO technique has been successfully used to correct the chromatic sextupole errors on the MAX-IV machine, however, it doesn't account for harmonic sextupoles, which are widely used on many other machines. Through generating vertical dispersion with chromatic skew quadrupoles, a measurable dependence of nonlinear optics on harmonic sextupoles can be observed from hybrid horizontal and vertical dispersive orbits. Proof of concept of our expanded technique was accomplished by simulations and beam measurements on the National Synchrotron Light Source II (NSLS-II) storage ring.

INTRODUCTION

Characterizing the nonlinear optics of storage rings is becoming more essential with the introduction of higher order multipole magnets in accelerator design. Errors from the higher order multipoles have been observed to degrade machine performance, such as reduction of dynamic aperture, energy acceptance, etc. Some efforts have been made to identify the nonlinear multipole errors by measuring local resonances [1] and distorted resonance driving terms [2], which requires a sophisticated Hamiltonian dynamics analysis. A more practical technique for measuring the nonlinear optics from off-energy closed orbits (NOECO) was reported and demonstrated on the MAX-IV ring [3]. Significant improvements on its dynamic aperture and beam lifetime were observed after correcting sextupole errors. Desired results were obtained while testing the NOECO technique on the ESRF-EBS ring as well [4]. However, the dependence of nonlinear optics on off-energy orbits is only measurable for chromatic sextupoles. This technique, however, doesn't apply to harmonic sextupoles, which do not see the first order linear dispersion. Harmonic sextupoles are used in almost every third-generation light source ring, and some fourth-generation diffraction-limited machines, such as the ALS-U ring [5]. They are even being used in the design of a future electron-ion collider ring [6]. As such, an expansion of the existing NOECO technique to correct for the harmonic sextupoles would be useful due to their common, integral use in current and future accelerator design. In the National Synchrotron Light Source II (NSLS-II) ring [7], the number of harmonic sextupoles is greater than the number of chromatic sextupoles (180:90). Therefore, correcting

harmonic sextupole errors is important for improving machine performance due to their greater influence. In this paper, we outline our expansion on the capabilities of existing sextupole correction techniques to accommodate for the harmonic sextupoles.

Some straightforward methods for calibrating harmonic sextupoles for correction would be (1) to temporarily convert them to chromatic ones; (2) to generate local orbit bumps through the sextupoles being calibrated. They are not practical when considering the limitations of routine operations of user facilities.

NONLINEAR OPTICS ON HYBRID DISPERSIVE ORBIT

When a sextupole sees vertical dispersion, its Hamiltonian reads as

$$H = \frac{p_x^2 + p_y^2}{2(1 + \delta)} + \frac{K_2}{3} [x^3 - 3x(y + \eta_y \delta)^2], \quad (1)$$

which includes a skew quadrupole component $2K_2\eta_y\delta \cdot xy$, with η_y the vertical dispersion, δ the beam momentum deviation, and sextupole strength $K_2 = \frac{1}{(B\rho)_0} \frac{\partial^2 B_y}{\partial x^2}$, normalized with the beam rigidity $(B\rho)_0$. Therefore, the nonlinear optics on off-energy orbits depend on the sextupole gradient, which can be utilized for their calibration and correction. A vertical dispersive wave can be generated through chromatic skew quadrupoles. In most light source rings, skew quadrupoles are widely equipped to control the residual vertical dispersion and linear coupling. Usually, a considerable amount of vertical dispersion can be generated, but only introduces weak coupling when the Betatron tune has sufficiently deviated from the linear difference/sum resonance. Thus, the nonlinear off-energy optics depends on not only chromatic sextupoles, but also on the original harmonic ones. In other words, horizontal harmonic sextupoles are converted into vertical chromatic ones, which makes their calibration and correction possible on hybrid dispersive orbits. In our studies, the NSLS-II ring double-bend achromat lattice was used to demonstrate these expanded capabilities.

At the NSLS-II ring, each odd-numbered cell is equipped with one 0.2 m long chromatic skew quadrupole (see Fig. 1). Their maximum gradients are $g_1 = 0.35 \text{ T} \cdot \text{m}^{-1}$, which is limited by the capacity of their power supplies. Assuming we can double their gradients to $g_1 = 0.70 \text{ T} \cdot \text{m}^{-1}$, a vertical dispersion wave with a ~ 0.1 m amplitude can be generated. The necessity for a double gradient is to increase the sensitivity of the nonlinear optics distortion to sextupoles. Although these gradients are twice as large as the maximum output of their power supplies, they are still quite weak compared to other operational quadrupoles with a maximum gradient of

* Work supported by US DOE Office of Science under Contract No. DE-SC0012704 operated by BNL

[†] yli@bnl.gov

MINIMIZING THE FLUCTUATION OF RESONANCE DRIVING TERMS FOR ANALYZING AND OPTIMIZING THE STORAGE RING DYNAMIC APERTURE

Zhenghe Bai*, Bingfeng Wei

National Synchrotron Radiation Laboratory, USTC, Hefei, China

Alexandre Loulergue, Laurent S. Nadolski, Ryutaro Nagaoka
Synchrotron SOLEIL, L'Orme des Merisiers, Saint-Aubin, France

Abstract

Minimization of resonance driving terms (RDTs) of nonlinear magnets such as sextupoles and octupoles is an essential condition for enlarging the dynamic aperture (DA) of a storage ring. We recently studied the correlation between minimizing the fluctuation or variation of RDTs along the ring and enlarging the DA. It was found that minimizing the RDT fluctuations is much more effective than minimizing the commonly-used one-turn RDTs in enlarging the DA, and that reducing low-order RDT fluctuations can also help reduce both higher-order RDT fluctuations and higher-order one-turn RDTs. In this paper, the DA analysis based on minimizing RDT fluctuations is further extended. By considering the RDT fluctuations including low- and high-frequency fluctuations, some nonlinear dynamics issues can be explained. The DA optimization is also studied based on numerically minimizing RDT fluctuations using genetic algorithms. Large DAs can be obtained, and the optimization is performed very fast.

INTRODUCTION

Enlarging the dynamic aperture (DA) of a storage ring is critical for improving beam injection efficiency and beam lifetime. At present, the numerical approach based on particle tracking and evolutionary algorithms has been intensively developed and successfully applied to the DA optimization of many storage ring light sources, which can in principle obtain the global best solution. But in this approach, it is hard to provide the physics for further nonlinear analysis and feedback on linear optics adjustment. Minimization of resonance driving terms (RDTs) [1] is a widely-used analytical approach, which has been used for nonlinear analysis and optimization for decades. In this traditional analytical approach, controlling RDTs and amplitude dependent tune shifts (ADTS) can give a larger DA, but it is only a necessary condition. Just recently, we found that minimizing the fluctuation or variation of RDTs along the ring is much more effective than minimizing the commonly-used one-turn RDTs in enlarging the DA [2], which can enhance the capability of this analytical approach.

In this paper, we will first briefly describe the correlation between minimizing RDT fluctuations and enlarging DA, and the physics behind this correlation. Then taking the SOLEIL II storage ring lattice as an example, this paper studies the DA analysis with low- and high-frequency RDT

fluctuations, and the DA optimization based on minimizing RDT fluctuations.

ANALYZING DA BASED ON MINIMIZING RDT FLUCTUATIONS

Correlation Between RDT Fluctuations and DA

For the hybrid multi-bend achromat (MBA) lattice and higher-order-achromat based MBA lattice, which have been adopted in many designs of 4th-generation synchrotron light sources, main nonlinear effects caused by sextupoles can be cancelled within a lattice cell. This kind of nonlinear cancellation is more effective than the nonlinear cancellation over some lattice cells, which was used in designing some 3rd-generation light sources. That is why the DAs of some 4th-generation light source designs can allow off-axis injection, even though their emittances are 1~2 orders of magnitude lower than those of 3rd-generation light sources. For the nonlinear cancellation within a lattice cell, the variation of RDTs along the longitudinal position is smaller than the case of the nonlinear cancellation over some lattice cells. This inspires us that reducing the variation or fluctuation of RDTs could be very beneficial for enlarging the DA.

Recently, we studied the correlation between minimizing RDT fluctuations and enlarging DA with different lattices [2]. In our study, the fluctuation of a RDT is quantitatively represented by the average RDT at the positions of sextupoles and octupoles. The results of DA analysis showed that minimizing RDT fluctuations is much more effective than minimizing one-turn RDTs. In other words, a nonlinear solution with smaller RDT fluctuations has a much higher probability of having a larger DA than a solution with smaller one-turn RDTs. In addition, by calculating RDT fluctuations, we can analyze which RDTs are likely to have a relatively large effect on the DA.

Physics Behind Minimizing RDT Fluctuations

We also studied the correlation between low-order RDTs and higher-order RDTs. It was found that reducing low-order RDT fluctuations can also help reduce both higher-order RDT fluctuations and higher-order one-turn RDTs [2]. By this logic, if higher-order RDT fluctuations are reduced, even higher-order RDTs can also be reduced. By using frequency map analysis, it was demonstrated that a 5th-order RDT of the SSRF lattice can be controlled if 3rd-order RDT fluctuations are reduced [2]. Besides, we also found that reducing 3rd-order RDT fluctuations can also help reduce

* baizhe@ustc.edu.cn

SINGLE LONGITUDINAL MODE GENERATION IN SLIPPAGE-DOMINATED TAPERED UNDULATOR SASE SOFT X-RAY FEL

D. C. Nguyen[†], C. Mayes, G. Stupakov, W. Lou, B. Dunham, xLight Inc., Palo Alto, CA, USA

Abstract

We study a short-pulsed SASE method called Slippage-dominated Tapered Undulator (STU) SASE to produce single longitudinal mode in each soft X-ray SASE pulse driven by an electron bunch with 10 fs bunch length and 16 pC bunch charge. STU-SASE uses both normal and inverse tapered undulators to select a single spike and increase its coherence length. Numerical simulations showing single-mode generation and narrow-lined spectra in a soft X-ray SASE FEL without seeding are presented.

SOFT X-RAY (BEUV) LITHOGRAPHY

A paradigm shift in light source utilization is required for the continuation of Moore's law scaling, the prediction that the number of transistors in an integrated circuit doubles every two years. To obtain smaller feature sizes, BEUV (beyond EUV) lithography at 6.x nm has been proposed [1]. SASE FELs can generate high-power soft X-rays, but they must produce spectrally narrow output to work with the narrow reflectivity curve of molybdenum-boron (MoB) multilayer mirrors [2]. While many ideas have been proposed to achieve fully coherent and narrow-band X-ray FELs [3, 4], only harmonic seeding [5] and self-seeding [6] have been experimentally demonstrated to narrow the output spectra of soft X-ray FELs. In this paper, we study a linac-based SASE FEL designed to produce substantial soft X-ray pulse energies and sufficiently narrow spectra to meet the need of BEUV lithography.

SINGLE-SPIKE SASE FEL

Slippage-dominated, Tapered Undulator SASE

It is well known that the coherence length in a SASE FEL is the slippage length over one gain length in the exponential regime. At saturation, the slippage length increases but the coherence length remains the same. In the tapered undulator where the FEL power continues to grow, the coherence length becomes longer by slippage in the tapered undulator length. Previous simulations using pC electron bunches with sub-fs electron bunch length have shown the possibility of generating a single spike (longitudinal mode) in each SASE pulse [7]. A more recent study suggests using an inverse taper to produce sub-fs X-ray pulses [8]. For many FELs, the electron bunch charge needs to be greater than a few pC and the FEL pulse energy at least 10 μ J. In this paper, we study a new method to generate single-spike SASE X-ray pulses based on slippage-induced lengthening of the coherence length, and single-mode selection via amplification and absorption in the tapered undulators of a SASE FEL without seeding.

The single mode selection is illustrated in the 2D plot of a single SASE spike in log-scale color codes (see Fig. 1). Slippage, as measured by the tilt of the radiation spike, is $\lambda/3\lambda_u$ before the taper start and increases to the full value of λ/λ_u in the taper. A second spike appears right before the taper start but is not amplified in the tapered sections.

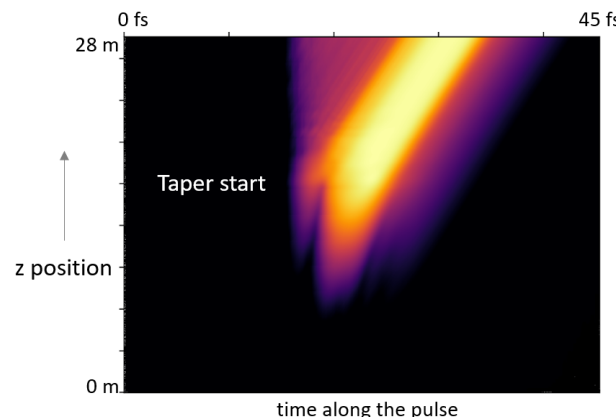


Figure 1: Evolution of a single spike along z and time.

We use the FEL code Genesis 1.3 version 4 [9] to model the STU-SASE FEL process. The electron beam, undulator and FEL parameters are listed in Table 1 below.

Table 1: STU-SASE FEL Parameters

Parameter	Value
Beam energy	1.333 GeV
Peak current	1.5 kA
Gaussian bunch FWHM	10 fs
Bunch charge	16 pC
Norm. emittance in x and y	1 μ m, 0.5 μ m
Undulator period	2.6 cm
Untapered undulator length	17 m
Untapered undulator K_0	2.22
Tapered undulator length	13 m
ΔK per taper section	0.02
Photon energy	186 eV
FEL ρ parameter	0.002
Average FEL pulse energy	40 μ J

Single-mode Generation in STU-SASE

Both normal and inverse tapered undulator are used in the single longitudinal mode generation. Figure 2 shows the energy phase space at the exit of the untapered undulators and the resonant energies of the untapered (black) and tapered (green=normal; red=inverse) undulator sections.

[†] dinh@xlight.com

COMPACT HOM-DAMPED RF CAVITY FOR A NEXT GENERATION LIGHT SOURCE*

H. Ego^{†,1}, KEK, Oho, Tsukuba, Ibaraki, Japan

T. Inagaki, H. Tanaka, RIKEN SPring-8 Center, Sayo, Hyogo, Japan

T. Asaka, N. Nishimori, QST, Sendai, Miyagi, Japan

T. Ohshima¹, T. Tomai, H. Yamaguchi¹, JASRI, Sayo, Hyogo, Japan

¹also at QST, Japan

Abstract

A beam-accelerating RF cavity with a new HOM-damping structure was designed in order to suppress coupled-bunch instabilities in a next generation light source with an ultra-low emittance and supplying X-rays approaching their diffraction limits. The TM₀₂₀ mode at 508.58 MHz is selected as a beam-accelerating mode because it has a high Q -value of 60,000 and a shunt impedance sufficient for beam acceleration and brings a compact HOM-damping structure to the cavity differently from massive types of cavities with waveguides or pipes extracting HOM power. Two shallow slots are cut on the cavity inner wall and materials absorbing RF waves are directly fitted into them. They work as HOM dampers without affecting the RF properties of the beam-accelerating mode. A prototype cavity of OFHC copper was fabricated to demonstrate the HOM-damping and generating an accelerating voltage of 900 kV in the cavity. Since the cavity was successful in operation up to 135 kW, the feasibility of both the high-power operation and the damping structure was proved. Four actual cavities were produced and installed to the new 3-GeV synchrotron radiation facility, NanoTerasu in Japan.

INTRODUCTION

Coupled-bunch instability (CBI) arising from high coupling impedances of higher-order modes (HOMs) in beam-accelerating RF cavities is one of the serious problems in the next generation storage ring. Therefore, RF cavities against the CBIs are indispensable for stable beam operation of the ring. We developed a new and compact type of HOM-damped cavity shown in Fig. 1 [1-3]. The beam-accelerating resonant mode of the cavity is the TM₀₂₀ mode. This mode enables HOM-absorbing materials to be directly embedded into the cavity body without using special waveguides or pipes usually occupying large spaces. Our HOM-damping structure makes the cavity body extremely compact and reduces the spaces occupied with the cavities in the storage ring packed in with accelerator components.

In the next section, we show the cavity structure, its RF characteristics and the HOM-damping mechanism. The last section represents the measurements on RF characteristics of the fabricated prototype cavity and the results of its high-power tests up to 135 kW.



Figure 1: RF cavity with the compact HOM-damping structure.

HOM-DAMPING MECHANISM

Cavity Structure

Figure 2 shows the schematic cross-sectional view of the cavity with the HOM-damping structure. The cavity has an inner diameter of 1040.4 mm and a beam-gap length of 206 mm. The cavity is a reentrant type with nose cones around the beam gap on the cavity inner wall. The cavity length between the beam-pipe flanges is 452 mm and we can accommodate plural cavities in short straight sections in a storage ring.

Two slots are opened in the cavity inner wall along the nodes of the axially symmetric magnetic fields of the TM₀₂₀ mode. 16 HOM dampers with 12 ferrite bars shown in Fig. 3 are directly bolted to the cavity body and the ferrite bars are exposed in the slots.

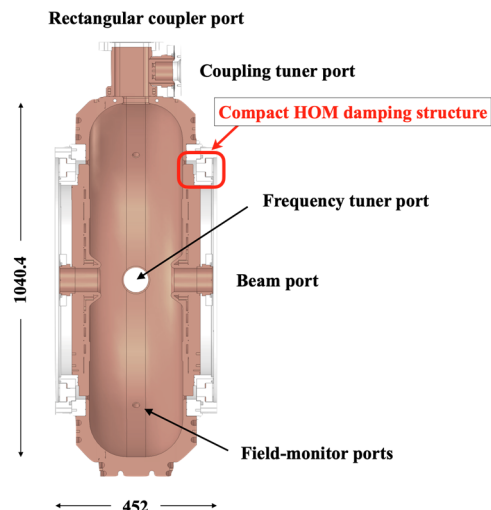


Figure 2: Cross-sectional view of the cavity.

* Work supported by the RIKEN SPring-8 upgrade program

[†] ego@post.kek.jp

Pyapas: A NEW FRAMEWORK FOR HLA DEVELOPMENT AT HEPS

Xiaohan Lu, Hongfei Ji, Yi Jiao, Jingyi Li, Nan Li, Cai Meng, Yuemei Peng,
 Haisheng Xu, Daheng Ji, YuanYuan Wei, Jinyu Wan, Gang Xu, Yaliang Zhao
 Institute of High Energy Physics, Chinese Academy of Sciences, Beijing, China

Abstract

The High Energy Photon Source (HEPS) is a 6 GeV, 1.3 km, 4th generation storage ring light source being built in Beijing, China. Compared to third-generation light sources, HEPS, as a fourth-generation light source, has a one to two orders of magnitude reduction in emittance. The number of magnets correspondingly increases by an order of magnitude, and there are higher demands for control precision. All of these pose new challenges for the development of HLA. The development of high-level applications (HLAs) for HEPS started in early 2021. A brand new framework named PYthon-based Accelerator Physics Application Set (*Pyapas*) was developed for HLA development. This paper will introduce the design of *Pyapas* and its application at HEPS.

INTRODUCTION

The High Energy Photon Source (HEPS) is a 6 GeV, 1.3 km, fourth-generation light source [1]. The construction started in Beijing, China, in the middle of 2019, and upon completion, it is expected one of world's brightest light source. The beam commissioning of Linac began in March 9 of this year, and the process acceptance of Linac completed three months later. Upon completion of a brief interlude for adjustments, the beam commissioning of booster started. The energy of booster successfully ramped to 6 GeV two weeks later [2]. As a fourth-generation light source, HEPS adopts a compact multi-bend achromat lattice design for the storage ring and uses a large number of combined magnets [3, 4]. The cross-talk effect between magnetic fields is significant, and the number of magnets has increased by an order of magnitude compared to the third-generation light sources, which introduce new challenges and requirements for tuning beam parameters.

Existing HLA development frameworks are mostly monolithic and not easily scalable [5, 6], which cannot meet the needs of HEPS' complex parameter tuning. And porting the existing framework is almost as much work as building it from scratch. In order to meet the requirements of HEPS, we decided to design a new HLA framework based on Python named *Pyapas* [7]. It adopts modular design philosophy to increase overall scalability. A dual-layer physical model module has been designed to meet the replaceability of online calculation models. In addition, the communication module, database module, and server module have all been specially designed to meet the needs of adjusting a large amount of parameters.

Based on *Pyapas*, we have completed the development of HLAs for the Linac [8] and successfully applied them to

beam commissioning [9], verifying the practicality and reliability of *Pyapas*. The development of HLAs for the booster and transfer lines [10, 11] has also been completed, and the development for the storage ring is nearing completion. This paper will briefly introduce the design of *Pyapas* and the progress of the development of HLAs for HEPS.

FRAMEWORK DESIGN

For a framework to develop HLA, the basic abilities include hardware communication, user interface development, database connection et.al. But for the high level physical application (HLPA), physical model and physical algorithm are more crucial part. Therefore the core of *Pyapas* is a dual-layer physical module. As shown in Fig. 1, there are two independent layers: device mapping layer and physical model layer. The device mapping layer corresponds to the real machine and is responsible for communicating with the machine, while the physical model [12] layer is responsible for online calculation based on the information read from the device mapping layer. The device mapping layer and the physical model layer are deeply decoupled and connected by connector, which only need to specify information such as the calculation model class name, unit conversion, and parameter name that needs to be called in the connector. This makes it very convenient to switch between different calculation models to meet the online calculation needs in different scenarios.

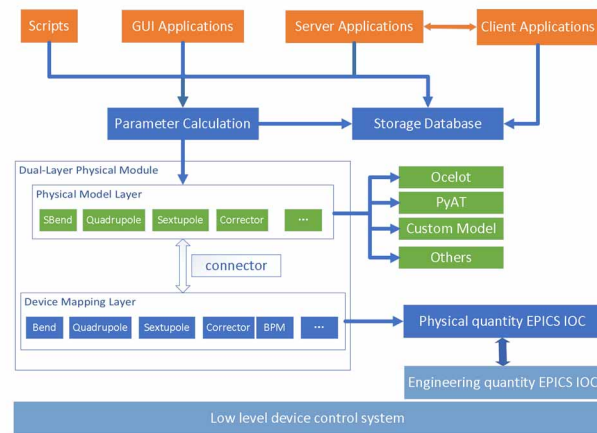


Figure 1: Pyapas framework.

In addition, to improve the scalability of the framework and reduce the development difficulty of developers, we adopt a modular design. Specifically, we analyze the functions involved in HLAs, and divide them into different modules for separate development. The modules are loosely coupled and specific application development is carried out through simple interface calls, which increases

* Work supported by NSFC12005239

† luxh@ihep.ac.cn

DESIGN OF THE TEST PLATFORM FOR HIGH AVERAGE CURRENT VHF ELECTRON GUN

Zipeng Liu^{1,2}, Houjun Qian^{1,2}, Guan Shu^{1,2}, Xudong Li^{1,2}, Zenggong Jiang^{1,2}, Haixiao Deng^{1,2,*}

¹Shanghai Synchrotron Radiation Facility, Shanghai, China

²Shanghai Advanced Research Institute, Shanghai, China

Abstract

Recently a high-average-current CW VHF electron gun is under construction at Shanghai Advanced Research Institute, which is aimed to develop the high average current and high beam quality technologies. The high average current electron source is the key component of a kW-power-order free electron laser facility. The average current and the frequency of this electron gun is 1-10 mA and 216.7 MHz, respectively. The energy of electron is over 500 keV, and repetition rate is about 1-9 MHz. To validate the performance of this instrument, a test platform has been designed. The R&D of its vacuum and diagnostics design are presented in this work.

INTRODUCTION

In recent years, several projects involving free electron lasers (FEL) and energy recovery linacs (ERL) facilities have been proposed and commissioned. These facilities require high repetition rates, low emittance, and high power. Some facilities, such as LCLS-II, SHINE, and APEX, have employed normal-conducting (NC) RF electron guns [1–4]. The electron gun (VHF) test platform in this work is under construction based on a NC continuous-wave (CW) RF photogun at the Shanghai Advanced Research Institute (SARI). The core of our photogun is a NC copper RF cavity operating at the VHF band, specifically at 216.7 MHz. This cavity generates a 22.5 MV/m accelerating field when supplied with nearly 90 kW of power. The accelerating gap measures 4 cm. To operate high quantum efficiency semiconductor photocathodes (Cs₂Te), an expected vacuum level of $10^{-10} - 10^{-9}$ mbar is necessary. Beam quality, including energy, normalized emittance, beam size, beam current, and the thermal emittance of the photocathode, significantly influences the electron source. The layout of the test platform is outlined in this paper, focusing mainly on diagnostics and vacuum design. The theoretical vacuum levels for the electron gun and test line are 3×10^{-8} mbar and 1×10^{-7} mbar, respectively. The main tube diameter is 50 mm, and the entrance diameter of the dump is 80 mm.

MANUSCRIPTS

The design objectives are presented in Table 1, and the layout of the test platform is illustrated in Fig. 1. The height of the beamline is 1.3 m. The beamline comprises a load lock, electron gun, solenoids, dipole, profile monitors, ICT (Integrated Current Transformer), and BPMs (Beam Position

Monitors). The positions of the main elements are indicated in Table 2.

Table 1: Design Objectives

Parameter	Value	Unit
Energy	>500	keV
Average current	>1	mA
Frequency	216.7	MHz
Repetition rate	1-9	MHz
Charge	200	pC

Table 2: Test Platform Layout

Element	Position	Unit
Electron gun	0	m
Solenoid 1,2	0.27,1.8	m
Laser injector	0.92	m
Profile 1,2,3	1.5,0.4(to the line),2.2	m
Dump	0.65(to the line)	m

Diagnostics Design

The essential characteristics of the electron gun's photocathode are crucial for the electron source. Therefore, this work includes simulations to measure beam energy, dark current, normalized emittance, and transverse momentum.

Dark current imaging Dark current is a primary focus of the electron source, particularly because superconducting linacs such as LCLS-II and SHINE require low dark currents for optimal acceleration quality and extended lifespan. Dark current imaging plays a role in enhancing the photo-cathode manufacturing process. As depicted in Equation 1, dark current emitted from the same position with varying transverse momentum should reach the same position on the profile by matching the strength of the solenoid ($M_{12} = 0$). The relationship between imaging magnification and the distance between the photo-cathode and the profile is demonstrated in Fig. 2b, where the primary emission of dark current is from the 5 mm center of the photo-cathode. As depicted in Fig. 2a, the dark current is imaged, resulting in a loss of transmission of the profile.

$$\begin{bmatrix} M_{11} & M_{12} \\ M_{21} & M_{22} \end{bmatrix} \begin{bmatrix} r_0 \\ r'_0 \end{bmatrix} = \begin{bmatrix} r \\ r' \end{bmatrix} \quad (1)$$

* denghx@sari.ac.cn

THE EXPERIMENTAL PROGRESS FOR THE STRONG FIELD TERAHERTZ RADIATION AT SXFEL

Kaiqing Zhang¹, Yin Kang^{2,3}, Cheng Yu¹, Chunlei Li¹, Bin Li¹, Chao Feng^{1,†}

¹Shanghai Advanced Research Institute, Shanghai, China

²University of Chinese Academy of Sciences, Beijing, China

³Shanghai Institute of Applied Physics, Shanghai, China

Abstract

Strong field Terahertz (THz) light source has been increasingly important for many scientific frontiers, while it is still a challenge to obtain THz radiation with high pulse energy at wide-tunable frequency. In this paper, we introduce an accelerator-based strong filed THz light source to obtain coherent THz radiation with high pulse energy and tunable frequency and X-ray pulse at the same time, which adopts a frequency beating laser pulse modulated electron beam. Here, we present the experimental progress for the strong filed THz radiation at shanghai soft X-ray free-electron laser (SXFEL) facility and show its simulated radiation performance.

INTRODUCTION

Terahertz (THz) radiation, with a frequency from 0.1 THz to several tens of THz, has been increasingly significant for many scientific frontiers, such as THz - triggered chemistry, single shot THz bioimaging and nonlinear physical [1]. The development of strong field THz radiation with a pulse energy on the order of millijoule (mJ) has provided new possibilities for studying various of new scientific phenomenon, such as strong field-novel material interactions, the high-harmonic generation of THz waves, nonlinear THz spectroscopy [2]. In recent years, the so-called THz pump and X-ray probe technique, which exciting the matter with a THz radiation and capturing the dynamic image by X-ray pulse, has been an important technique to measure the basic properties of matters such as magnetization, conductivity and even crystal lattice, or study the dynamic process of matter [3].

One main barrier for the application of strong field THz is lack of THz source with high pulse energy and tunable frequency. Currently, the strong THz radiation is mainly produced by the ultrafast laser [4], laser produced plasma [5] and electron accelerator-based techniques [6]. For the ultrafast laser and laser produced plasma techniques, it cannot generate synchronized high-power X-ray and strong field THz radiation at the same time. The electron accelerator-based technique has been treated as one reliable method to obtain strong field THz radiation, and many electron-accelerator-based THz light source also has been proposed. The electron accelerator can produce THz radiation by several methods: coherent synchrotron radiation (CSR) [7], coherent transition radiation (CTR) [8] and

undulator radiation [9]. In recent years, FEL facilities around the world, including LCLS-II, FLASH, European XFEL and Swiss-FEL have produced high power X-ray and strong-field THz radiation at the same time by adopting an afterburner and compressing the duration of electron beam into one THz period [10]. However, generating THz radiation with a frequency above 10 THz needs to suppress the electron beam duration below 100 fs, which can be a challenge for the most existing FEL facilities.

In this paper, we introduce an electron accelerator-based strong field THz radiation technique, which can produce THz radiation with high pulse energy and tunable frequency from 0.1 THz to 40 THz by using a frequency beating laser modulated electron beam. Here, we present the experimental progress, including the frequency beating laser pulse, THz undulator, THz diagnostic line, for the strong THz radiation at shanghai soft X-ray free-electron laser (FEL) (SXFEL) facility. To show the possible performance, simulation results with the basic parameters of SXFEL are also given.

WORKING PRINCIPLE

Figure 1 shows the layout of the introduced THz radiation technique [11, 12]. The working principle can be expressed as following: The electron is firstly produced from a photocathode gun with a beam energy of several keV, and then the beam is accelerated to a beam energy above 1 GeV by the LINAC, and the pulse duration of electron beam is also be suppressed by the LINAC. After that, the relativistic electron beam is sent into a modulation section together with a frequency beating laser pulse. Figure 2 shows the layout of the frequency beating laser. An ultrafast laser pulse with an initial pulse length of σ is stretched by a grating pair to generate large frequency chirps, and the laser pulse undergoes a frequency-dependent modulation phase modulation, the phase can be expressed as [13]:

$$\phi(\omega) = \phi(\omega_0) + \tau_0(\omega - \omega_0) + \frac{(\omega - \omega_0)^2}{2\mu} + \dots,$$

where τ_0 is the group delay at ω_0 , μ is the carrier frequency sweep rate (linear chirp rate), $\mu = \frac{d\omega}{dt}$. At the same time, the pulse length of laser pulse is also stretched from σ to σ_n , where σ_n can be calculated by $\sigma_n = \sigma\sqrt{(1 + 4/\mu^2\sigma^4)}$. And then, a beam splitter is introduced to separate the stretched laser pulse into two pulses, one of them passes through an optical delay line, which will introduce a time delay τ . The laser pulses are recombined, which can form a quasi-sinusoidal chip modulation of the

* Work supported by the National Natural Science Foundation of China, grant number 12105347, 12275340

† email address: fengc@sari.ac.cn

DESIGN OF THE BEAM DISTRIBUTION SYSTEM OF SHINE*

S. Chen[†], X. X. Fu, H. X. Deng, B. Liu, Shanghai Advanced Research Institute, Shanghai, China
 B. Y. Yan, University of Chinese Academy of Sciences, Beijing, China

Abstract

For feeding the three parallel undulator lines by the CW beam of a single SRF linac simultaneously, a beam switchyard between the linac and undulator lines is designed with the consideration of bunch-by-bunch beam separation and beam quality per. In this work, the schematic design of the beam switchyard for bunch-by-bunch beam separation of CW beam is described, and the current lattice design of the linac-to-undulator deflection branches and the start-to-end tracking simulation results are presented.

INTRODUCTION

As a high repetition rate XFEL and extreme light facility, the SHINE project is now under construction near the SSRF and ShanghaiTech campus [1,2]. High quality electron beam is generated by a VHF gun in CW mode with a repetition rate up to about 1 MHz [3]. A superconducting RF linac with two bunch compressors then accelerates the electron beam to about 8 GeV. The electron beam is used to feed the FEL undulator complex with three parallel undulator lines, referred to as FEL-I (3-15 keV), FEL-II (0.4-3 keV) and FEL-III (10-25 keV) respectively. In addition, spaces are reserved for future upgrade of more undulator lines.

For the simultaneous operation of multiple undulator lines with different parameters and operation modes in SHINE, a beam switchyard is located in between the SRF linac and the undulator lines complex. In the beam switchyard, the 1 MHz CW electron beam should be separated bunch-by-bunch in an arbitrarily programmable pattern and then delivered to each undulator line through the corresponding linac-to-undulator (LTU) branch respectively. In this work, we present the physics design of the beam switchyard for SHINE.

MAIN LAYOUT

A schematic view of the SHINE is seen in Fig. 1. Most of the beam equipment will be installed in the tunnels and shafts about 30 m underground. Electron beam starts from the injector in #1 shaft and is accelerated by the SRF linac in a 1.4 km long tunnel. The three undulator lines are installed in two of the undulator tunnels: FEL-I and FEL-II in the middle undulator tunnel and FEL-III in the west undulator tunnel. All the three undulator lines are parallel to the linac line, in the same vertical plain but not collinear. The horizontal distance between the three undulator line and the linac is about +1.85 m for FEL-II, -1.45 m for FEL-I and -8.95 m for FEL-III, where '+'('−') denotes left(right) to the linac beam direction. The linac tunnel and the undulator tunnels

are connected by the #2 shaft. Some key beam parameters of SHINE are listed in Table 1.

Table 1: SHINE Main Beam Parameters

Parameter	Value	Unit
Beam Energy (E_0)	8.0	GeV
Slice Energy Spread (σ_E/E_0)	~0.01	%
RMS Norm. Emittance (ϵ_n)	≤0.45	μm · rad
Bunch Frequency (f_{rep})	1000	kHz
Bunch Charge (Q)	10~300	pC
Bunch Length (l_b)	~100	fs
Peak Current (I_{pk})	≥1500	A

The beam switchyard section starts from the end part of the linac tunnel, passes through the #2 shaft and ends at the entrance of the undulator lines. Electron bunches from the linac should be separated and delivered either to the three undulator lines or to a 800-kW beam dump in the middle of #2 shaft. Starts from the end of the SRF linac, a linac-to-dump (LTD) line brings the undeflected bunches to the main dump. Three LTU deflection branches extract bunches from the LTD line in the sequence of LTU-2, LTU-3, and LTU-1. This arrangement avoids the conflict of the three LTU branches and reserves spaces for future extension of more LTU branches for more undulator lines.

KICKER-SEPTUM MODULE

An electron bunch that is wanted by an undulator line should be firstly extracted from the 1 MHz CW electron bunch train without affecting the bunches to other directions. Typically it is realized by pulsed kicker magnets. For maximizing the available beam modes that can be provided to the user experiments and their flexibility of switching, the kicker magnets should be able to perform a stable bunch-by-bunch kick to the electron beam and, what's more, should be programmable for arbitrary distribution pattern. Considering the beam parameter and the limited geometry, a single kicker magnet could not meet the requirements independently. Therefore, the actual scheme is based on a set of small angle vertical kicker magnets combined with a DC Lamberson septum magnet, which can be a compact scheme with high enough frequency and stability.

The configuration of the kicker-septum module is seen in Fig. 2. The fast kicker set and the DC Lamberson septum magnet are inserted in a FODO cell with about 24 m period. The fast kicker set consists of 8(+2) special designed lumped-inductance kicker magnets with a total deflection angle of about 0.8 mrad [4]. The pole of the kicker magnet is out of vacuum so that ceramic vacuum chamber should be used. To reduce the wakefields, the ceramic vacuum chamber should

* Work supported by the Natural Science Foundation of Shanghai (22ZR1470200).

[†] chens@sari.ac.cn

DESIGN AND COMMISSIONING OF THE BEAM SWITCHYARD FOR THE SXFEL-UF*

Si Chen[†], Kaiqing Zhang, Zheng Qi, Tao Liu, Chao Feng, Haixiao Deng, Bo Liu, Zhentang Zhao
Shanghai Advanced Research Institute, CAS, Shanghai, China

Abstract

A beam switchyard is designed for the Shanghai soft X-ray FEL user facility to enable parallel operation of its two FEL lines. It is designed to keep the beam properties like low emittance, high peak charge and small bunch length from being spoiled by various beam collective effects such as the dispersion, coherent synchrotron radiation and micro-bunching instability. In this work, the detailed physics design of the beam distribution system is described and the recent commissioning result is reported.

INTRODUCTION

The Shanghai soft X-ray FEL (SXFEL) user facility aims to open the way of various application fields of XFEL in China [1, 2]. It is designed to cover the whole water window range, i.e., X-ray in wavelength range of 2.3 nm ~ 4.4 nm. To accomplish this, the beam energy is accelerated to about 1.5 GeV by a normal conducting linac with a series of S-band and C-band RF structures. The bunch repetition rate is about 50 Hz. Two parallel undulator lines are installed in the undulator hall. Directly downstream of the linac it is a SASE-FEL line with radiation wavelength about 2 nm, which is named as the SBP line. A fully-coherent seeded-FEL line, which is renamed as the SUD line, is about 3 m right side of the SBP line with the radiation wavelength about 3 nm. The schematic layout of the SXFEL-UF is shown in Fig. 1. Some main beam parameters of SXFEL-UF are shown in Table 1.

Table 1: Main Parameters of SXFEL user facility Linac

Parameter	Value	Unit
E	1.5~1.6	GeV
σ_E/E (rms)	$\leq 0.1\%$	
ε_n (rms)	≤ 1.5	mm-mrad
l_b (FWHM)	≤ 0.7	ps
Q	500	pC
I_{pk}	≥ 700	A
f_{rep}	50	Hz

For the simultaneous operation of the two FEL lines, a beam switchyard is located between the linac and the undulator section. The electron bunch train from the linac is separated and directed in two subsequent directions: either to the SBP line or to the SUD line. Due to the high

requirements of the externally seeded FEL, the beam switchyard should ensure a stable and precise transportation of the electron beam, while maintaining desirable beam quality properties such as low emittance, high peak charge, and short bunch length. In the following sections, the physics design and commissioning results of such a beam switchyard are described in detail.

BEAM SWITCHYARD DESIGN

General Layout

Since the two FEL lines lie parallel in the undulator hall, the deflection line uses a dog-leg structure to bring the kicked beam to the entrance of the seeding-FEL line. Due to the limitation of the longitudinal distance, the total deflection angle of the dog-leg is about 6° . The two reverse angle bending magnets of the dog-leg are replaced by two identical but symmetrical double-bend-achromatic (DBA) structures for reducing the deflection angle of a single bending magnet. An in-vacuum lumped-inductance kicker magnet acts as the first 3° bending magnet of the entrance DBA, with the capability of performing bunch-by-bunch beam separation and programmable for arbitrary separation pattern. To guarantee the beam trajectory stability in the SUD line, the field repetitive jitter of the kicker magnet should be less than 100 ppm.

Optics Design for CSR & MBI Suppression

Emittance growth due to coherent synchrotron radiation is a crucial beam dynamic issue of a dog-leg beam switchyard. It is necessary and possible to suppress the CSR induced emittance growth by well designed beam optics in an achromatic deflection structure. A straightforward method for mitigating emittance growth involves adjusting the beam size at the bending magnet, thereby reducing the strength of the CSR kick. Another method involves achieving mirror symmetry in the lattice of the switchyard dog-leg and adjusting the betatron phase advance between the two DBA cells to be an odd multiple of π , which is referred to as the "optics balance" method [3]. With this method, the CSR induced longitudinal dispersion and transverse kick can be well canceled at the exit of the switchyard dog-leg. The betatron functions and dispersion functions of such an optics design for SXFEL-UF are shown in Fig. 2.

Special attention should also be paid to the micro-bunching instability in the beam switchyard with multi-bend deflection line, especially for the seeded-FEL scheme which requires a smoother longitudinal phase space for more effective density modulation. For this purpose, a small bending magnet (micro-bend) is inserted in the middle of the DBA

* This work was supported by the Natural Science Foundation of Shanghai (22ZR1470200).

[†] chens@sari.ac.cn

SYMMETRIC COMPTON SCATTERING: A WAY TOWARDS PLASMA HEATING AND TUNABLE MONO-CHROMATIC GAMMA-RAYS

L. Serafini*, A. Bacci, C. Curatolo, I. Drebot, M. Rossetti Conti, S. Samsam
 INFN-MI, INFN-LASA, Milan, Italy
 V. Petrillo¹, A. Puppini¹, UNIMI, Milan, Italy
¹also at INFN-MI, Milan, Italy

Abstract

We analyze the transition between Compton Scattering and Inverse Compton Scattering (ICS), characterized by an equal exchange of energy and momentum between the colliding particles (electrons and photons). In this Symmetric Compton Scattering (SCS) regime, the energy-angle correlation of scattered photons is cancelled, and, when the electron recoil is large, monochromaticity is transferred from one colliding beam to the other. Large-recoil SCS or quasi-SCS can be used to design compact intrinsic monochromatic γ -ray sources based on compact linacs, thus avoiding the use of GeV-class electron beams and powerful laser/optical systems as required for ICS sources. At very low recoil and energy collisions (about 10 keV energy range), SCS can be exploited to heat the colliding electron beam, which is scattered with large transverse momenta over the entire solid angle, offering a technique to trap electrons into magnetic bottles for plasma heating.

INTRODUCTION

The Inverse Compton Scattering (ICS) effect regards the interaction between highly relativistic electrons and laser beams, within an inverse kinematics set-up where the electron loses energy and momentum in favor of the incident photon, that is back-scattered and up-shifted to much larger energies. Compton sources are devices developed and operating in many laboratories [1] with plenty of applications. In this paper, we analyze the transition between direct Compton (DC) effect, occurring when the electron is at rest, and ICS. In this case, the colliding particles exchange an equal amount of energy and momentum, and we call this regime Symmetric Compton Scattering (SCS). Unlike in all other radiations emitted with a Lorentz boost, SCS scattered photon energy indeed no longer depends on the scattering angle, so that the back-scattered radiation beam becomes intrinsically monochromatic. SCS is characterized by the transfer of monochromaticity from one colliding beam to the other, so that when a large bandwidth photon beam collides under SCS conditions with a monoenergetic electron beam, the back-scattered photon beam results to be monochromatized. The possible applications ranges in many fields. SCS or quasi-SCS at large recoil could allow to design compact sources of intrinsic monochromatic γ -rays alimented by low energy MeV electron bunches, thus avoiding the use of GeV-class accelerators and powerful laser/optical systems, actu-

ally needed by ICS sources [2]. On the other hand, the SCS effect at low recoil can provide an electron heater based on X-rays.

SYMMETRIC COMPTON SCATTERING

In the Compton scattering, the photon energy ($E'_{\text{ph}} = \hbar\omega'$, with ω' being the photon angular frequency and \hbar the reduced Planck constant) scattered at an angle θ is given by:

$$E'_{\text{ph}}(\theta) = \frac{(1 + \beta)\gamma^2}{\gamma^2(1 - \beta \cos \theta) + \frac{X}{4}(1 + \cos \theta)} E_{\text{ph}}, \quad (1)$$

where the incident photon energy is $E_{\text{ph}} = \hbar\omega$, $\beta = v_e/c$ is the dimensionless electron velocity (c being the speed of light), $\gamma = 1/\sqrt{1 - \beta^2}$ is electron Lorentz factor and X is the electron recoil factor,

$$X = \frac{4E_e E_{\text{ph}}}{(m_0 c^2)^2} = \frac{4\gamma E_{\text{ph}}}{m_0 c^2} = 4\gamma^2 \frac{E_{\text{ph}}}{E_e}, \quad (2)$$

with m_0 the electron rest mass and $E_e = \gamma m_0 c^2$.

We call Symmetric Compton Scattering (SCS) the regime of transition between DC and ICS [3], where the energy/momentum transfer between photons and electrons is balanced. The maximum photon energy closely approaches the electron energy. Referring to Eq. (1), the dependence on θ of E'_{ph} cancels when: $\frac{X}{4} = \beta\gamma^2$, a condition valid when the photon and electron energies satisfy the relation $E_{\text{ph}} = \beta E_e$, corresponding to equal electron and photon momenta with opposite directions $\vec{p}_e = -\vec{p}_{\text{ph}}$. Moreover, we can introduce an asymmetry factor $A = \beta\gamma^2 - \frac{X}{4}$, that vanishes ($A = 0$) in SCS regime, assumes large positive values ($A \rightarrow \gamma^2$) in ICS regime (that is indeed characterized by $X \ll 4\beta\gamma^2$) and negative values in DC when $\beta = 0$.

The energy of the scattered photons is $E'_{\text{ph}} = E_{\text{ph}}$, uniformly in θ .

The asymmetry factor A is negative in DC regime, where $\beta = 0$ and $\gamma = 1$, and $A = -\lambda_C/\lambda$. In ICS regime the asymmetry factor A is positive and scales like γ^2 .

Figure 1 shows the dependence of E'_0 vs. T_e and of the recoil factor X in different regimes (DC, SCS, ICS).

Another unique characteristic of Symmetric Compton Scattering, that does not occur in any other electron-photon collision, is that: $E_{\text{ph}} = \beta E_e$, $E'_{\text{ph}} = E_{\text{ph}}$ and $E'_e = E_e$, i.e., the energies of electron and photon do not change before and after SCS. This is represented by the $A = 0$ line plotted in Fig. 1.

* luca.serafini@mi.infn.it

INJECTION INTO XFELs, A REVIEW OF TRENDS AND CHALLENGES

C. Davut^{*,1,3}, O. Apsimon^{1,3}, S. S. Percival^{2,3}, and B. L. Milityn^{2,3}

¹The University of Manchester, Manchester, UK

²STFC UKRI, Daresbury, UK

³Cockcroft Institute of Accelerator Science and Technology, Daresbury, UK

Abstract

In this contribution, we review the low-energy electron injectors for the existing X-ray Free-Electron Laser (XFEL) facilities, focusing on the buncher and booster sections. The technology choices are parallel to the increasing demand for stricter six-dimensional phase space quality. The current capabilities for beam parameters and future requirements are laid out, alongside a discussion on challenges and technological bottlenecks. In light of this review, preliminary results for a high-capability injector providing a high repetition rate and continuous wave emission are presented as an option for the UK XFEL.

INTRODUCTION

XFEL facilities are an unprecedented tool for probing matter at the atomic and molecular scales. The concept of the Free-Electron Laser (FEL) was introduced in the early 1970s [1], and since then developments in FEL technology led to the construction of XFEL facilities. The first lasing in the vacuum ultra-violet range was achieved in 2005 at the Deutsches Elektronen-Synchrotron (DESY) [2]. The FLASH user facility commenced operation in the same year and extended its capabilities into the soft X-ray range. A milestone was reached in 2009 when the Linac Coherent Light Source (LCLS) at the SLAC National Accelerator Laboratory achieved X-ray lasing, starting a new era of X-ray science [3]. Since then, ongoing efforts have focused on advancing XFEL capabilities with the exploration of different concepts such as multi-colour, two-pulse X-rays, variable polarisation states, high spectral purity X-rays, higher brightness X-rays, sub-femtosecond and attosecond X-ray pulses by manipulating the electron bunch before self-amplified spontaneous emission (SASE) takes place [4]. However, increasing demand in beam quality through expanding the scope of XFEL applications leads to upgrades of existing facilities [5, 6] and motivates the construction of new ones.

One such machine, the UK XFEL, is currently undergoing the Conceptual Design and Options Analysis phase based on the published science case [7]. An exhaustive science case for UK XFEL demonstrated a community preference for high repetition rate, photon energy, energy per pulse, and some additional features such as high repetition rate laser seeding, high spectral purity X-rays, attosecond pulses across all photon energies, combining X-rays with other advanced capabilities for EUV/gammas to have a unique X-ray light source [8].

UK XFEL aims to operate across a large portion of the repetition rate-photon energy parameter space as shown in Fig. 1. In light of the science case requirements, UK XFEL has been proposed to operate at a 1 MHz repetition rate that will be likely driven by an 8 GeV beam generated using superconducting technologies. A more detailed discussion on the technologies proposed to be used based on the preliminary focus of the UK XFEL can be found in [7].

High brightness plays a central role in determining the ability of a light source to access new domains of ultra-fast X-ray science [9]. Therefore, the main design objective for the UK XFEL injector is to explore the minimum possible transverse slice emittance at the end of the injector.

The preliminary design of the UK XFEL proposes the use of a normal conducting very high frequency (VHF) gun operating either at the 6th or 7th subharmonic of the main linac RF frequency. The VHF gun will be followed by a single or 2-cell buncher operating at either harmonic or subharmonic of the main linac RF frequency to compress bunches to short lengths. Following that, a booster section will bring the beam to the emittance-dominated regime, where the energy of the beam reaches ~ 220 MeV after acceleration. A magnetic chicane will then perform the final bunch compression before the main linac. The design goal of the UK XFEL injector is preserving the transverse core slice emittance while compressing the bunch as much as possible and delivering it to the main linac at a high repetition rate.

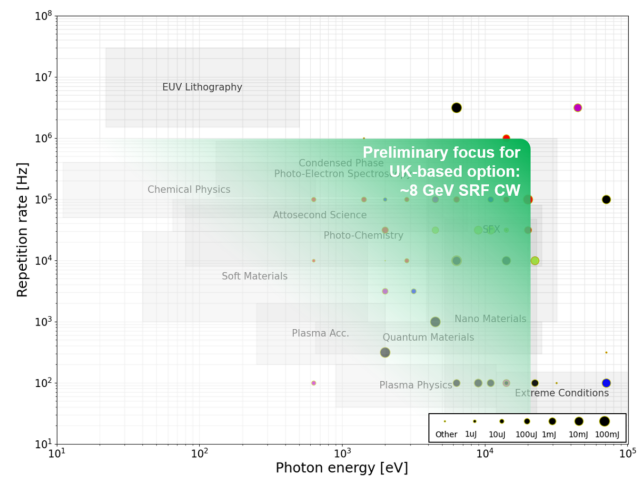


Figure 1: Research areas potentially covered by the UK XFEL, based on the preliminary repetition rate and photon energy capabilities. Figure courtesy of [7].

* can.davut@manchester.ac.uk

AN INTRODUCTION TO THE UK XFEL CONCEPTUAL DESIGN AND OPTIONS ANALYSIS

D. J. Dunning*, D. Angal-Kalinin, J. A. Clarke, J. R. Henderson, S. L. Mathisen, B. L. Militsyn, M. D. Roper, E. W. Snedden, N. R. Thompson, D. A. Walsh, P. H. Williams, ASTeC, STFC Daresbury Laboratory and Cockcroft Institute, Sci-Tech Daresbury, Warrington, UK P. Aden, B. D. Fell, Tech. Dept., STFC Daresbury Laboratory, Sci-Tech Daresbury, Warrington, UK J. L. Collier, J. S. Green, Central Laser Facility, STFC Rutherford Appleton Laboratory, Didcot, UK J. P. Marangos, Department of Physics, Imperial College London, Blackett Laboratory, London, UK

Abstract

In October 2022, the UK XFEL project entered a new phase to explore how best to deliver the advanced XFEL capabilities identified in the project's Science Case. This phase includes developing a conceptual design for a unique new machine to fulfil the required capabilities and more. It also examines the possibility of investment opportunities at existing XFELs to deliver the same aims, and a comparison of the various options will be made. The desired next-generation capabilities include transform-limited operation across the entire X-ray range with pulse durations ranging from 100 as to 100 fs; evenly spaced high rep. rate pulses for enhanced data acquisition rates; optimised multi-colour FEL pulse delivery and a full array of synchronised sources (XUV-THz sources, electron beams and high power/high energy lasers). The project also incorporates sustainability as a key criteria. This contribution gives an overview of progress to date and future plans.

INTRODUCTION

In early 2019, the UK initiated a project to develop the science case for a UK XFEL, which was published in 2020 [1, 2]. Subsequent exercises demonstrated the support of the UK community and in June 2022, UK Research and Innovation announced funding for the next phase of the project: a 3-year conceptual design and options analysis (CDOA), which started in October 2022. This phase includes developing a conceptual design for a unique new UK machine, alongside examining investment opportunities at existing facilities e.g. [3–12], both with the aim of realising 'next-generation' XFEL capabilities (the features of which are discussed below). By the end of this phase of the project (October 2025) we will have:

- mapped out how best to deliver advanced XFEL capabilities identified in the Science Case;
- explored a conceptual design for a unique new machine that can fulfil all required capabilities;
- examined other investment options and collaborations in existing XFELs;
- updated the Science Case to feed into the process and inform future decisions;
- held multiple Townhall Meetings around the UK engaging with the user community;

* david.dunning@stfc.ac.uk

- investigated the socioeconomic impact of a next generation XFEL.

Year 1 has so far focused on the project launch, surveying the science requirements, preliminary engagement with overseas XFEL facilities, planning the Townhall meetings and initial conceptual design and layout work. Informed by work this year, Year 2 will focus on R&D targeting gaps in key physics and technology areas, including collaborative work with overseas XFEL facilities, and the continuation of Townhall meetings and other workshops. In Year 3, R&D activities will continue and the final CDOA report will be written, detailing the preferred options; including associated costs, socio-economic analysis, and an update to the Science Case. This paper gives an overview of progress to date.

NEXT-GENERATION XFEL CAPABILITIES

Starting from our Science Case, our project clearly sets an emphasis on enhancing XFEL capabilities and on widening access to such capabilities, defined as follows:

- Transform-limited operation across the entire X-ray range (initial focus on 0.1 - 20 keV and 100 as - 100 fs).
- High efficiency facility, with a step change in the simultaneous operation of multiple end stations.
- Evenly spaced, high rep. rate pulses to match samples & detectors.
- Improved synchronisation/timing data with external lasers to < 1 fs.
- Widely separated multiple colour X-rays to at least one end station.
- Full array of synchronised sources: XUV-THz, e-beams, high power & high energy lasers at high rep. rate.

This list of features results from both the Science Case and work in this phase, including a detailed survey of our science team, results of which are shown in Fig. 1. We are presently focusing our preliminary activities on the capabilities listed above, particularly the first two, which we consider to be the most challenging and fundamental to the machine design (see sections below). Other requested capabilities, e.g., higher photon energies will be considered beyond the preliminary focus and are briefly summarised below.

The options will ultimately be assessed on a range of criteria including the above capabilities, technology readiness level, environmental sustainability and cost.

TRANSVERSE OPTICS-BASED CONTROL OF THE MICROBUNCHING INSTABILITY

A. D. Brynes*, E. Allaria, G. De Ninno, S. Di Mitri, D. Garzella, G. Perosa, C. Spezzani
 Elettra-Sincrotrone Trieste S.C.p.A., Trieste, Italy
 C.-Y. Tsai

Department of Electrotechnical Theory and Advanced Electromagnetic Technology,
 Huazhong University of Science and Technology, Wuhan, China

Abstract

A number of recent experimental and theoretical studies have investigated novel techniques for suppressing the microbunching instability in high-brightness linac-based light sources. This instability has long been studied as one of the causes of reduced longitudinal coherence in these machines. It is commonly suppressed using a laser heater. This contribution presents recent developments which use an optics-based scheme to mitigate the microbunching instability in the FERMI free-electron laser, paving the way towards reversible beam heating techniques that could improve the performance of future machines.

INTRODUCTION

High-brightness electron bunches are a fundamental requirement for producing high-intensity, narrow-bandwidth free electron laser (FEL) pulses [1]. The 6D beam brightness is described by the phase space volume occupied by the beam: in the transverse plane, a bright beam has a small emittance, whereas the requirements for the longitudinal properties of the beam are a high current density and a low slice energy spread [2, 3]. One of the key factors that can reduce the brightness of the electron beam as it is accelerated on its path towards the FEL undulators is the microbunching instability [1, 4, 5], which arises due to a variety of collective interactions between particles in the beam and its environment [6]. This instability can result in a beam that has a non-uniform longitudinal density profile, and an increased slice energy spread [7, 8], thereby reducing the quality of the light produced in the FEL [9, 10].

Various methods have been proposed and tested to mitigate the development of this instability, and to preserve the beam brightness up to the entrance of the FEL [11]. The most widely used of these methods is the laser heater [12, 13], a device which increases the uncorrelated slice energy spread in the beam (to an acceptable level). However, other methods can lead to the suppression of small-scale modulations in the beam without resorting to this irreversible dilution of the beam phase space [14–23]. In this contribution, a method of controlling the microbunching content in the beam is exploited at the FERMI FEL [24]. The transverse optics functions of the beam are varied along the linac-to-FEL transfer line (also known as the ‘spreader’), and it is observed that the FEL performance can be improved simply using quadrupole magnets.

* alexander.brynes@elettra.eu

THEORY

The one-dimensional bunching factor $b(k)$ [25–27] is used to characterize the depth of modulations in the electron bunch as a function of wavenumber. This parameter is given by the Fourier transform of the current profile. The ratio between the final and initial bunching factors – $b_f(k)$ and $b_i(k)$, respectively – is known as the microbunching gain $G(k) = b_f(k)/b_i(k)$. In the absence of collective effects, the final bunching factor is given by:

$$b_f(k) = b_i(k_0) \exp\left(-\frac{1}{2}(k_f R_{56} \sigma_{\delta,0})^2\right) \times \exp\left(-\frac{1}{2}k_f^2 \left[\epsilon_{x,0} \beta_{x,0} \left(R_{51} - \frac{\alpha_{x,0}}{\beta_{x,0}} R_{52} \right)^2 - \frac{\epsilon_{x,0}}{\beta_{x,0}} R_{52}^2 \right]\right). \quad (1)$$

The R_{5x} parameters give the linear components of the 6×6 transfer matrix [28], and ϵ , β and α are the initial horizontal emittance and Twiss parameters of the beam. The final wavenumber k_f is given by $k_i C$, with C the compression factor of the lattice. For full derivations of the influence of the collective effects mentioned above on the microbunching gain, the reader is referred to Refs.[12, 13, 16, 25, 27, 29–32].

Coherent synchrotron radiation (CSR) [26, 27], geometric wakefields in accelerating structures [33], and longitudinal space-charge (LSC) [13, 34–36] are all examples of collective effects that can drive the microbunching instability during the electron beam acceleration and compression process.

It can be seen from Eq. (1) that the final bunching factor can be reduced by increasing either $\sigma_{\delta,0}$, R_{56} , or \mathcal{H}_x . The third of these terms, otherwise known as the dispersion invariant, is given by the term in square brackets within the second exponential of Eq. (1). Previous work undertaken at FERMI [18] has demonstrated that a non-isochronous spreader line ($|R_{56}| > 0$) can reduce the spectral bandwidth of the FEL pulse; in this contribution, a similar effect is observed by varying the dispersion invariant \mathcal{H}_x .

MEASUREMENT METHODS

While a full measurement of the electron bunch longitudinal phase space, and the modulations therein, can be captured through the use of a vertical RF deflector and a bending magnet [37], this analysis method can be complicated [7, 8]. Alternatively, as mentioned above, the microbunching

NON-DESTRUCTIVE VERTICAL HALO-MONITORS ON THE ESRF ELECTRON BEAM

K. Scheidt

European Synchrotron Radiation Facility, Grenoble, France

Abstract

The ESRF EBS storage ring has now among its electron beam diagnostics two independent units of vertical Halo-monitor. They use the available X-rays in a non-used Front-End, emitted from standard 0.56 T dipole magnets in the EBS lattice. These instruments measure continuously at a 2 Hz rate the so-called ‘far-away’ halo level, i.e. in a zone of roughly 1-3 mm away from the beam centre.

Both units are yielding excellent and well-correlated results with data of both the beam lifetime and of our 128 Beam Loss Detectors, and this as a function of the beam current, the filling-patterns, the vertical emittance, and the quality and incidents of the vacuum.

NON-DESTRUCTIVE MEASUREMENTS OF THE VERTICAL BEAM HALO

The Extreme Brilliant Source (EBS) ring at the European Synchrotron Radiation Facility (ESRF) is operational since mid-2020, generating coherent and bright X-rays for the scientific users. The X-rays are generated by an electron beam of 6 GeV and 200 mA, with horizontal and vertical emittances of 120 pm and 10 pm. A large range of diagnostics are in operation since the commissioning to measure the parameters, characteristics and behaviour of the beam [1, 2]. This 10 pm emittance implies that the beam’s vertical size is in a range of roughly 4.5 to 13 σ .

However, it is easily verified that a non-negligible beam population exists at some millimetres vertical distance from the beam-centre by inserting a vertical scraper and measuring the signal from a down-stream Beam Loss Detector (BLD). However, such method is destructive to the beam and not useable for assessing the halo population while serving normal users’ operation (USM).

In 2014, in the old ESRF ring, a non-destructive vertical Halo-monitor based on imaging the X-rays from an available bending magnet beam-port was conceived and installed [3]. It was successfully operated and yielded excellent results until the disassembly of that ring for the subsequent installation of the new low emittance lattice of EBS in 2019. However, implementing a similar Halo-monitor in EBS was more complicated due to the constraints of the much smaller vacuum chamber, the weaker field strength of the available magnet source (now 0.56 T while 0.86 T before) and the longer distances between the essential components (now 6.8 m while before 4.2 m). These disadvantages were partly compensated by the availability of now non-used bending magnet Front-Ends, and this allowed a low-cost installation in cells 10 and 11 of two identical devices without any modification to the vacuum chambers in the EBS.

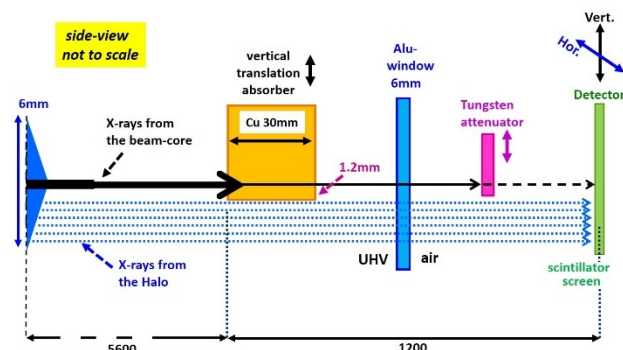


Figure 1: The main components and the paths of the X-rays of both the beam-core and that of the halo population.

Explanation of the Concept and its Components

The main components are shown in Fig. 1 in the vertical plane together with the (simplified) trajectory of the X-rays that are emitted from the electrons (at extreme left of the picture) and travel towards the detector (extreme right) which is a two-dimensional X-ray imager read-out by a standard camera. It is important to note that the X-rays from the central beam-core are many orders of magnitude stronger than those emitted from the electrons that make up the weak halo population. The specificity in our concept is to attenuate this powerful X-ray beam by an absorber that is vertically positioned so to intercept that beam.

However, the X-rays of typically 60 keV have a small but not a zero divergence as is supposed in the illustration. In fact, this divergence amplitude is 1E-9 for a divergence angle of 200 μ rad. Therefore, the absorber (at roughly 6m from the source) needs to be positioned at least 1.2 mm below the central axis, so to reduce this unwanted divergence signal to a negligible level compared to the weak level of the X-rays emitted by the halo. Consequently, it implies that this system can only detect the halo levels at roughly 1 to 3 mm distance from the beam-core.

The UHV of the Front-End is separated from the free air by a 6 mm thick Aluminium window. Further downstream a movable attenuator (1 mm thick Tungsten) provides flexibility in attenuation, followed by the detector that can be precisely positioned with a two-axis translation stage.

This detector is protected by a 5 mm thick lead box, and contains a 2 mm thick LYSO scintillator (15 x 15 mm), a double chicane with 3 mirrors, a set of achromat lenses and a CMOS camera and covers an 8 x 6 mm field of view.

The Fig. 2 shows a typical image (left) and its vertical profile (right). The beam-core signal there is produced by the main beam with its X-rays very strongly attenuated by the 30mm Copper, the 6 mm Aluminium and the 1 mm Tungsten. While for the halo signal beneath, the X-rays are only attenuated by the 6 mm Aluminium window. In the

Content from this work may be used under the terms of the CC-BY-4.0 licence (© 2023). Any distribution of this work must maintain attribution to the author(s), title of the work, publisher, and DOI

NONLINEAR DYNAMICS MEASUREMENTS AT THE EBS STORAGE RING

N. Carmignani*, L. Carver, L. Hoummi, S. Liuzzo, T. Perron, S. White
ESRF, Grenoble, France

Abstract

The Extremely Brilliance Source (EBS) is a 4th generation synchrotron light source and it has been in user operation since August 2020 at the ESRF. Several measurements to characterise the nonlinear dynamics have been performed in 2023: nonlinear chromaticity, second order dispersion and detuning with amplitude. The results of the measurements are shown and compared with simulations.

INTRODUCTION

The EBS has been in user operation since August 2020 at the ESRF [1]. The nonlinear dynamics model of the storage ring has been improved by adding the cross talk effect of some magnets to their neighbors [2]. The Touschek lifetime of the machine reached the design values already in the first year of user operation [3] and it is improved regularly by online nonlinear optimization [4]. The horizontal dynamic aperture and therefore the injection efficiency is still slightly lower than the one predicted by the model [3].

In order to better understand the disagreement with the model of the horizontal dynamic aperture, in 2023 we performed a series of nonlinear dynamics measurements and we compared them with the accelerator model.

In the next section we will show the measurements of transverse detuning with amplitude and in the following the measurements of high order chromaticity and second order dispersion. For all the cases, a comparison with the theoretical model is shown.

DETUNING WITH AMPLITUDE

Measurement Technique

In order to measure the detuning with amplitude we need to excite coherent oscillations of the beam at increasing amplitudes and measure the frequency of the free oscillations.

A kicker magnet able to excite the beam for about 1 turn, either in horizontal or vertical, will be installed in the ESRF-EBS storage ring in 2024. The four injection kickers can be used to excite horizontally the beam, but their field has a raising time of about 70 μ s (see Fig. 1) [5]. The four injection kickers are usually pulsed with a current of about 1.6 to 1.9 kA.

Since the pulsed power supplies limit the minimum sent currents to a few hundreds of Amperes, we excited the beam by powering all the four kickers at full current except for the kicker K3, that was powered with reduced current. The described distribution of currents generates a bump that is not perfectly closed. In Fig. 2, the turn by turn (TBT) orbit



Figure 1: Pulse shape of the injection kickers.

in the first beam position monitor (BPM), which is located inside the injection bump, is shown for different current reductions of the kicker K3 power supply. The injection oscillations are dumped in about 100 turns because of the decoherence due to the high chromaticity. The radiation damping is a slower effect that lasts a few thousands turns.

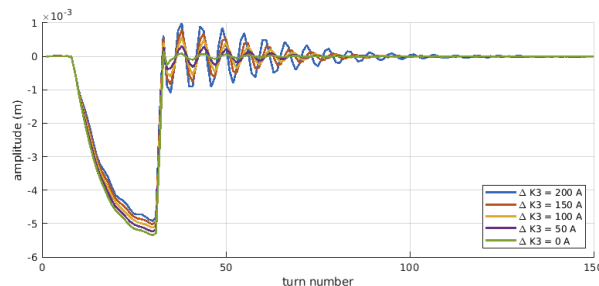


Figure 2: Orbit at the BPM number 1, which is inside the injection bump, during the ramp rise and after it goes off in about 1 turn. The oscillations are dumped quickly because of strong decoherence due to the high chromaticity.

The tune is extracted from the first 130 turns of oscillations using 5 consecutive measurements in all the 320 BPM. In order to increase the resolution of the FFT, a zero-padding of the signal with 12000 samples has been added to the measurements. A histogram of the 320 x 5 tune measurements for a single amplitude is shown in Fig. 3. The standard deviation of the histogram is about 5×10^{-4} and it is considered as the measurement error for the tune. From the peak to peak oscillation amplitude at each BPM, knowing the beta functions, we can extract the action of the beam and compute the tune shift with amplitude.

The vertical tune can be measured in the same way. Even if the injection kickers produce a horizontal excitation, some smaller vertical oscillations can be observed and can be used to measure the vertical tune as a function of horizontal amplitude of oscillations.

* nicola.carmignani@esrf.fr

EVOLUTION OF EQUILIBRIUM PARAMETERS RAMP INCLUDING COLLECTIVE EFFECTS IN THE DIAMOND-II BOOSTER

R. Husain^{1,2,†}, R.T. Fielder¹, I.P.S. Martin¹, P.N. Burrows²

¹Diamond Light Source Ltd., Oxfordshire, UK

²John Adam Institute, University of Oxford, Oxfordshire, UK

Abstract

Efficient top-up injection into the Diamond-II storage ring will require upgrading the booster lattice for a beam emittance of < 20 nm·rad and a bunch length of < 40 ps, including when operating with high single-bunch charge. The small vacuum chamber dimensions will drive the resistive wall instability and may adversely affect equilibrium parameters along the beam energy ramp. In addition, various diagnostic and vacuum chamber components will generate geometric impedances which may further disrupt the equilibrium parameters. Based on the detailed engineering designs, impedance models of the major components have been simulated using CST Studio and included in ELEGANT tracking simulations of the booster. In addition, the effects of synchrotron radiation emission and intra-beam scattering on the equilibrium parameters during the ramp are studied.

INTRODUCTION

Diamond Light Source is to be upgraded with an advanced low emittance storage ring, Diamond-II, using a multi-bend achromat lattice [1] to provide space for more beamlines and to increase the brightness and coherence of the photon beams. For efficient beam injection into the Diamond-II storage ring, the injector system also needs to be upgraded [1, 2]. This includes a new low emittance booster synchrotron with beam emittance < 20 nm·rad and bunch length < 40 ps at the 3.5 GeV extraction energy. The lower emittance is required to achieve off-axis beam accumulation into the reduced dynamic aperture of the new storage ring. A shorter bunch length will ensure a proper matching with the storage ring RF bucket so that energy errors during synchrotron oscillations for the injected beam remain small. The major Diamond-II booster parameters are given in Table 1, more lattice details can be found in Refs. [1-3].

The Diamond-II booster should be capable of accelerating high-charge single bunches or multi-bunch trains without degradation of the equilibrium parameters such as beam emittance, bunch length and energy spread. The beam energy needs to be raised from the injection energy of 100 MeV to 3.5 GeV at extraction. During the beam energy ramp process, the equilibrium parameters change due to synchrotron radiation (SR) emission. These parameters may deviate from the equilibrium values due to high intensity collective effects [4] such as coupling impedance (resistive wall and geometric impedance) and intra-beam scattering (IBS). Another important contribution comes from

higher order modes (HOMs) in the RF cavities. If the beam impedance interaction become strong it may result in large disruption of the electron bunch and equilibrium parameters and could eventually lead to beam loss.

In this paper, we present simulation studies of the evolution of the equilibrium parameters during the beam energy ramp. These have been done considering a high-charge single bunch including impedances, SR and IBS effects with physical apertures applied.

Table 1: Main Parameters of the Diamond-II Booster

Parameters	At 100 MeV	At 3.5 GeV
Circumference	163.85 m	
Betatron tunes	12.41 / 5.38	
Chromaticity	+1 / +1	
Momentum comp. factor	5.65×10^{-3}	
Damping times	[156.3, 173.1, 91.5] s	[3.67, 4.04, 2.13] ms
Energy loss/turn	0.63 eV	947.5 keV
Natural beam emittance	14.1 pm·rad	17.3 nm·rad
Natural energy spread	2.5×10^{-5}	8.6×10^{-4}
Bunch length	0.55 ps	38 ps
RF Voltage	200 kV	2 MV
Energy acceptance	2.8 %	0.93 %
RF frequency	499.51 MHz	

BOOSTER RAMP PROFILE

For the present studies, the energy and voltage ramp profiles of the Diamond booster are as follows. The beam energy is raised from 100 MeV to 3.5 GeV (compared to 3 GeV in the existing booster) with a biased sinusoidal waveform at 5 Hz repetition rate. At the injection energy the RF voltage is 200 kV. This provides sufficient energy acceptance (2.8 %) for the energy errors during initial synchrotron oscillations of the injected bunch. This voltage is kept constant up to 1.93 GeV and then increases with the fourth power of energy up to 2 MV at the extraction.

BOOSTER IMPEDANCE MODEL

The Diamond-II booster consists of a large number of components which contribute to the overall impedance. Initial engineering designs of the major components have been completed and an impedance database has been generated. A vacuum vessel of stainless steel has been selected with two different circular apertures with radii 18.3 mm (in the injection/extraction sections) and 11.5 mm (in the arc sections). In addition, there are four in vacuum ferrite kickers (one for the injection and three for beam extraction). Two ceramic breaks of 10 mm length and inner radius

* Work supported by the United Kingdom Science and Technology Facilities Council via the John Adams Institute, University of Oxford.

† riyasat.husain@diamond.ac.uk

SIMULATED COMMISSIONING FOR DIAMOND-II STORAGE RING FROM ON-AXIS TO OFF-AXIS INJECTION

H.-C. Chao*, I. P. Martin, Diamond Light Source, Oxfordshire, UK

Abstract

The Diamond-II storage ring commissioning simulations have continued based on the previous results where on-axis injected beams are captured. The next goal is to enlarge the dynamic aperture so that off-axis injection can be achieved. The procedures include beam based alignment, beta-beating correction and linear optics correction. Details of the implementations are discussed and the simulation results are presented. In the end, we are able to reach off-axis injection which allows accumulation.

INTRODUCTION

The Diamond-II project [1] features a storage ring using a modified hybrid six-bend achromat lattice. The parameters of the current baseline lattice are listed in Table 1.

Table 1: Diamond-II Storage Ring Parameters

Parameter	Value	Unit
Energy	3.5	GeV
Circumference	560.56	m
Number of Straight Sections	48	
Betatron Tune (H/V)	54.14 / 20.24	
Natural Chromaticity (H/V)	-68 / -89	
Damping Partition (J_x)	1.88	
Natural Emittance	162	pm-rad
Momentum Compaction Factor	1.03	10^{-4}
Energy Loss Per Turn (w/o IDs)	723	keV
Rad. Damping Time (H/V/L)	9.7 / 18.1 / 16.0	ms
Natural Energy Spread [†]	9.4	10^{-4}
Natural Bunch Length [†]	3.5	mm
Synchrotron Tune [†]	0.0025	
Beta Functions (H/V) [‡]	8.44 / 3.41	m

[†] Estimated with only main RF total voltage = 1.42 MV

[‡] At long straight centres

The general commissioning strategies and some preliminary simulation results were presented in the previous study [2], including initial estimates for storage ring error tolerances. Since that time, prototyping and alignment trials have begun, ensuring all sources of error are minimised within the practical engineering constraints. As such, the error specifications continue to evolve.

In the follow-up study [3], the revised error tolerances are given and some alternative methods for early-stage commissioning are discussed. Initial commissioning stages were simulated for 200 random machines, up to the phase when an on-axis injected beam is captured. The demonstrated dynamic apertures, estimated by particle tracking with more

than one synchrotron period, are large enough to capture on-axis injected beams efficiently.

At this stage the beam current will be low (< 1 mA), but sufficient to detect a closed orbit and betatron tunes. In addition, the RF frequencies and phases are already adjusted to minimise the synchrotron oscillation of the captured beam.

In this paper the plans for the subsequent commissioning will be discussed, together with some details of the implementation and simulation results.

COMMISSIONING RECIPES AND SIMULATIONS

The next goal of commissioning is to enlarge the dynamic aperture to switch from on-axis injection to off-axis injection for accumulation. The current subsequent commissioning recipes are as follows.

1. Very first time closed orbit correction and chromaticity correction,
2. Set up ab-initio BPM offsets,
3. Preliminary beam based alignment (BBA),
4. Preliminary beta-beating correction (BBC),
5. Integer tune correction,
6. Further iterations of BBA and linear optics correction.

During the course of commissioning a tune scan can always be performed to ensure a good beam transmission whenever needed. The tune response matrix used is constructed from the ideal lattice with 7 families of quadrupoles (excluding strong quadrupoles). Some of the commissioning procedures are detailed as follows.

First Closed Orbit Correction

The Tikhonov parameter [4] used to regularise the corrector strengths is set very weak ($\alpha = 1000$). As shown in Fig. 1, the rms BPM readouts are slightly improved to a few hundreds μm and an extreme case is fixed.

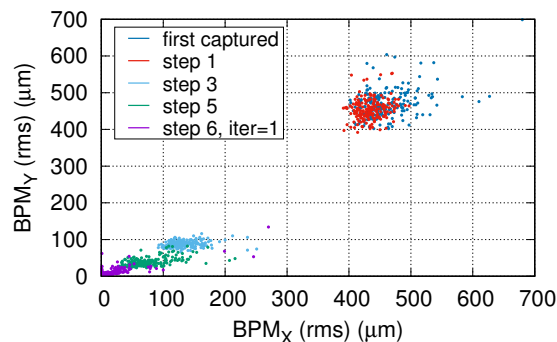


Figure 1: RMS BPM readouts at different steps.

* hung-chun.chao@diamond.ac.uk

SPECIAL OPERATIONAL MODES FOR SLS 2.0

J. Kallestrup*, M. Aiba, Paul Scherrer Institut, 5232 Villigen PSI, Switzerland

Abstract

The SLS 2.0 storage ring will achieve low emittance and high brightness while maintaining large dynamic aperture and lifetime comparable to the present SLS. Special operational modes are investigated to further explore the potential of the lattice. In this contribution, the first considerations on such modes for the SLS 2.0 are outlined. A promising high-brightness mode, increasing brightness by up to 25% at insertion devices with minor deterioration to dynamic and momentum aperture is presented. The use of round beams and its impact on beam dynamics and the beamlines in the SLS 2.0 portfolio is discussed.

INTRODUCTION

One of the main goals of the SLS 2.0 is to minimize the natural emittance of the machine, thereby generating significantly higher brightness than the existing SLS. This is achieved using a seven-bend achromat with longitudinal gradient bends and reverse bends [1, 2]. In this contribution we explore two possible operational modes for SLS 2.0. We investigate the option of a high-brightness mode which lowers the beta-functions at the insertion device (ID) source points. Finally, we show a possible implementation of round beams in SLS 2.0 in combination with one of the high-brightness lattice options, and evaluate the impact on both machine and beamline performance.

HIGH-BRIGHTNESS MODE

Motivation

The goal of the SLS 2.0 lattice design has been to create a lattice that provides an order-of-magnitude higher brightness and higher coherent flux than the existing SLS, without compromising with the dynamic and momentum aperture of the machine [2]. This leads to an ambitious, but realistic design. However, the brightness of IDs can be increased by optimizing the beta-functions in the straight sections further.

We follow the definitions of brightness and spatial coherence as given in [3], defined as:

$$\mathcal{B} = \frac{\Phi_{\text{ph}}}{4\pi^2 \sigma_{\text{Tx}} \sigma_{\text{Tx}'} \sigma_{\text{Ty}} \sigma_{\text{Ty}'} (d\omega/\omega)}, \quad (1)$$

and

$$\frac{\Phi_{\text{coh}}}{\Phi_{\text{ph}}} = \frac{\lambda^2}{16\pi^2 \sigma_{\text{Tx}} \sigma_{\text{Tx}'} \sigma_{\text{Ty}} \sigma_{\text{Ty}'}}, \quad (2)$$

where Φ_{ph} and Φ_{coh} are the total and spatially coherent flux, λ is the photon wavelength, σ_{Tu} and $\sigma_{\text{Tu}'}$ are the effective photon source size and divergence defined as

$$\sigma_{\text{Tu}} = \sqrt{\beta_u \epsilon_u + \frac{\lambda L}{8\pi}}, \quad (3)$$

and

$$\sigma_{\text{Tu}'} = \sqrt{\frac{(1 + \alpha_u^2)}{\beta_u} \epsilon_u + \frac{\lambda}{2L}}, \quad (4)$$

where β_u and α_u are the Twiss parameters at the ID source point. The SLS 2.0 portfolio contains IDs of several different lengths. The brightness and the coherence depends on the ID length, L , and we compute them for a range of $1 \leq L \leq 3$ m, corresponding to the actual IDs to be installed.

In the following, first the possibilities for brightness improvement without physically modifying the storage ring are investigated. Next, the option of increasing the gradient of quadrupoles will be considered.

The linear optics changes will be restricted to the straight sections to avoid modifying the optimized arc optics. This also means that the equilibrium emittances will remain unchanged.

The baseline SLS 2.0 lattice is designed such that the betatron phase advances along each straight section are the same constant values. The super-periodicity for on-momentum particles is therefore as high as the number of arcs: 12 (“pseudo symmetry”). To maintain good dynamic and momentum aperture, it is beneficial to keep the pseudo symmetry and, hence, the phase advance must be increased equally in all straight sections.

For each proposed solution, a genetic algorithm is used to optimize the nonlinear magnets in the lattice to maximize Touschek lifetime, τ_T . Piwinski’s formula for the Touschek lifetime is used [4], with the nominal “flat beam emittances” $\epsilon_x = 149$ pm rad and $\epsilon_y = 10$ pm rad. All tracking simulations are performed in Accelerator Toolbox [5, 6].

We are interested in the relative increase in brightness and coherence between the baseline SLS 2.0 lattice and the new high-brightness solutions. The denominators of Eqs. (1) and (2) both scale as $(\sigma_{\text{Tx}} \sigma_{\text{Tx}'} \sigma_{\text{Ty}} \sigma_{\text{Ty}'})^{-1}$, meaning that the scaling of brightness and coherence will be the same, and we will therefore only report impacts on brightness.

Solutions-A: Unaltered Machine Layout

Two options are investigated for an unaltered machine layout: increasing the horizontal tune by a full integer (“solution A-1”) or increasing the vertical tune by 0.56 (“solution A-2”). A comparison between the baseline and new Twiss parameters in the straight sections is shown in Table 1, and the relative brightness increases for IDs of the three lengths are shown in Fig. 1 for solution A-1 and A-2 as solid and dashed lines, respectively. Qualitatively, short IDs have the largest gain in brightness. Solution A-1 provides the biggest increase around the soft x-ray region of 1 keV photon energies, while solution A-2 is most beneficial around hard x-rays at 10 keV. Long straight sections benefit in a broader spectral range; for high photon energies this stems from the smaller values of α_x and α_y at the source points.

* jonas.kallestrup@psi.ch

PROGRESS OF THE HEPS ACCELERATOR CONSTRUCTION AND LINAC COMMISSIONING*

C. Meng[†], J. S. Cao, Z. Duan, D. Y. He, P. He, H. F. Ji, Y. Jiao[†], W. Kang, J. Li, J. Y. Li[†], X. H. Lu, Y. M. Peng, H. M. Qu, S. K. Tian, J. Zhang, J. R. Zhang, H. S. Xu, G. Xu, W. M. Pan
 Key Laboratory of Particle Acceleration Physics and Technology, Institute of High Energy Physics, Chinese Academy of Sciences, Beijing, China

Abstract

The High Energy Photon Source (HEPS) is the first fourth-generation synchrotron radiation source in China that has proceeded on the track of construction. The accelerator complex of the light source is composed of a 7BA storage ring, a booster injector, a Linac pre-injector, and three transfer lines. In order to provide high-bunch-charge beams for the storage ring, the booster was designed to be capable of both beam acceleration from low injection energy to extraction energy and charge accumulation at the extraction energy by means of accepting electron bunches from the storage ring. The Linac was built using S-band normal conducting structures, and can provide electron beam with pulse charge up to 7 nC. This paper reports the progress of the construction of the accelerators, including the installation of the storage ring, the pre-commissioning tests of the booster, and commissioning of the Linac. In particular, the beam commissioning of the Linac will be introduced in detail.

INTRODUCTION

The High Energy Photon Source (HEPS) [1, 2] is the first fourth-generation synchrotron radiation source based on a 6-GeV diffraction-limited storage ring [3, 4] that is currently under construction in China. The accelerator complex of the HEPS comprises an injector and a storage ring. The injector consists of a 500-MeV Linac [5, 6], a full-energy booster [7], a low energy transfer line connecting the Linac and booster and two high energy transfer lines that transport beams between the storage ring and booster [8]. The layout of HEPS accelerator is shown in Fig. 1 and the overall design goals of the light source are listed in Table 1.

The storage ring consists of 48 modified hybrid 7BAs, which were grouped in 24 periods with circumference of 1360.4 m. The Booster consists of 4 FODO structure lattice with circumference of 454.07 m. The optical functions and layouts of the storage ring and booster are shown in Fig. 2. The swap-out injection scheme [9] is adopted, so the booster employs the “high-energy accumulation” scheme. In order to meet the requirements of the injection and beam commissioning, a high bunch charge scheme of the Linac was adopted [5] with bunch charge of 7 nC. The layout and tunnel of the Linac are shown in Fig. 2.

Considering the long injection interval in the ring, the injector adopts an energy-saving design, the Linac operates in burst mode, and the booster adopts a novel ramping-table-controlled scheme. For the burst mode of the Linac, each macro-RF pulse has 1 to 10 RF pulse and the RF pulse repetition rate is 50 Hz. The interval time of the macro-RF pulse is decided by the injection rate. For the booster ramping-table-controlled scheme, the booster can realize the stop and start at any energy. The power supply and the cavity can be ramped according to the ramping-table, every time there is a clock trigger, take a step, and wait without the clock trigger. The schematic diagram is shown in Fig. 3. When no injection is needed, the booster is in a low-power waiting phase without repeated ramping.

In this paper, we introduce the brief construction process of the HEPS, and present the latest results of beam commissioning.

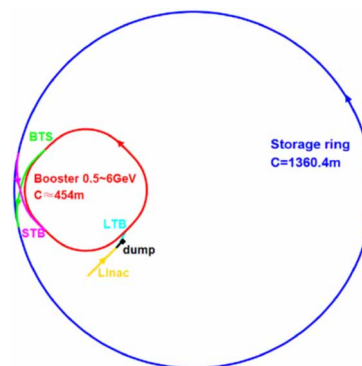


Figure 1: Layout of the HEPS accelerator.

Table 1: Main Parameters of The HEPS

Parameter	Value	Unit
Energy	6	GeV
Beam current	200	mA
Horizontal natural emittance	60	pm·rad
Brightness	$>1 \times 10^{22}$	phs/s/mm ² /mrad ² / 0.1%BW
Circumference	1360.4	m

CONSTRUCTION

Construction of the HEPS starts in June 2019 with a construction period of 6.5 years, which means it will be completed by the end of 2025. The milestone of the HEPS construction are as follows:

* Work supported by the High Energy Photon Source (HEPS) project, a major national science and technology infrastructure project, National Natural Science Foundation of China (NSFC12005239) and the Youth Innovation Promotion Association CAS (2019016)

[†] mengc@ihep.ac.cn, jiaoyi@ihep.ac.cn, jingyili@ihep.ac.cn

USEFUL FORMULAS AND EXAMPLE PARAMETERS SET FOR THE DESIGN OF SSMB STORAGE RINGS

Xiujie Deng*, Alex Chao¹, Wenhui Huang, Zizheng Li, Zhilong Pan, Chuanxiang Tang
 Tsinghua University, Beijing, China

¹also at Stanford University, Menlo Park, USA

Abstract

A promising accelerator light source mechanism called steady-state microbunching (SSMB) has been actively studied in recent years. Here we summarize some important formulas for the design of SSMB storage rings. Generally we group our formulas into two categories, i.e., a longitudinal weak focusing storage ring for a desired radiation wavelength $\lambda_R \gtrsim 100$ nm, and a transverse-longitudinal coupling, or a generalized longitudinal strong focusing, storage ring for a desired radiation wavelength $1 \text{ nm} \lesssim \lambda_R \lesssim 100$ nm. In each category, we have presented an example parameters set for the corresponding SSMB storage ring, to generate kW-level infrared, EUV and soft X-ray radiation, respectively.

INTRODUCTION

In Ref. [1], we have conducted indepth theoretical and experimental studies on the steady-state microbunching (SSMB) mechanism [2–18], which promises high-power narrow-band coherent radiation, with wavelength ranging from THz to soft X-ray. To make our investigations more useful for practitioners, especially concerning the parameters choice for an SSMB storage ring, here in this paper we present some important formulas and example parameters set for the design of SSMB storage rings.

LONGITUDINAL WEAK FOCUSING SSMB

The effective modulation voltage of a laser modulator using a planar undulator is [19]

$$V_L = \frac{[JJ]K}{\gamma} \sqrt{\frac{4P_L Z_0 Z_R}{\lambda_L}} \tan^{-1} \left(\frac{L_u}{2Z_R} \right). \quad (1)$$

in which γ is the Lorentz factor, $[JJ] = J_0(\chi) - J_1(\chi)$ and $\chi = \frac{K^2}{4+2K^2}$, J_n is the n -th order Bessel function of the first kind, $K = \frac{eB_0}{m_e c k_u} = 0.934 \cdot B_0[\text{T}] \cdot \lambda_u[\text{cm}]$ is the undulator parameter, determined by the peak magnetic flux density B_0 and period of the undulator λ_u , c the speed of light in free space, P_L is the modulation laser power, $Z_0 = 376.73 \Omega$ is the impedance of free space, Z_R is the Rayleigh length of the laser, L_u is the undulator length. The linear energy chirp strength around zero-crossing phase is related to the laser and modulator undulator parameters according to $h = \frac{eV_L}{E_0} k_L$, with E_0 the particle energy, $k_L = 2\pi/\lambda_L$ the modulation laser wavenumber.

Linear stability of the longitudinal motion requires $0 < h\eta C_0 < 4$, where C_0 is the ring circumference, η is the phase

slippage factor of the ring. In a longitudinal weak focusing ring ($\nu_s \ll 1$), the longitudinal beta function at the laser modulator is

$$\beta_{zS} \approx \sqrt{\frac{\eta C_0}{h}}. \quad (2)$$

The synchrotron tune is $\nu_s \approx \frac{\eta}{|\eta|} \frac{\sqrt{h\eta C_0}}{2\pi}$. The natural bunch length at the laser modulator is $\sigma_{zS} = \sigma_{\delta S} \beta_{zS}$, where $\sigma_{\delta S} = \sqrt{\frac{C_q \gamma^2}{J_s \rho}}$ is the natural energy spread, with ρ the bending radius of dipole in the ring, $C_q = \frac{55\lambda_e}{32\sqrt{3}} = 3.8319 \times 10^{-13} \text{ m}$, $\lambda_e = \frac{\lambda_e}{2\pi} = 386 \text{ fm}$ is the reduced Compton wavelength of electron, J_s is the longitudinal damping partition number. The micro-bucket half-height is $\hat{\delta}_{\frac{1}{2}} = \frac{2}{\beta_{zS} k_L}$.

If there is a single laser modulator in the ring, and if longitudinal damping partition $J_s = 2$, then the theoretical minimum bunch length and longitudinal emittance in a longitudinal weak focusing ring with respect to the bending radius ρ and angle θ of each bending magnet are

$$\begin{aligned} \sigma_{z,\min} [\mu\text{m}] &\approx 4.93 \rho^{\frac{1}{2}} [\text{m}] E_0 [\text{GeV}] \theta^3 [\text{rad}], \\ \epsilon_{z,\min} [\text{nm}] &\approx 8.44 E_0^2 [\text{GeV}] \theta^3 [\text{rad}]. \end{aligned} \quad (3)$$

Coherent undulator radiation power at the odd- H -th harmonic from a transversely-round electron beam is

$$P_{H,\text{peak}} [\text{kW}] = 1.183 N_u H \chi [JJ]_H^2 F F_{\perp}(S) |b_{z,H}|^2 I_P^2 [\text{A}], \quad (4)$$

where N_u is the number of undulator periods, $[JJ]_H^2 = \left[J_{\frac{H-1}{2}}(H\chi) - J_{\frac{H+1}{2}}(H\chi) \right]^2$, with $\chi = \frac{K^2}{4+2K^2}$, and the transverse form factor $F F_{\perp}(S) = \frac{2}{\pi} \left[\tan^{-1} \left(\frac{1}{2S} \right) + S \ln \left(\frac{(2S)^2}{(2S)^2+1} \right) \right]$, with $S = \frac{\sigma_{\perp}^2 \omega}{L_u}$ and σ_{\perp} the RMS transverse electron beam size, $b_{z,H}$ is the bunching factor at the H -th harmonic, and I_P is the peak current.

Based on the above formulas, here we present an example parameters set in Tab. 1 of a longitudinal weak focusing SSMB storage ring, aimed for high-power infrared radiation generation. As can be seen, such a compact SSMB storage ring can be used for high-power infrared radiation generation. The requirement on the stored laser power is easy to realize in practice. All the other parameters listed are also within practical range. A sharp reader may notice that the microbucket half-height is only twice the natural energy spread of the electron beam. Therefore, in addition to the shallow microbuckets, we need a larger bucket, for example a barrier bucket formed by an induction linac, to

* dengxiujie@mail.tsinghua.edu.cn

WHY IS THE COHERENT RADIATION FROM LASER-INDUCED MICROBUNCHES NARROWBANDED AND COLLIMATED

Xiujie Deng*, Alex Chao¹, Tsinghua University, Beijing, China
¹also at Stanford University, Menlo Park, CA, USA

Abstract

There are two reasons: one is the long coherence length of radiation from microbunches imprinted by the modulation laser, the second is the finite transverse electron beam size. In other words, one is due to the longitudinal form factor, and the other the transverse form factor of the electron beam. Here we study the role of these form factors in shaping the energy spectrum and spatial distribution of microbunching radiation. The investigations are of value for cases like steady-state microbunching (SSMB), coherent harmonic generation (CHG) and free-electron laser (FEL).

GENERAL FORMULATION

For simplicity, as the first step we consider only the impacts of particle position x , y and z , but ignore the particle angular divergence x' , y' and energy deviation δ , on the radiation. We will discuss the requirement of applying this approximation and the impact of beam divergence and energy spread in the end of this paper. With this simplification, the spectrum of radiation from an electron beam with N_e electrons is related to that of a single electron according to

$$\left. \frac{d^2W}{d\omega d\Omega}(\theta, \varphi, \omega) \right|_{\text{beam}} = N_e^2 |b(\theta, \varphi, \omega)|^2 \left. \frac{d^2W}{d\omega d\Omega}(\theta, \varphi, \omega) \right|_{\text{point}} \quad (1)$$

with θ and φ being the polar and azimuthal angles in a spherical coordinate system, respectively, and

$$b(\theta, \varphi, \omega) = \int_{-\infty}^{\infty} \int_{-\infty}^{\infty} \int_{-\infty}^{\infty} \rho(x, y, z) e^{-i\omega \left(\frac{x \sin \theta \cos \varphi + y \sin \theta \sin \varphi + z}{\beta c} \right)} dx dy dz, \quad (2)$$

in which β is the particle velocity normalized by the speed of light in vacuum c and for relativistic beam can be approximated as 1, and $\rho(x, y, z)$ is the normalized charge density satisfying $\int_{-\infty}^{\infty} \int_{-\infty}^{\infty} \int_{-\infty}^{\infty} \rho(x, y, z) dx dy dz = 1$. When the longitudinal and transverse dimensions of the electron beam are decoupled, we can factorize $b(\theta, \varphi, \omega)$ as

$$b(\theta, \varphi, \omega) = b_{\perp}(\theta, \varphi, \omega) \times b_z(\omega), \quad (3)$$

where

$$b_{\perp}(\theta, \varphi, \omega) = \int_{-\infty}^{\infty} \int_{-\infty}^{\infty} \rho(x, y) e^{-i\omega \left(\frac{x \sin \theta \cos \varphi + y \sin \theta \sin \varphi}{c} \right)} dx dy, \quad (4)$$

and

$$b_z(\omega) = \int_{-\infty}^{\infty} \rho(z) e^{-i\omega \frac{z}{\beta c}} dz. \quad (5)$$

Note that $\rho(x, y)$ and $\rho(z)$ are then the projected charge density. $b_z(\omega)$ is the usual bunching factor found in literature and is independent of the observation angle. This however is not true for $b_{\perp}(\theta, \varphi, \omega)$. For example, for an x - y decoupled transversely Gaussian beam, we have

$$|b_{\perp}(\theta, \varphi, \omega)|^2 = \exp \left\{ - \left(\frac{\omega}{c} \right)^2 \left[(\sigma_x \sin \theta \cos \varphi)^2 + (\sigma_y \sin \theta \sin \varphi)^2 \right] \right\}, \quad (6)$$

where $\sigma_{x,y}$ are the RMS beam size in the horizontal, and vertical dimension, respectively.

In order to efficiently quantify the impact of the transverse and longitudinal distributions of an electron beam on the overall radiation energy spectrum, here we define the transverse and longitudinal form factors of an electron beam as

$$FF_{\perp}(\omega) = \frac{\int_0^{\pi} \sin \theta d\theta \int_0^{2\pi} d\varphi |b_{\perp}(\theta, \varphi, \omega)|^2 \frac{d^2W}{d\omega d\Omega}(\theta, \varphi, \omega) \Big|_{\text{point}}}{\int_0^{\pi} \sin \theta d\theta \int_0^{2\pi} d\varphi \frac{d^2W}{d\omega d\Omega}(\theta, \varphi, \omega) \Big|_{\text{point}}}, \quad (7)$$

and

$$FF_z(\omega) = |b_z(\omega)|^2, \quad (8)$$

respectively. The overall form factor is then

$$FF(\omega) = FF_{\perp}(\omega) FF_z(\omega). \quad (9)$$

The total radiation energy spectrum of an electron beam is related to that of a single electron by

$$\left. \frac{dW}{d\omega} \right|_{\text{beam}} = N_e^2 FF(\omega) \left. \frac{dW}{d\omega} \right|_{\text{point}}. \quad (10)$$

LONGITUDINAL FORM FACTOR

Cleanly Separated Microbunch Train

When there are multiple microbunches cleanly separated from each other with a distance of the modulation laser wavelength λ_L , like that in some of the SSMB scenarios [1–3], the longitudinal form factor is that of the single microbunch multiplied by a macro form factor,

$$FF_{z\text{MB}}(\omega) = FF_{z\text{SB}}(\omega) \left(\frac{\sin \left(N_b \frac{\omega \lambda_L}{c} \right)}{N_b \sin \left(\frac{\omega \lambda_L}{c} \right)} \right)^2, \quad (11)$$

where the subscripts _{MB} and _{SB} mean multi bunch and single bunch, respectively, and N_b is the number of

* dengxiujie@mail.tsinghua.edu.cn

OPTICAL STOCHASTIC COOLING IN A GENERAL COUPLED LATTICE

Xiujie Deng*, Tsinghua University, Beijing, China

Abstract

Here we present a formalism of optical stochastic cooling in a 3D general coupled lattice. The formalism is general, and can treat a variety of damping and diffusion mechanisms within a single framework. We expect the work to be of value for the development of future light source.

GENERAL FORMALISM OF STORAGE RING PHYSICS

Particle state vector $\mathbf{X} = (x, x', y, y', z, \delta)^T$ is used throughout this paper, with its components meaning the horizontal position, horizontal angle, vertical position, vertical angle, longitudinal position, and relative energy difference of a particle with respect to the reference particle, respectively. The superscript T means the transpose of a vector or matrix. Following Chao's solution by linear matrix (SLIM) formalism [1], we can introduce the definition of the generalized beta functions in a 3D general coupled storage ring lattice as

$$\beta_{ij}^k = 2\text{Re} \left(\mathbf{E}_{ki} \mathbf{E}_{kj}^* \right), \quad k = I, II, III, \quad (1)$$

where $*$ means complex conjugate, the sub or superscript k denotes one of the three eigenmodes, $\text{Re}()$ means the real component of a complex number or matrix, \mathbf{E}_{ki} is the i -th component of vector \mathbf{E}_k , and \mathbf{E}_k are eigenvectors of the 6×6 symplectic one-turn map \mathbf{M} with eigenvalues $e^{i2\pi\nu_k}$, satisfying the following normalization condition

$$\mathbf{E}_k^\dagger \mathbf{S} \mathbf{E}_k = \begin{cases} i, & k = I, II, III, \\ -i, & k = -I, -II, -III, \end{cases} \quad (2)$$

and $\mathbf{E}_k^\dagger \mathbf{S} \mathbf{E}_j = 0$ for $k \neq j$, where † means complex conjugate transpose, and

$$\mathbf{S} = \begin{pmatrix} 0 & 1 & 0 & 0 & 0 & 0 \\ -1 & 0 & 0 & 0 & 0 & 0 \\ 0 & 0 & 0 & 1 & 0 & 0 \\ 0 & 0 & -1 & 0 & 0 & 0 \\ 0 & 0 & 0 & 0 & 0 & 1 \\ 0 & 0 & 0 & 0 & -1 & 0 \end{pmatrix}. \quad (3)$$

Since the one-turn map is a real symplectic matrix, for a stable motion, we have

$$\nu_{-k} = -\nu_k, \quad \mathbf{E}_{-k} = \mathbf{E}_k^*. \quad (4)$$

Using the generalized beta function, we can write the eigenvector component as

$$\mathbf{E}_{kj} = \sqrt{\frac{\beta_{jj}^k}{2}} e^{i\phi_j^k}. \quad (5)$$

And according to definition we have

$$\beta_{ij}^k = \sqrt{\beta_{ii}^k \beta_{jj}^k} \cos(\phi_i^k - \phi_j^k). \quad (6)$$

Similarly, here we introduce the definition of imaginary generalized beta functions as

$$\hat{\beta}_{ij}^k = 2\text{Im} \left(\mathbf{E}_{ki} \mathbf{E}_{kj}^* \right), \quad k = I, II, III, \quad (7)$$

where $\text{Im}()$ means the imaginary component of a complex number or matrix. Further we can define the real and imaginary generalized Twiss matrices of a storage ring lattice corresponding to three eigen mode as

$$(\mathbf{T}_k)_{ij} = \beta_{ij}^k, \quad (\hat{\mathbf{T}}_k)_{ij} = \hat{\beta}_{ij}^k, \quad k = I, II, III. \quad (8)$$

Due to the symplecticity of the one-turn map, we have

$$\mathbf{T}_k^T = \mathbf{T}_k, \quad \hat{\mathbf{T}}_k^T = -\hat{\mathbf{T}}_k, \quad (9)$$

where T means transpose. The generalized Twiss matrices at different places are related according to

$$\begin{aligned} \mathbf{T}_k(s_2) &= \mathbf{R}(s_2, s_1) \mathbf{T}_k(s_1) \mathbf{R}^T(s_2, s_1), \\ \hat{\mathbf{T}}_k(s_2) &= \mathbf{R}(s_2, s_1) \hat{\mathbf{T}}_k(s_1) \mathbf{R}^T(s_2, s_1), \end{aligned} \quad (10)$$

with $\mathbf{R}(s_2, s_1)$ being the transfer matrix from s_1 to s_2 .

The action or generalized Courant-Snyder invariants of a particle are defined according to

$$J_k \equiv \frac{\mathbf{X}^T \mathbf{G}_k \mathbf{X}}{2}, \quad k = I, II, III, \quad (11)$$

where

$$\mathbf{G}_k \equiv \mathbf{S}^T \mathbf{T}_k \mathbf{S}. \quad (12)$$

It is easy to prove that J_k are invariants of a particle when it travels around the ring, from the symplectic condition $\mathbf{R}^T \mathbf{S} \mathbf{R} = \mathbf{S}$. The three eigenemittance of a beam containing N_p particles are defined according to

$$\epsilon_k \equiv \langle J_k \rangle = \frac{\sum_{i=1}^{N_p} J_{k,i}}{N_p}, \quad k = I, II, III, \quad (13)$$

where $J_{k,i}$ means the k -th mode invariant of the i -th particle.

Assume there is a perturbation \mathbf{K} to the one-turn map \mathbf{M} , i.e., $\mathbf{M}_{\text{per}} = (\mathbf{I} + \mathbf{K}) \mathbf{M}_{\text{unp}}$. From canonical perturbation theory [2], the tune shift of the k -th eigen mode is then

$$\Delta\nu_k = -\frac{1}{4\pi} \text{Tr} \left[\left(\mathbf{T}_k + i\hat{\mathbf{T}}_k \right) \mathbf{S} \mathbf{K} \right], \quad (14)$$

where $\text{Tr}()$ means the trace of a matrix. This formula can be used to calculate the real and imaginary tune shifts due to symplectic (for example lattice error) and non-symplectic

* dengxiujie@mail.tsinghua.edu.cn

A RECURSIVE MODEL FOR LASER-ELECTRON-RADIATION INTERACTION IN INSERTION SECTION OF SSMB STORAGE RINGS BASED ON THE TRANSVERSE-LONGITUDINAL COUPLING SCHEME

Cheng-Ying Tsai*, Huazhong University of Science and Technology, Wuhan, China
 Xiujie Deng, Tsinghua University, Beijing, China

Abstract

Recently, a mechanism of steady-state microbunching (SSMB) in the storage ring has been proposed and investigated. The SSMB aims to maintain the same excellent high repetition rate, close to continuous-wave operation, as the storage ring. Moreover, replacing the conventional RF cavity with a laser modulator for longitudinal focusing, the individual electron bunches can be microbunched in a steady state. The microbunched electron bunch train, with an individual bunch length comparable to or shorter than the radiation wavelength, can not only produce coherent powerful synchrotron radiation but may also be subject to FEL-like collective instabilities. Our previous analysis was based on the wake-impedance model. In this paper, we have developed a recursive model for the laser modulator in the SSMB storage ring. In particular, the transverse-longitudinal coupling scheme is assumed. Equipped with the matrix formalism, we can construct a recursive model to account for turn-by-turn evolution, including single-particle and second moments. It is possible to obtain a simplified analytical expression to identify the stability regime or tolerance range for non-perfect cancellation.

INTRODUCTION

Recently there has been a growing interest in the mechanism of the so-called steady-state microbunching (SSMB) in a storage ring proposed as a potential new light source [1–5]. The existing literature for the studies of electron dynamics in the laser modulators mainly focuses on single-particle dynamics, e.g., Refs. [6–9], or the radiation output characteristics based on the prescribed electron trajectories [10, 11]. The collective dynamics occurring in the laser modulators has only recently been studied [12–14] using the wake-impedance model for the case of a *single* laser modulator.

In a current design a pair of two laser modulators, where the radiator is sandwiched, is considered; see Fig. 1. In this work we propose an alternative model to study the laser-electron-radiation interaction in the laser modulators of SSMB storage rings based on the transverse-longitudinal coupling (TLC) scheme [10], by constructing a recursive model to account for multi-pass radiation dynamics in nonlinear regime to analyze multi-bunch multi-turn dynamics [9]. In the model there are two options for us to study the dynamics: non-perfect kick model and FEL-like model.

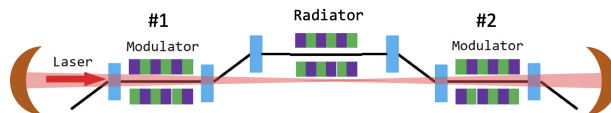


Figure 1: Conceptual schematic layout of SSMB laser modulator based on TLC scheme. The two laser modulators can be independent.

THEORETICAL FORMULATION

In the recursive formulation, the laser-electron-radiation dynamics can in principle be nonlinear. However the energy chirp is linearized; therefore the validity is limited to $\sigma_z \ll \lambda_L$. We assume the microbunch circulates clockwise. Considering the state vector $[y \ y' \ z \ \delta]^T$ at the middle of the storage ring (e.g., at RF or main-ring laser modulator), the transport from which to the insertion entrance can be formulated as a half ring $\mathbf{R}_{1/2}$, which is

$$\begin{pmatrix} \cos \pi \nu_y & \beta_y \sin \pi \nu_y & 0 & 0 \\ -\frac{1}{\beta_y} \sin \pi \nu_y & \cos \pi \nu_y & 0 & 0 \\ 0 & 0 & \cos \pi \nu_s & \beta_z \sin \pi \nu_s \\ 0 & 0 & -\frac{1}{\beta_z} \sin \pi \nu_s & \cos \pi \nu_s \end{pmatrix}, \quad (1)$$

where β_y, ν_y and β_z, ν_s parametrize the transverse and longitudinal motions, respectively. The synchrotron tune ν_s is determined by the RF/laser modulator of the storage ring with the slippage factor η_{ring} and the circumference C_{ring} . Here we have implicitly assumed Courant-Snyder functions are the same at the RF, the entrance and exit of the insertion section. The insertion section begins from the vertical bending magnet

$$\mathbf{M}_B = \begin{pmatrix} 1 & 0 & 0 & 0 \\ 0 & 1 & 0 & R_{46} \\ -R_{46} & 0 & 1 & 0 \\ 0 & 0 & 0 & 1 \end{pmatrix}, \quad (2)$$

and the following first laser modulator

$$\mathbf{M}_{LM}^{(1)} = \begin{pmatrix} 1 & N_u \lambda_u & 0 & 0 \\ 0 & 1 & 0 & 0 \\ 0 & 0 & \cos \chi^{(1)} & \frac{R_{56,LM}}{\chi^{(1)}} \sin \chi^{(1)} \\ 0 & 0 & \frac{h^{(1)}}{\chi^{(1)}} \sin \chi^{(1)} & \cos \chi^{(1)} \end{pmatrix}, \quad (3)$$

with N_u, λ_u the number and period length of the undulator, $\chi^{(1)} = \sqrt{-R_{56,LM} h^{(1)}}$, $R_{56,LM}, h$ being the longitudinal

* jcytsai@hust.edu.cn

AN INVERSE-COMPTON SCATTERING SIMULATION MODULE FOR RF-TRACK

A. Latina*, V. Muşat¹, CERN, Geneva, Switzerland
¹also at The University of Oxford, Oxford, UK

Abstract

A simulation module implementing Inverse-Compton scattering (ICS) was added to the tracking code RF-Track. The module consists of a special beamline element that simulates the interaction between the tracked beam and a laser, making RF-Track capable of simulating a complete ICS source in one go, from the electron source to the photons. The description of the laser allows the user to thoroughly quality the laser in terms of wavelength, pulse energy, pulse length, incoming direction, M^2 parameter, aspect ratio, polarisation and whether the laser profile should be Gaussian or uniform. Furthermore, as the code implements fully generic expressions, the scattering between photons and different particles than electrons can be simulated. A benchmark against CAIN showed excellent agreement and that RF-Track outperforms CAIN in terms of computational speed by orders of magnitude.

INTRODUCTION

Light sources based on Inverse Compton Scattering are attracting growing attention due to their compactness, high brilliance, and the capability to reach a wide range of photon energies, from X-rays (few keV) to gamma rays (few MeV), the latter inaccessible to most light sources including synchrotrons.

Inverse Compton scattering takes place when a charged particle transfers a fraction of its momentum to a photon, increasing its energy. The maximum final photon energy achievable in an ICS interaction occurs in case of a *head-on* collision. If the initial energy of the photon is E_i , the final energy E_f is given by

$$E_f = 4\gamma^2 E_i,$$

where γ is the relativistic factor of the scattering particle [1]. In the case of ultra-relativistic electrons, the photon's energy can increase by several orders of magnitude.

While designing an ICS source, the simulation of ICS is crucial to assess the scattered photons' spectral properties, bandwidth, and angular distribution. The most accredited code for simulating Inverse Compton Scattering is probably CAIN, written by Yokoya et al. [2]. CAIN is a stand-alone Monte Carlo program that simulates beam-beam interactions involving high-energy electrons, positrons, and photons. The code covers the classical and quantum domains in linear and weakly nonlinear regimes. The interaction is described as the scattering between particles and has been extensively tested and compared to experimental results.

Despite its excellent reputation, the practical application of CAIN towards optimising an ICS-based facility is hindered by two primary limitations: (1) it operates rather slowly, and (2) as a standalone code, it requires an interface with conventional particle tracking codes that can transport electrons through the accelerator to the interaction point (IP), making integrated performance optimisation challenging.

To circumvent these limitations, the author of this paper developed a simulation module as a part of the tracking code RF-Track [3]. Since RF-Track can track particles with any charge through an accelerator while accounting for the effects of space charge, beam loading, wakefields, etc., this module enables the simulation of an ICS source from cathode to X-rays in one go. This unlocks a thorough optimisation of the source being designed.

The module was written in parallel C++ and showed simulation speed orders of magnitude faster than CAIN. This paper provides a detailed description of the implementation and two benchmarking cases.

IMPLEMENTATION

To the user, the collision point consists of a specialised lattice element called "LaserBeam" that simulates the scattering between the tracked beam and a laser. This element allows the user to define the key laser parameters: wavelength, pulse energy, pulse length, incoming direction (which can be arbitrarily chosen over the entire solid angle), the M^2 parameter, the aspect ratio, the degree of linear polarisation (optional), and whether the laser beam has a Gaussian or a uniform profile.

LaserBeam is a time-dependent element that the user can synchronise to the beam or an absolute clock. Like any other RF-Track's lattice element, it can be arbitrarily displaced by any offset and angle, allowing for misalignment imperfection studies. The element can have a length or be thin; in either case, the entire three-dimensional structure of the bunch is reconstructed during the computation.

The scattering is computed in the rest frame of the charged particle as a Monte Carlo process. When the photon's energy is much lower than the particle's rest energy, its absolute momentum and wavelength remain unchanged during the collision. In this case, the scattering is elastic and is called *Thomson scattering*. Proper *Compton scattering* occurs at higher photon energies when there is a momentum transfer between the particle and the photon, and the scattering is inelastic. After the computation of the scattering, the phase-space variables of particle and photon are updated and moved back to the laboratory frame, where tracking continues for both species.

* andrea.latina@cern.ch

RECENT DEVELOPMENTS OF THE cSTART PROJECT

M. Schwarz*, A. Bernhard, E. Bründermann, B. Härer, D. El Khechen, A. Malygin,
 M.J. Nasse, G. Niehues, A. Papash, R. Ruprecht, J. Schäfer, M. Schuh, N. Smale,
 P. Wesolowski, Ch. Widmann, A.-S. Müller
 Karlsruhe Institute of Technology, Karlsruhe, Germany

Abstract

The combination of a compact storage ring and a laser-plasma accelerator (LPA) can serve as the basis for future compact light sources. One challenge is the large momentum spread (about 2 %) of the electron beams delivered by the LPA. To overcome this challenge, a very large acceptance compact storage ring (VLA-cSR) was designed as part of the compact Storage ring for Accelerator Research and Technology (cSTART) project. The project will be realized at the Karlsruhe Institute of Technology (KIT, Germany). Initially, the Ferninfrarot Linac- Und Test-Experiment (FLUTE), a source of ultra-short bunches, will serve as an injector for the VLA-cSR to benchmark and emulate LPA-like beams. In a second stage, a laser-plasma accelerator will be used as an injector, which is being developed as part of the ATHENA project in collaboration with DESY and the Helmholtz Institute Jena (HIJ). The small facility footprint, the large-momentum spread bunches with charges from 1 pC to 1 nC and lengths from few fs to few ps pose challenges for the lattice design, RF system and beam diagnostics. This contribution summarizes the latest results on these challenges.

INTRODUCTION

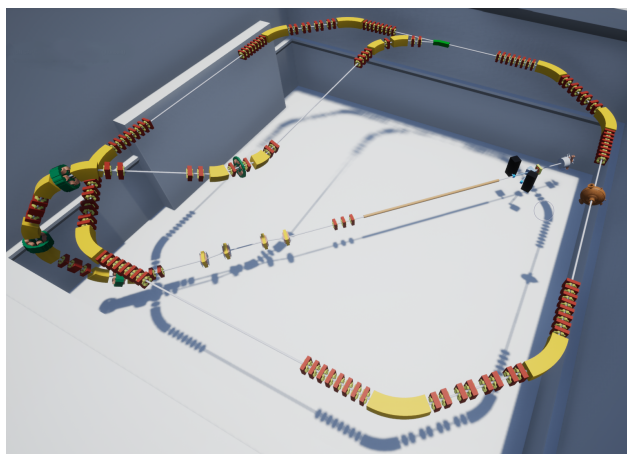


Figure 1: Artistic view of the cSTART project. The cSTART storage ring at a height of about 3.5 m is connected to the FLUTE injector by a complex 3D transfer line. The LPA (not shown) will be at the same height as the storage ring and uses the last part of the transfer line of FLUTE for injection.

Laser-based plasma acceleration can deliver electron bunches with high peak current and ultra-short bunch lengths

* markus.schwarz@kit.edu

Table 1: Main Parameters of the cSTART Storage Ring

Parameter	Value	Unit
Circumference	43.2	m
Energy range	40 to 60	MeV
Injection rate	10	Hz
Injection type	one-turn swap-out	–
Beam storage time	100	ms
Bunch charge	1 to 1000	pC
Revolution period	144	ns
Revolution frequency	6.94	MHz
Incoherent energy loss	0.54	eV
Damping time (h, v, l)	29.5, 26.5, 12.6	s
Coherent energy loss (1 pC, 20 fs)	160	keV
Critical frequency f_{crit}	37.7	THz
Tune (h, v, l)	5.18, 1.66, 0.023	1
Momentum compaction:		
nominal	14.8×10^{-3}	1
reduced- α	3.9×10^{-3}	1
RF frequency	500	MHz
RF voltage	500	kV
Harmonic number	72	1
Vacuum pressure	1×10^{-8}	mbar

on a compact facility footprint. This makes LPAs attractive candidates for light sources, since ultra-short bunches emit intense coherent radiation in the THz regime [1]. However, their large beam divergence and energy spread require dedicated beam transport systems and insertion devices [2]. Moreover, their repetition rate is limited to a few Hz compared to MHz at storage rings.

The cSTART project develops the infrastructure and technology necessary for a compact LPA-based light source. A key component is the construction of a very-large momentum acceptance compact storage ring to inject and store sub-ps short electron bunches. One injector is a LPA developed in cooperation with DESY and HIJ [3]. The linac-based accelerator FLUTE [4] will serve also as injector to provide well-defined LPA-like bunches for benchmarking and to further explore injection of ultra-short, 10 fs-range electron bunches. An artistic view of the cSTART storage ring on top of FLUTE is shown in Fig. 1. In storing a sub-ps short bunch, the ring would act as a “multiplier” to push the few Hz injection rate to a MHz repetition rate.

With two different injectors, the beams at cSTART cover a large region in parameter space. In simulations, the LPA beam achieved a bunch charge of 20 pC with mean energy of

OPERATING LIQUID METALJET X-RAY SOURCES FOR MATERIALS RESEARCH

Mirko Boin, Roland Mainz, Manuela Klaus, Daniel Apel, Paul H. Kamm, Robert C. Wimpory,
Francisco García-Moreno, Guido Wagener, Christoph Genzel,
Helmholtz-Zentrum Berlin für Materialien und Energie GmbH, Berlin, Germany

Abstract

Even on the 100th anniversary of the death of Wilhelm Conrad Röntgen the demand for applications of his discovery of X-rays is not diminishing. On the contrary, both academic and industrial research and development need X-ray generating devices with ever-improving properties to meet the current challenges of science and technology. For this reason, the development of next-generation synchrotrons is being driven forward and made available to users worldwide. Nevertheless, the availability of synchrotron beamtime will always remain limited, even with the most brilliant sources for ultra-fast and high-throughput experiments. That is why the operation of and research with decentralized laboratory equipment becomes just as important. In this context, Helmholtz-Zentrum Berlin (HZB) has commissioned Excillum's MetalJet X-ray devices providing photon energies in the hard X-ray regime. Technical specifications of these sources, the HZB diffractometer lab installations and selected examples are shown. A comparison to synchrotron measurements is made to benchmark the performance of the available setups.

INTRODUCTION

Non-destructive testing methods utilizing conventional laboratory (desktop) X-ray sources have become a successful tool for more and more academic and industrial research purposes, such that their physical limits, for example according to the material's penetration depths, have been extended using high-energy synchrotron photons. Furthermore, high-brilliance synchrotron photons have made fast in-situ and in-operando experiments possible.

However, the increasing demand for measurement time at such facilities contrasts with their availability – the beamtime at synchrotron sources is very limited. Moreover, as a rule, the access to the beamlines cannot be obtained promptly. Waiting times of half a year or longer are quite common in this field. Synchrotron beamlines are usually overbooked many times. Hence, it seems sensible and necessary in several ways to use suitable laboratory X-ray sources as well. With their help, numerous questions can be answered which do not necessarily require the use of expensive and in their availability mostly very limited large-scale facilities.

It is the motivation of this work to address the lack of beamtime with the development of tailored measurement and evaluation methods including the implementation of appropriate experimental hardware using laboratory X-ray sources. Here, novel X-ray sources are presented that help to transport a number of applications from the synchrotron

to decentralized laboratories and thus make the analysis of microstructural properties available to a larger community.

LIQUID METALJET X-RAY SOURCES

Inside laboratory and desktop X-ray devices electrons are extracted from a cathode and accelerated within an electric field into the direction of an anode, where their deceleration leads to an energy conversion into heat and X-rays. In general, the X-ray power of all electron-impact X-ray sources is limited by the thermal power loading of the anode. In solid-anode technology, the surface temperature of the anode must be cooled down and stay well below its melting point to avoid damage. Consequently, the yield in terms of photon flux of conventional fixed-anode X-ray tubes is rather low compared to synchrotron radiation. Although the X-ray output can be increased significantly with the use of rotating-anode tubes, the melting limitation of the solid anode material remains.

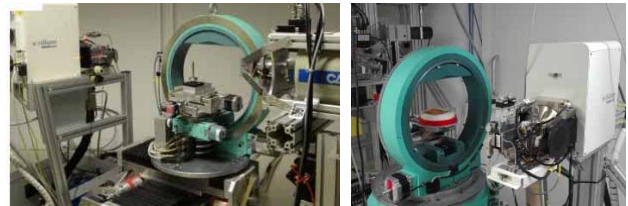


Figure 1: Photographs of the LIMAX-70 (left) and LIMAX-160 (right) laboratories.

In contrast, a liquid metal anode changes this condition since the limitation to maintain the target at well below the melting point is inexistent – the material is already molten. This approach is implemented by the MetalJet products available from the Swedish company Excillum. Two of their MetalJet D2 X-ray sources have been installed at HZB to equip a suite of the so-called LIMAX laboratories (see Fig. 1) for microstructural, residual stress and imaging characterizations. These sources continuously supply fresh target material. The liquid anode, composed of a Ga-In alloy liquid already at room temperature, is provided via a closed high-pressure circuit at 190 bars. A very fine liquid metal jet of a diameter of about 180 μm is formed with the help of a nozzle. The electrons are released by a LaB₆ cathode and accelerated into the direction of the liquid anode under a voltage of 70 kV and 160 kV respectively. With the help of focusing optics a very well-defined electron spot of down to 5 μm \times 5 μm is created at the edge of the metal jet. The X-ray spectrum emitted consists of a broad range of Bremsstrahlung (the white beam) up to 70 keV and 160 keV respectively, depending on the excitation voltage. In addition, and due to the extremely high-power loading,

MULTI-FELOs DRIVEN BY A COMMON ELECTRON BEAM

C.-Y. Tsai*, Huazhong University of Science and Technology, Wuhan, China

Y. Zhang†, Thomas Jefferson National Accelerator Facility, Newport News, VA, USA

Abstract

Generating a free-electron laser (FEL) requires a high-brightness electron beam. To produce multiple FELs, the linac beam must be shared to enable one beam driving an undulator. This leads to a reduced average current and compromised FEL performance. Recently, a concept of multiple FELs driven by one electron beam was proposed, which enables reduction of equipment and improvement of productivity. We present here a simulation study based on an extended 1-D FEL oscillator model to demonstrate this concept. The system consists of two FEL oscillators arranged side-by-side and one electron beam passing through them. As such, the second, downstream oscillator is driven by bunches already been used once, while the first oscillator always receives fresh bunches from the linac. The study shows lasing could be achieved for both oscillators, their radiation intensities at saturation are comparable, thus meet needs of users. The concept also enables a potential application using a circular ring such that an oscillator can be driven alternately by fresh linac bunches and from used bunches in the circular ring. Extending the concept to cases of more than two FEL oscillators driven by one beam is also explored.

CONCEPT OF THE SCHEME

In 1984 Colella and Lucio [1] proposed the feasibility of a low-gain FELO emitting at $2 \sim 3 \text{ \AA}$ using silicon single crystal diffraction around a right angle. With significant advance in accelerator technologies over the past 40 years, an electron beam with multi-GeV energy, multi-pC bunch charge, lower than $1 \mu\text{m}$ of the normalized emittance, and smaller than 10^{-4} of the energy spread can now be produced. In 2008 K.-J. Kim et al. [2] re-evaluated the idea and proposed using an FEL oscillator mode based on a high-repetition rate ERL-SRF and GeV electron beam to produce coherent radiation at 1 \AA . Currently, the FEL community is actively investing in the development of x-ray FELO construction.

XFELo is a small-gain FEL, its undulator is much shorter compared to those used for SASE-like single-pass FELs, thus the radiation fields are built up slowly through many rounds in the optical cavity. Therefore, it is expected that the backreactions, namely interaction of the radiation fields on electrons, are usually much weaker, at least before the radiation fields reach saturation, and likely so after. As a consequence, perturbation on electrons, i.e., distortion of bunch phase space distribution, over each pass of individual short undulator is relatively small. This fact suggests that these lightly used bunches might be undegraded enough for driving next XFELos in serial [3]. With proper design beam

parameters, the electron bunches could be reused multiple times before being extracted and sent to beam dump. There will be a small reduction of gain for used bunches due to backreactions, but that could be compensated by lower losses in the optical cavity and it may also take more rounds of the light pulse to grow in the optical cavity. Eventually the radiation fields will reach a similar level of laser intensity at saturation, since the latter is determined by a balance of gain in undulator and combined loss of reflective crystal mirrors and radiation outcoupling.

MODEL DESCRIPTION

In this paper, we use a simple two-XFELo system to illustrate the concept, similar to the model used in Ref. [4]. The FELos are arranged side-by-side as shown in Fig. 1. The driving electron beam from the source and SRF linac passes through undulators of the two XFELos while interacting with and amplifying the radiation fields in both undulators. The spent electron bunch is extracted and goes to a beam dumper. At meantime, the next fresh bunch from the SRF linac enters the dual undulator system.

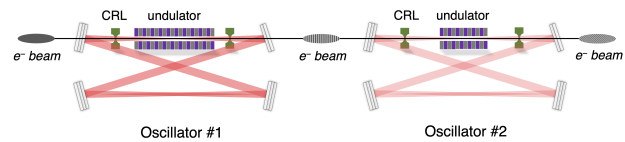


Figure 1: Conceptual schematic layout for the two-oscillator scheme. Bragg mirrors, consisting of three high-reflectivity mirrors and one mirror used for outcoupling, and two Be compound refractive lenses (CRLs) used for focusing are employed to form the oscillator. This design allows two independent users to conduct experiments.

The overall performance of the two x-ray FEL oscillators in serial is analyzed using an extended 1-D FEL model

$$\frac{d\theta_j}{d\tau} = p_j, \quad \frac{dp_j}{d\tau} = -\left(Ae^{i\theta_j} + c.c.\right), \quad \frac{dA}{d\tau} = \langle e^{-i\theta_j} \rangle + i\delta A \quad (1)$$

where τ is the scaled time along the undulator $\tau = 2\omega_u \rho t$, $\omega_u = c\beta_z k_u$, β_z is the longitudinal electron velocity along the undulator, $k_u = 2\pi/\lambda_u$ with λ_u the undulator period. The

Pierce parameter $\rho = \left[\frac{1}{\gamma_r^3} \frac{I_b}{I_A} \frac{K^2 [JJ]^2}{32\pi} \frac{\lambda_u^2}{2\pi\sigma_\perp^2} \right]^{\frac{1}{3}}$ with $[JJ] = J_0(\chi) - J_1(\chi)$, $\chi = \frac{K^2}{4+2K^2}$, $K \approx 0.934\lambda_u[\text{cm}]B_u[\text{T}]$, $J_{0,1}$ being the 0th and 1st order of Bessel functions of the first kind. Here (θ_j, p_j) for $j = 1, 2, \dots, N_e$ are the j -th electron phase space coordinate, with $p_j = \frac{\gamma_j - \gamma_r}{\rho\gamma_r}$. γ_r is the resonant electron energy (in unit of electron rest mass energy) satisfying the resonance condition $\lambda_r = \frac{\lambda_u}{2\gamma_r} \left(1 + \frac{K^2}{2}\right)$, $\omega_r = c k_r$,

* jcytsai@hust.edu.cn

† yzhang@jlab.org

HEAT LOAD AND RADIATION PULSE OF CORRUGATED STRUCTURE AT SHINE FACILITY

Junjie Guo¹, Duan Gu², Zhen Wang², Meng Zhang^{2,*}, Qiang Gu², Haixiao Deng^{2,†}

¹Zhangjiang laboratory, Shanghai, China

²Shanghai Advanced Research Institute, Chinese Academy of Sciences, Shanghai, China

Abstract

Corrugated structure modules are being proposed for installation after the end of the linac and before the undulator regions of SHINE facility, where it has been used for energy chirp control and as a fast kicker for two color operation of the FEL. When ultra-relativistic bunch of electrons passing through corrugated structure will generate strong wakefield, we find most of the wake power lost by the beam is radiated out to the sides of the corrugated structure in the form of THz waves, and the remaining part cause Joule heating load on the corrugated structure wall. In this paper, we estimate the Joule power loss and radiation pulse power of the corrugated structure in SHINE facility.

INTRODUCTION

In order to eliminate residual energy chirps in superconducting linear accelerator (linac)-driven X-ray FEL facilities, there are currently two traditional ways: one involves exploiting the resistive-wall wakefield induced by the beam pipe; another option, which involves running the beam ‘off-crest,’ is inefficient and costly, especially for ultrashort bunches in FEL facilities [1]. As far as SHINE linac [2, 3] is concerned, the electron bunch length is less than 10 fm after passing through the second bunch compressor. Therefore, the beam energy spread cannot be effectively compensated by chirping the RF phase of the main linac. The SHINE linac adopts the corrugated structure (Fig. 2) to dechirp the energy spread [4].

When an ultra-short electron bunch passing through very small gap corrugated structure, strong wake effect be generated to manipulate the phase space of the electron bunch. Most of the power radiates out along the opening of the corrugated structure, and only a small amount of power causes a heat load on the metal wall of the corrugated structure. The paper is organized as follows. In the 2nd section, the main parameters of corrugated structure in Shine Facility are introduced briefly, and the distribution wake power lost by the beam through the corrugated structure is also described. In the 3rd section total wake power lost by beam are investigated, and the heat load and distribution of the corrugated structure are calculated by numerical simulation. The 4th section introduces a radiation pulse generated by corrugated structure, and calculate the centre frequency and length of the pulse at the outlet of the corrugated structure, as well as the length of the required cooling water pipe. The final section summarizes the results and significance of this paper.

* zhangmeng@sari.ac.cn

† denghx@sari.ac.cn

THE DISTRIBUTION OF WAKE POWER LOST BY THE BEAM THROUGH THE CORRUGATED STRUCTURE

Schematic diagram of the corrugated structure is shown in the Fig. 1, the red ellipse indicates the on-axis bunch. The transverse directions are denoted x and y, with x pointing into the page, and z represents the longitudinal direction. The corrugated structure parameters are the radius a , the depth h , the period p and the gap width t . The parameters for the corrugated structure and for the exciting bunch to be used in simulations presented below are given in Table 1

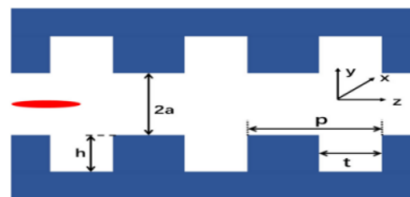


Figure 1: Schematic diagram of the corrugated structure.

Table 1: Parameters for the corrugated structure and for the exciting bunch.

Parameter	Value
Plate length, L (m)	2
Gap, a (mm)	0.7
Depth, h (mm)	0.5
Period, p (mm)	0.5
Longitudinal gap, t (mm)	0.25
Width, w(mm)	12.7
W/2a	9.07
Energy, E (GeV)	8
Charge per bunch, Q (pC)	100
Beam current, I (kA)	1.5
Bunch length (RMS), σ (μm)	5

According to the previous work by K. Bane [5–7], in a flat corrugated structure of a finite length, the wakefield energy loss experienced by a relativistic beam of charged particles is partly absorbed in the walls as Joule heat and partly generates a THz pulse that leaves the structure just behind the driving particle. The energy per unit length lost by the beam to the wake is then given by the sum:

$$P_w = P_h + (P_{\text{rad}})_z + (P_{\text{rad}})_x \quad (1)$$

UPGRADES OF HIGH LEVEL APPLICATIONS AT SHANGHAI SOFT X-RAY FEL FACILITY

H. Luo, D. Gu, Z. Wang, K.-Q. Zhang, T. Liu,

Shanghai Advanced Research Institute (SARI-CAS) Chinese Academy of Sciences, Shanghai, China

Abstract

The Shanghai soft X-ray free-electron laser(SXFEL) facility has made significant progress in recent years with the rapid, upgraded iterations of the high level software, including but not limited to energy matching, orbit feedback and load, beam optimization, etc. These tools are key components in operation and experiment of free electron laser facility. Some key applications are presented in this paper.

INTRODUCTION

Based on the principle of the free-electron lasers [1], the output of the free-electron laser drifts and fluctuates with the instability of the electron beam energy, the instability of the angle and position of the electron beam, the instability of each device due to environmental changes, and the instability of the device itself. A stable electron beam is the key to obtaining a stable free-electron laser. The commissioning of the e SXFEL user facility started in spring of 2021 [2], and in 2023, the SXFEL facility has been opened to the public and user experimental research has been carried out, placing a higher demand on the stability of the entire device. In order to maintain the long-term high-quality operation of the SXFEL facility, with the joint efforts of our team, through the interaction and access of applications and hardware systems implemented by the Experimental Physics and Industrial Control System (EPICS [3]), we developed and put online a set of processed beam-tuning high-level applications (SXFEL HLA) written in python language in 2022. Based on these applications, we can achieve rapid recovery and long-term stable operation of SXFEL, and practice has confirmed the reliability and sophistication of this software, which has played an indispensable role in the tuning and operation of SXFEL. This article will report on some key applications. The main window of SXFEL's high level applications is shown in Fig. 1

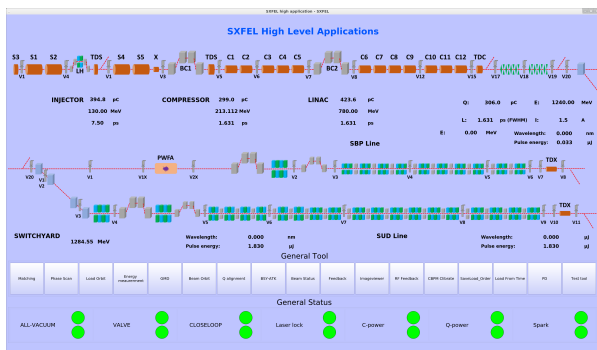


Figure 1: The main window of SXFEL's high level applications.

MATCHING

We all know that the focusing of the electron beam in the transverse direction is crucial to the stability of the beam and the amplification of the FEL, and through theoretical simulation calculations, we can get the target reasonable focusing state of the beam. Therefore, in order to get the focusing state we want, we design and develop the Matching module (shown in Fig. 2), which divides the matching of the beam into linear section, beam distribution section, SBP oscillator section and SUD oscillator section. The Energy Measurement module measures the energy and Emittance Measurement module measures the Twiss parameters, and the measurement results are placed in the background through the soft IOC for the Matching module to call. The inverse solution of the inlet parameters by this Twiss parameter is then solved by the theoretical simulation method of the Matching module.

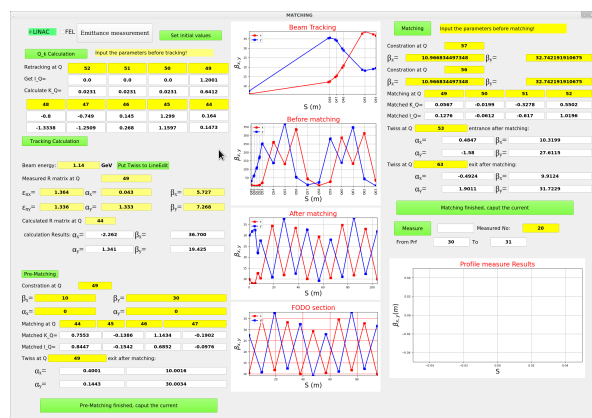


Figure 2: Matching Window.

ORBIT CONTROL MODULES

Combined with these applications: LoadOrbit, Orbit, ImageViewer and BPM Calibrate, orbit feedback (shown in Fig. 3) is one of the key feedbacks to maintain high quality and long term stability of the SXFEL facility. For the consideration of the flexibility, ease of use and reliability of the application, we have linked the orbit feedback with the newly developed tuning tools: LoadOrbit, Orbit, ImageViewer and BPM Calibrate.

The BPM may drift in phase with changes in ambient temperature and humidity. In order to ensure the accuracy of the beam position measured by the BPM, we regularly use the high-level application BPM Calibrate (shown in Fig. 4) to detect and calibrate the phase drift of the BPM, which

PHYSICS DESIGN AND BEAM DYNAMICS OPTIMIZATION OF THE SHINE ACCELERATOR

Duan Gu*, Xuan Li, Zhen Wang, Meng Zhang,

Shanghai Advanced Research Institute, Chinese Academy of Sciences, Shanghai, China

Abstract

Shanghai High Repetition Rate X-ray Free Electron Laser and Extreme Light Facility (SHINE) is a hard X-ray FEL facility which is driven by a 1.3 km superconducting Linac, aims to provide high repetition rate pulses up to 1 MHz. We present the physics design of the SHINE accelerator and considerations of beam dynamics optimizations. Start-to-end simulation results show that, a high brightness electron beam with over 1500 A quasi-flat-top current can be attained which fully meet the requirements of FEL lines. Furthermore, the design of bypass line is discussed.

INTRODUCTION

In recent years, high-repetition-rate XFEL based on superconducting Linac draws increasing attention due to its unique capability of providing Ångström performance at high average power. Several facilities have been built in the world such as EXFEL [1] and LCLS-II [2].

The SHINE facility currently under construction at SARI aims to deliver FEL pulses between 0.4 keV and 25 keV, which enable research in various fields, including biology, chemistry, and material science. To meet the requirements of FEL performance, the Linac of SHINE should provide 8 GeV high brightness electron beam up to 1 MHz, with normalized emittance of $< 0.5 \mu\text{m}$ at nominal 100 pC and peak current over 1500 A. In this paper, we describe the beam dynamics studies including longitudinal working point optimization and lattice matching. Then the detailed start to end simulation results are presented. Finally, the design of a bypass line design is also discussed.

LAYOUT AND MAIN PARAMETERS

At the end of the injector, the bunch length is 1 mm and the peak current is about 10 A. In the Linac section, the beam will be further accelerated to 8 GeV in four acceleration sections (L1, L2, L3 and L4) which consist of seventy-five 1.3 GHz superconducting cryomodules. To obtain the desired peak current, the beam will be compressed to over 1500 A in two bunch compression sections (BC1 and BC2). In addition, two 3.9 GHz cryomodules are used before BC1 as linearizer.

Two beam collimation sections (COL0 and COL1) are placed before L1 and after BC1 to remove undesired stray electrons which can make the serious damages to the sensitive part of the machine. And a metallic corrugated structure section (DCP) is designed to cancel the linear chirp

of the electron beam at the exit of the Linac. The transverse magnetic focusing is carefully optimized to minimize the emittance dilution due to transverse wakes, momentum dispersion and coherent synchrotron radiation in bending magnets. The layout of the SHINE Linac is shown in Fig. 1. The main parameters are listed in Table 1.

Table 1: Main parameters of the SHINE Linac

Parameter	Value	Unit
Beam energy	8	GeV
Bunch charge	100	pC
Max Rep-rate	1	MHz
Projected emittance	< 0.5	μm
Peak current	> 1500	A
Sliced energy spread	< 0.015	% _{rms}

LONGITUDINAL BEAM DYNAMICS

The electron beam is generated by a VHF gun and then accelerated to about 100 MeV then the beam is transported in to the L1 (two cryomodules) where the beam will be accelerated to 326 MeV. Off-crest acceleration creates the desired correlated energy spread along the bunch in the first compressor BC1. The two 3.9 GHz cryomodules tuned at the 3rd harmonic of 1.3 GHz frequency is placed right before the first bunch compressor BC1. The function of the structure is to provide cubic corrections of the correlated momentum distribution along the bunch in presence of the sinusoidal RF time curvature and the magnetic compressors non-linearity, which also decelerates the beam to 265 MeV. The beam is compressed in BC1 from 1 mm to 0.13 mm, the peak current is increased to 80 A accordingly.

The L2 structure (18 cryomodules) is located between the first and second bunch compressor, which accelerates the electron beam from 265 MeV to 2.2 GeV. It also provides the residual energy chirp needed for the second compressor BC2, in which the peak current will be further increased to over 1500 A. After BC2 the beam is accelerated to its final 8 GeV energy in the L3 and L4 structure (54 cryomodules).

The X-ray FEL refers using an electron beam with low emittance, small energy spread and a high core current to generate coherent radiation through the undulator, it's critical to avoid the single-spike or double-horn type beam current distribution. the final beam current profile is preferred to be a so-called "flat-top" distribution [3].

Meanwhile, the beam jitters including peak current, beam energy and beam arrival time also sensitive to longitudinal parameters such as RF settings. To achieve this, the

* gud@sari.ac.cn

LAYOUT OF THE UNDULATOR-TO-DUMP LINE AT THE SHINE*

Tao Liu[†], Zheng Qi, Zhangfeng Gao, Si Chen, Haixiao Deng, Bo Liu
Shanghai Advanced Research Institute, Chinese Academy of Sciences, Shanghai, China
Nanshun Huang, Zhangjiang Lab, Chinese Academy of Sciences, Shanghai, China

Abstract

The Shanghai High repetition rate XFEL and Extreme light Facility as the first hard X-ray free-electron laser (FEL) facility in China, is currently under construction in the Zhangjiang area, Shanghai. It aims to deliver X-ray covering photon energy range from 0.4 to 25 keV, with electron beam power up to 800 kW. Downstream of the undulator line, the beam transport design of the undulator-to-dump line is critical which is mainly used for realization of FEL diagnostics based on transverse deflecting structure and beam absorption in the dump. In this manuscript we describe the current layout of this system.

INTRODUCTION

In recent years, the high-repetition-rate XFEL based on superconducting LINAC attracts increasing attention due to its ability to generate radiation pulse with higher average brightness and plays an important role in many research fields. The Shanghai High repetition rate XFEL and Extreme light facility (SHINE) aims to join the exclusive XFEL club as one of the most advanced user facilities by delivering femtosecond X-ray pulses with high repetition rate. It is designed to deliver photons between 0.4 keV and 25 keV with repetition rate up to 1 MHz using a superconducting LINAC [1,2]. It consists of an 8 GeV continuous-wave superconducting RF Linac, 3 undulator lines, 3 X-ray beamlines and 10 experimental stations in phase-I, which has started its construction from April of 2018.

For the nominal parameters of the electron beam output at the SHINE, the operating beam energy is 8 GeV with repetition rate up 1 MHz and bunch charge of 100 pC, so that it would provide electron with beam power up to 800 kW. According to the current design requirements, there are four beam dump lines at 8 GeV, as shown in Fig. 1. One of them is the linac-to-dump (L2D) line, which is mainly used for the beam energy and energy spread measurements. The other three are the undulator-to-dump (U2D) lines, ensuring that the electron beam transport into and absorbed in the dumps. To take the commissioning and operation into consideration at the SHINE, the design of the three U2D lines mainly meets the following three basic abilities. The first one is absorbing electron beam power up to 800 kW in the dump, the second one is measurements of the incoming beam en-

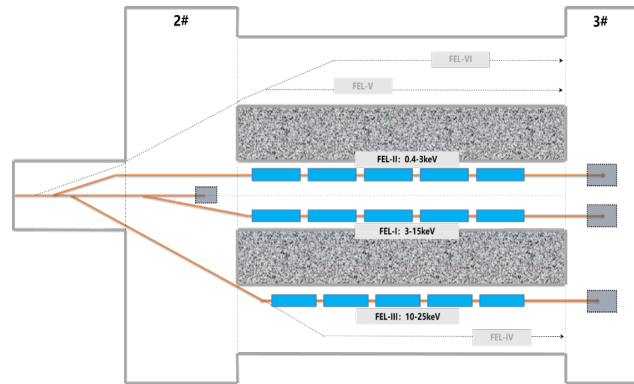


Figure 1: Undulator system at the SHINE. Main dump is located at the beam switch-yard system in the tunnel 2#, and the other three dumps are at the downstream of the undulator systems in the tunnel 3#.

ergy and energy spread, and the third one is measuring the longitudinal phase space of the electron beam. It is worth mentioning that beam expanding and rotation are required for dump absorbing, together with beam longitudinal phase space measurement online. The total length of the U2D line is approximately 90 m, in which the distance from the analyzing magnets to the dump is less than 20 m. This means the beam transport design of the line is great challenging under severe spatial constraints. Besides, the magnets are also specified to operate within the beam energy range from 4.0 to 10.0 GeV.

LAYOUT OF THE U2D LINE

The electron beam specifications at the SHINE are given in Table 1. On the one hand, due to such high beam power up to 800 kW, the specific dump design is essential associated with beam expanding and rotation. On the other hand, beam longitudinal phase space measurement should be operated online and the time resolution should be the femtosecond level since the bunch length is about 30 fs.

The design of the three U2D lines are very similar with slightly different arrangement in details. Therefore, we take the U2D line of the FEL-I undulator beamline as an example. As shown in Fig. 2, the scheme design is as follows:

1) A set of quadrupoles is required upstream of the transverse deflection structure (TDS) to match the beta functions of the electron beam at the center of the TDS, which aims to achieve ultra-high time resolution.

2) X-band TDS introducing transverse-to-longitudinal correlation is to present the longitudinal phase space of the electron beam and the measurement of several related beam and FEL parameters.

* Work supported by the National Natural Science Foundation of China (11905277, 12122514, 11975300), the CAS Project for Young Scientists in Basic Research (YSBR060), the Shanghai Natural Science Foundation (23ZR1471300), the Youth Innovation Promotion Association CAS (2023302), and the CAS-Helmholtz International Laboratory on Free Electron Laser Science and Technology (HZXM2022500500).

[†] liut@sari.ac.cn

MULTICHROMATIC FREE-ELECTRON LASER GENERATION THROUGH FREQUENCY-BEATING IN A CHIRPED ELECTRON BEAM

Zheng Qi^{1,*}, Chao Feng^{1,2}

¹Shanghai Advanced Research Institute, Chinese Academy of Sciences, Shanghai, China

²University of Chinese Academy of Sciences, Beijing, China

Abstract

We propose a simple method to generate mode-locked multichromatic free-electron laser (FEL) through a longitudinal phase space frequency-beating in a chirped electron beam. Utilizing the two stage modulator-chicane setups in Shanghai Soft X-ray FEL facility, together with a chirped electron beam, we are going to imprint a frequency-beating effect into the electron beam. Hence periodic bunching trains can be formed and can be used to generate mode-locked FEL radiation pulses. Theoretical analysis and numerical simulations are given out to demonstrate the performance of the method. The results indicate that mode-locked FEL in temporal and frequency domain can be formed at the 18th harmonic of the seed laser, with the central wavelength being about 14.58 nm and the peak power over 2 GW.

INTRODUCTION

Mode locking is an essential concept and technique in conventional lasers. It's of great importance in the generation of ultrashort laser pulses and in the stable control of the laser phase. For the state-of-the-art X-ray free electron lasers, mode-locked lasing has also been proposed and pursued for the last decade [1, 2]. Mode-locked XFELs could provide new opportunities for high resolution x-ray spectroscopy and attosecond sciences. The FEL community has proposed and studied several methods for mode-locked FEL lasing. Generally mode-locked FEL lasing requires an initial energy modulation or density modulation with fixed phase relation imprinted into the electron beam. And then mode locking amplifiers with undulator and delay-chicane modules are needed for the amplification.

In this study, we propose a simple method to generate mode-locked multichromatic FEL through a longitudinal phase space frequency-beating in a chirped electron beam. The schematic layout is show in Fig 1. The layout mainly consists of two modulator-chicane setups and a radiator. The electron beam is coming from the upstream beam switchyard, and it is manipulated to have an energy chirp in the head and tail of the electron beam. Two seed lasers with identical wavelength are employed in the two modulator. The chirped electron beam first get an energy modulation in modulator-1, the chicane-1 with a relatively small dispersion will then slightly change the imprinted energy modulation wavelength since the whole electron beam has an energy chirp. The electron beam will then get an energy modulation in modulator-2, and in chicane-2 the energy modulation

is converted into density modulation. Through proper optimizations of the parameters, periodic bunching trains can be formed in the electron beam, and high harmonic bunching can also be formed. And then the electron beam will go through the radiator for mode-locked high-gain harmonic generation (HGHG) FEL radiation.

We will give a brief analysis of the electron beam phase space evolution in the scheme. First of all, we need to define some variables. The dimensionless energy deviation of a particle is defined as $p = (E - E_0)/\sigma_E$, where E_0 is the central energy of the electron beam and σ_E is the rms energy spread. The initial longitudinal beam distribution can be written as

$$f(p) = \frac{1}{\sqrt{2\pi}} \exp(-p^2/2) \quad (1)$$

with a linear energy chirp and an energy modulation, the electron beam energy becomes

$$p_1 = p + c \frac{E_0}{\sigma_E \sigma_s} z + A_1 \sin(k_1 z) \quad (2)$$

where c is the relative linear energy chirp, A_1 is the energy modulation strength, k_1 is the wavenumber of the seed laser. After DS1, the electron longitudinal position becomes

$$z_1 = z + R_{56}^1 p_1 \sigma_E / E_0 \quad (3)$$

and the beam distribution now is

$$\begin{aligned} f(p, z) &= \frac{1}{\sqrt{2\pi}} \exp\left\{-\frac{1}{2}\left[p - c \frac{E_0}{\sigma_E \sigma_s} (z - R_{56}^1 p \sigma_E / E_0) - A_1 \sin(k_1 (z - R_{56}^1 p \sigma_E / E_0))\right]^2\right\} \\ &= \frac{1}{\sqrt{2\pi}} \exp\left\{-\frac{1}{2}\left[p - \frac{cE_0}{\sigma_E \sigma_s} z + cR_{56}^1 p / \sigma_s - A_1 \sin(k_1 z - R_{56}^1 k_1 p \sigma_E / E_0)\right]^2\right\} \end{aligned} \quad (4)$$

define $C = \frac{cE_0}{\sigma_E \sigma_s}$, $\xi = k_1 z$, $B_1 = R_{56}^1 k_1 \sigma_E / E_0$, we can simplify the formula as follows

$$f(p, \xi) = \frac{1}{\sqrt{2\pi}} \exp\left\{-\frac{1}{2}\left[p - C\xi/k_1 + CB_1 p/k_1 - A_1 \sin(\xi - B_1 p)\right]^2\right\} \quad (5)$$

through the second energy modulation and the second dispersion section, the electron beam energy and the electron longitudinal positions are now

$$\begin{aligned} p_2 &= p_1 + A_2 \sin \xi \\ z_2 &= z_1 + R_{56}^2 p_2 \sigma_E / E_0 \end{aligned} \quad (6)$$

* qiz@sari.ac.cn

PRELIMINARY DESIGN OF HIGHER-ORDER ACHROMAT LATTICE FOR THE UPGRADE OF TAIWAN PHOTON SOURCE

N. Y. Huang*, M. S. Chiu, P. J. Chou, H. J. Tsai, H. W. Luo, F. H. Tseng, G. H. Luo
 National Synchrotron Radiation Research Center, Hsinchu, Taiwan

Abstract

We study the upgrade of Taiwan Photon Source (TPS) with energy saving as the prime objective. The upgrade design is dubbed TPS-II. To accommodate the constraints imposed by the existing TPS tunnel, we choose the higher-order achromat (HOA) lattice configuration which is composed of the 5BA and 4BA cells. This HOA lattice produces a natural beam emittance about 131 pm·rad for a 3 GeV, 518.4 m storage ring. The on-momentum dynamic aperture is about 8 mm and the estimated Touschek life time reaches around 5.7 hours at total beam current of 500 mA. As a result of the ultralow beam emittance, the brightness and coherence fraction (CF) of the photon beam are improved with a factor of several tens especially in the photon wavelength around 0.1 nm. The challenges and preliminary results of this HOA lattice design will be presented.

INTRODUCTION

The present trend of development for storage ring light sources is steering towards the design of diffraction-limited storage rings (DLSRs), a trend that has been substantiated by the successful establishment and operation of prominent facilities such as MAX-IV, SIRIUS, and ESRF-EBS [1-3]. In the continuum of this evolution, TPS as one of the bright third-generation storage rings since 2015 [4], we plan to upgrade the machine toward DLSR for a brighter synchrotron radiation light source and a green energy-oriented facility.

Globally, several advanced technologies are undergoing examination to propel the development of green energy particle accelerator. These innovations encompass diverse strategies, including the substitution of permanent magnets for electromagnets, the design of a compact accelerator with higher gradient accelerating structures, the reduction of unnecessary power consumption, the enhancement of electric power transfer efficiency and so on. Among these, a storage ring lattice configuration capable of producing an electron beam emittance toward the diffraction limit is one of the keys for energy saving. Directly impact to the users is the increase of coherent photon numbers and brightness which enable the shorter experiment sampling time and reduction of waste heat.

According to the analytical estimation, the relative brightness and CF with respect to the present TPS operation conditions improves by a factor of few tens as the electron beam emittance is reduced to one hundred pm·rad from the current TPS lattice (Fig. 1). There are several possible schemes under study such as H7BA, H6BA, 5BA and

* huang.ny@nsrc.org.tw

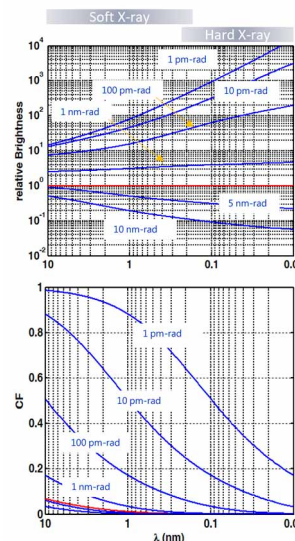


Figure 1: The estimated improvements from TPS to TPS-II on the relative brightness and CF. The red line represents the present operation conditions of TPS ($\epsilon_0 = 1.6 \text{ nm}\cdot\text{rad}$, 500 mA). This calculation employs undulator with the same magnet length and period numbers, optics function of $(\beta_x, \beta_y) = (5.353, 1.73) \text{ m}$, and $\eta_x = 0 \text{ m}$.

HOA for TPS upgrade [5]. In this report, we delve into the initial design stages of a HOA lattice configuration bounded by the constraints and challenges we are facing.

TPS TOWARD TPS-II

TPS is a 3 GeV, 518.4 m storage ring with the 4-DBA lattice configuration per super-period. There are totally 24 straight sections available for insertion devices (IDs). To use the existing infrastructure of accelerating tunnel, the upgrade design must keep all the source points of ID beam-lines fixed. The current long straight section (LSS) to short straight section (SSS) length ratio is large, at 12:7, making it challenging to keep identical unit cells in a super cell while preserving the same source points for the insertion devices and sufficient SSS lengths. Therefore, we have adopted the HOA configuration that is based on the combination of 5-4-4-5 Multi-Bend-Achromat lattice. It is a similar strategy that proposed by SOLEIL-U to overcome the existing constraints in the tunnel [6].

The linear optics function of one TPS-II supercell is shown in Fig. 2. The number of dipole magnets in the ring is increased from 48 to 108. As predicted by the scaling law, $\epsilon_0 \propto \theta^3$, the beam emittance of the basic HOA scheme is estimated about 430 pm·rad due to the reduction in bending angle. Additionally, the inclusion of combined dipole

Content from this work may be used under the terms of the CC-BY-4.0 licence © 2023. Any distribution of this work must maintain attribution to the author(s), title of the work, publisher, and DOI

SIMULATION STUDY OF ORBIT CORRECTION BY NEURAL NETWORK IN TAIWAN PHOTON SOURCE

M. S. Chiu[†], C. Felix, Y. S. Cheng, F. H. Tseng, H. J. Tsai, G. H. Luo

National Synchrotron Radiation Research Center, Hsinchu, Taiwan

Abstract

Machine learning has been applied in many fields in recent decades. Many research articles also presented remarkable achievements in either operation or designing of the particle accelerator. This paper focuses on the simulated orbit correction by neural networks, a subset of machine learning, in Taiwan Photon Source. The training data for the neural network is generated by accelerator toolbox (AT).

INTRODUCTION

The Taiwan Photon Source (TPS) [1,2] is designed as a 3 GeV synchrotron light source, encompassing a 518.4 m circumference. The lattice structure of the storage ring consists of 24 Double-Bend Achromat (DBA) cells, providing 18 short straight sections (7m) and 6 long straight sections (12 m). Three long straight sections, located at 3-fold symmetric position, adopt symmetrical double mini- β_y lattice in which a set of quadrupole triplet is installed in the middle of the long straight section to accommodate double undulators. Figure 1 shows the optical functions of the double mini- β_y lattice for 1/3 TPS.

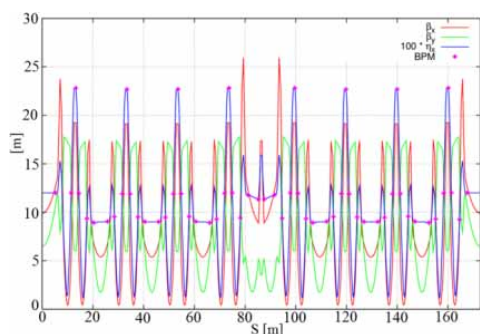


Figure 1: Optical functions of the double mini- β_y lattice for 1/3 TPS storage ring.

Each DBA cell is outfitted with 7 beam position monitors (BPMs). Two BPMs installed in the injection section are unused. There are six additional BPMs installed in three double mini- β_y sections. The TPS storage ring employs 72 horizontal and 96 vertical corrector magnets to define the electron golden orbit, which is monitored by 172 BPMs. In routine operation for user experiments and maintaining long-term orbit stability, each insertion device is equipped with orbit feed-forward table to compensate itself 1st and 2nd order residual integral fields, while gap or phase of the insertion device are moving. Additionally, TPS storage ring is also equipped with a fast

orbit feedback systems involving 96 fast correctors (FC) in horizontal and vertical direction, and the RF feedback system.

Figure 2 shows the positions of BPMs, slow orbit corrector magnets (trim coil wound on the sextupoles) and fast orbit corrector magnets in a DBA cell.

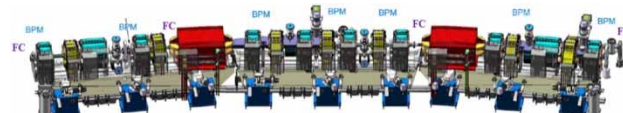


Figure 2: DBA cell in TPS storage ring. Dipole is printed in red colour. Quadrupole is in blue colour. Sextupole is in yellow. Slow orbit corrector magnets are the trim coils wound on the sextupole magnets.

In daily operation for user experiments, the orbit correction and control uses a measured orbit response matrix and singular value decomposition (SVD) algorithm. BPMs are used to monitor the electron beam's orbit, apply SVD to calculate the pseudoinverse of the orbit response matrix, the desired strengths of the corrector magnets can be derived, then apply the calculated current to corrector magnets to bring the electron orbit closer to the target orbit. This traditional method is rooted in physics and well-established principles of beam dynamics in particle accelerators. However, applying machine learning to particle accelerators is growing. D. Schirmer [3, 4] published a paper talking about orbit correction with machine learning at the synchrotron light source DELTA. We also try to create a neural network model to do orbit correction to explore the benefits and drawbacks of utilizing machine learning for orbit correction in TPS storage ring.

MACHINE LEARNING

Machine learning (ML) is a subset of artificial intelligence (AI). It can enable computers to learn from large amounts of data and make predictions or decisions without being explicitly programmed. ML can be roughly classified into three types: supervised learning, unsupervised learning, and reinforcement learning. In supervised learning, the model is trained on labeled datasets, meaning that the input data is paired with output or target values. The goal of supervised learning is to search for a mapping from inputs to outputs. Once adeptly trained, the model can make precise predictions or classifications when encountered with new or unseen data. In unsupervised learning, the model works with unlabeled data and learns patterns without predefined outcomes. It's often used for clustering and dimension reduction. In reinforcement learning, agents learn by interacting with an environment to achieve specific goals.

[†] chiu.ms@nsrrc.org.tw

THE ALIGNMENT RESULTS OF THE TANDEM EPU AT TAIWAN PHOTON SOURCE

F. H. Tseng, T. Y. Chung, H.-Y. Huang, C. M. Cheng, C.-Y. Hua, Y. M. Hsiao, Y. C. Liu[†]
 National Synchrotron Radiation Research Center,
 Hsinchu Science Park, Hsinchu, Taiwan, R. O. C.

Abstract

Since its inauguration for user applications in 2016, the Taiwan Photon Source (TPS) has facilitated numerous research endeavors. The current investigation focuses on the alignment results of a tandem Elliptically Polarizing Undulator (EPU) situated within an extended double minimum beta y long straight section. The objective is to augment the photon flux of the synchrotron light generated by the tandem EPU via accurate alignment and using a phase shifter to attain temporal coherence. A cross-correlation function is employed to scrutinize the beam parameters associated with the source points to evaluate the temporal coherence of the two light sources emitted from the tandem EPU.

INTRODUCTION

The TPS is a 3 GeV storage ring with a 6-fold symmetry Double Bend Achromat (DBA) lattice structure [1]. Spanning a circumference of 518.4 m, it comprises 24 cells, 18 six-meter-long straights, and six 12-meter-long straights. Tandem undulators are allocated to three 12-meter-long straights, which separate eight cells to maintain the symmetry of optical functions. A quadrupole triplet is positioned in the center of the 12-meter-long straight to minimize the beta y at the core of each undulator [2]. Figure 1 compares optical functions with and without the quadrupole triplet. The tandem undulator beamline was designed to double its flux. However, since TPS began user operation in 2016, only one undulator has been accessible to the three beamlines.

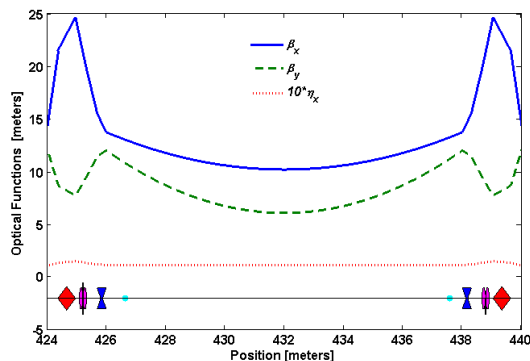


Figure 1a: Optical functions without the quadrupole triplet in the 12-meter-long straight.

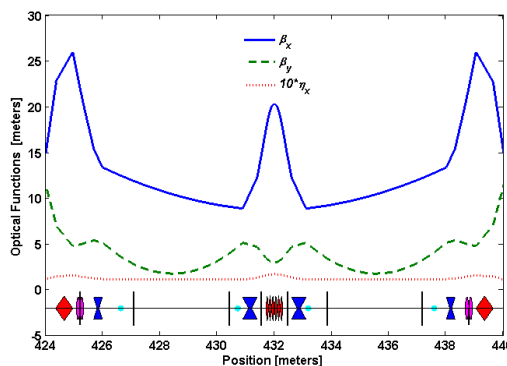


Figure 1b: Optical function with the help of quadrupole triplet to minimize the β_y at the core of each EPU.

Beamline 41A at the TPS consists of two branches [3]: high-resolution resonant inelastic X-ray scattering (RIXS) and coherent soft X-ray scattering. Both branches share the same equipment, such as the monochromator, slits, and front-end focusing optics. The light source comes from two elliptically polarized undulators (EPU) placed one after another in a 12-meter-long straight with a unique design to double the light's brilliance. Each EPU is 3.2 m long with a 48 mm period. Figure 2 presents the tandem EPUs and quadrupole triplet configuration and shows the locations of beam position monitors (BPM) and the pairs of correctors for local orbit feedback.

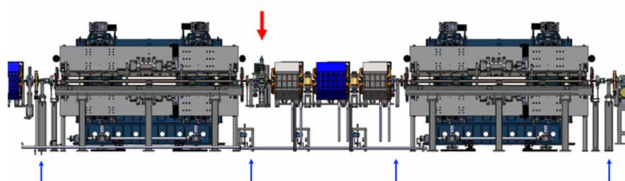


Figure 2: Tandem EPUs and quadrupole triplet configuration, locations of four BPMs (small blue arrow) and the pairs of correctors (black dot) for local orbit feedback, the red arrow indicates the location of the phase shifter.

The EPU tandem is designed to achieve a brilliance greater than 1×10^{20} photons per second per mrad^2 per mm^2 with a 0.1% bandwidth in the energy range from 400 to 1200 eV. In this range, the photon flux in the central cone is over 1×10^{15} photons per second. The calculated beam sizes are roughly 386 μm horizontally and 28-35 μm vertically at the full width at half-maximum (FWHM). Based on the photon energy range, the beam divergences are 42-61 μrad horizontally and 33-52 μrad vertically at FWHM.

[†] email address yichihl@nsrc.org.tw

SOME BEAM DYNAMIC ISSUES IN THE HALF STORAGE RING

Jingyu Tang*, Penghui Yang, Gangwen Liu, Yihao Mo, Anxing Wang, Zhouyu Zhao, Tianlong He
 Zhenghe Bai University of Science and Technology of China, Hefei, China

Abstract

HALF (Hefei Advanced Light Facility) is a fourth-generation synchrotron light source that just started construction in 2023. With 2.2 GeV in energy, 350 mA in beam current and 86 pm.rad in emittance, the HALF storage ring faces several beam dynamics challenges. This presentation gives the recent study on some of these issues, in particular the beam collimation and the influence and compensation of the insertion devices. For beam collimation, different beam loss mechanisms have been studied, and the Touschek scattering and beam dumping are considered the two major effects in designing the collimation system. Then two collimators with movable horizontal blades and fixed passive vertical blades are being designed, with the main focus on the collimation efficiency and impedance. For the influence of the insertion devices, it is found that some of the long-period undulators have a high impact on the beam dynamic aperture due to low beam energy and originally small dynamic aperture. The local compensation methods for both linear and non-linear effects have been studied. Instead of the traditional compensation method by electrical wires, the method of using two combined magnets with quadrupole and octupole fields at the two ID ends in restoring the dynamic aperture is also studied and compared.

INTRODUCTION

HALF is a fourth-generation synchrotron light source. After many years of design study and R&D efforts, now it enters the construction phase of 2023-2028 [1-2]. The accelerator complex consists of a full-energy linac of 2.2 GeV and a storage ring of 20 periods with a circumference of 480 m. Figure 1 shows the lattice functions of one period. The main design parameters of the storage ring are listed in Table 1.

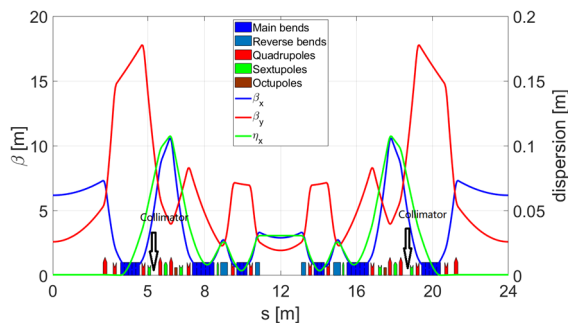


Figure 1: The lattice functions and magnet layout of the HALF storage ring (with collimator positions marked).

Table 1: Main Parameters of the HALF Storage Ring

Parameter	Value
Energy [GeV]	2.2
Current [mA]	350
Circumference [m]	479.86
Number of cells	20
Natural emittance [pm·rad]	85.8
Transverse tunes (H/V)	48.19/17.19
$\beta_x/\beta_y/\eta$ @ long straight [m]	6.78/2.55/0.00
$\beta_x/\beta_y/\eta$ @ mid-straight [m]	2.51/1.95/0.03
Arc lattice	modified hybrid 6BA
Straight sections [m]	20*5.5, 20*2.2
RF frequency [MHz]	499.8

With a relatively low beam energy of 2.2 GeV, a modest beam current of 350 mA and a very small beam emittance of 86 pm.rad, the HALF storage ring faces several beam dynamics challenges. In this paper, we present the preliminary study results of some beam dynamics issues, including beam loss mechanisms, beam collimation, influences of the insertion devices (ID) on the beam dynamics and compensation methods.

BEAM LOSS MECHANISMS IN THE HALF STORAGE RING

Beam losses become much more important in fourth-generation synchrotron light sources, as compared to third-generation light sources, mainly due to the much higher loss rate and much smaller beam size. The beam loss knowledge is not only important for the design of the tunnel shielding but also for the safe operation of the machine, since a critical beam loss may damage the accelerator devices. A study on the loss mechanisms in the HALF storage ring was conducted. The following beam loss mechanisms are considered the most important: the Touschek scattering loss, beam loss during the injection, beam loss or dumping when the abnormal functions of the facility occur and intentional shutdown is launched, and beam losses in the non-standard operation modes.

The Touschek Scattering Loss

The Touschek scattering loss is the most important beam loss in the HALF storage ring. Due to that both the beam size and momentum aperture (MA) in fourth-generation light sources are significantly smaller than those in third-generation light sources, the Touschek scattering as the principal beam loss mechanism leads to a significant reduction in beam lifetime. In the normal operation mode

* jytang@ustc.edu.cn

OPTICS FOR AN ELECTRON COOLER FOR THE EIC BASED ON AN ELECTRON STORAGE RING*

J. Kewisch[†], A. Fedotov, X. Gu, Y. Jing, D. Kayran, I. Pinayev, S. Seletskiy
 Brookhaven National Laboratory, Upton, NY, USA

Abstract

An electron cooler based on a storage ring is one of the options to improve the luminosity in the Electron-Ion Collider (EIC). The transverse emittance of the electrons in the cooler is driven by the quantum excitation in dipoles and wigglers, as well as by both beam-beam scattering with the ions and intra-beam scattering of the electrons in the regions with a non-zero dispersion. The resulting demand to minimize a dispersion conflicts with the need of a sufficient dispersion in sextupoles for chromaticity correction. In this report we discuss our studies of several approaches to electron ring lattice, including those typically used in light sources, and present resulting compromise between various requirements.

INTRODUCTION

The Electron-Ion Collider is being designed at the Brookhaven National Laboratory, with an anticipated start of construction in 2025. This machine will allow colliding 10 GeV electrons with 275 GeV protons. An important feature of this accelerator will be a luminosity of $10^{34} \text{cm}^{-2} \text{sec}^{-1}$. After injection the beam emittance of the ions, and therefore the luminosity, will degrade because of intra-beam scattering (IBS). In order to maintain a high integrated luminosity the ion beams must be cooled.

In the current design of the EIC Micro-bunched Electron Cooling (MBEC) [1] is selected as a promising new technique for cooling dense hadron beams. An alternative method is the traditional electron cooling, invented by Gersh Budker at INP, Novosibirsk, in 1966. Electron cooling has been tested in many applications and has been proven to work well with bunched beams in the LEReC cooler [2] at BNL. However, the EIC would be the first application with hadron energies greater than 10 GeV. The EIC operates at 100 GeV and 275 GeV.

The cooling rate of an electron cooler with bunched beams is proportional to:

$$\frac{1}{\tau} \propto \frac{r_e^2 m_e c Z^2 \Lambda_c}{A m_p} \frac{1}{\gamma^2} \frac{N_e}{\epsilon_{xn} \epsilon_{yn} \sigma_z \sigma_\delta} \frac{L_{CS}}{C_{ring}} \quad (1)$$

where N_e is the number of electrons, L_{CS} is the length of the cooling section, C_{ring} is the ring circumference, Λ_c is the Coulomb log, ϵ_{xn} , ϵ_{yn} are the normalized electron beam emittances, and γ is the Lorenz factor. The cooler becomes less effective with higher energies and we must increase the length and the electron current as well as maintain low emittances to achieve sufficient cooling rates.

The choices for the electron accelerator are a linac or a storage ring. When a photo-cathode is used in a linac the beam emittance is small, since each bunch is used only once for cooling the ions, but the electron current is limited by the life time of the cathode.

In a storage ring the beam current can be higher, but the emittance results from the equilibrium of heating of the beam by radiation excitation, intra-beam scattering of the electrons, heating by the ions (beam-beam scattering), and the radiation damping. It turns out that the IBS comprises a significant portion of the heating and strongly influences the design of the ring. Everywhere where the dispersion function is non-zero IBS couples the higher longitudinal temperature into the transverse direction and increases the emittance.

In an electron cooler the central velocity of the electrons and ions must be the same. With an ion energy of 275 GeV the required electron energy is only 150 MeV. As the radiated power is proportional to the 4th power of the energy it is therefore necessary to increase the radiation damping with wiggler magnets.

LAYOUT

The layout of the ring is shown in Fig. 1. It is shaped like a racetrack, with the cooling section being located in one straight section and the wigglers located in the other. Figure 2 shows the Twiss functions.

The arcs comprise only a small fraction of the circumference. It is not practical to concentrate the sextupoles for chromaticity correction in the arcs. We opted to eliminate the sextupoles from the arcs and use a tightly focused FODO lattice. Doing that allows keeping the dispersion small and minimizing IBS. We tried to use a double-bend-achromat lattice, but that did not decrease the beam emittance and increased the natural chromaticity significantly. The sextupoles are placed in the cooling section and the wiggler section.

In the cooling section the electrons overlay the ion bunch. It is 190 m long to maximize the interaction between electrons and ions. There are no magnetic focusing elements which results in large beta functions. An optical telescope reduces the beta functions at both ends to the small beta functions in the arcs. The non-zero dispersion in the cooling section allows redistributing longitudinal cooling into the horizontal direction [3]. It also allows placing sextupoles in the cooling section. However, since the phase advance over the whole cooling section is less than 90 degrees, placing many sextupoles would be detrimental to the dynamic aperture.

* Work supported by Supported by the US Department of Energy, Contract DE-SC0012704

[†] jorg@bnl.gov

DETERMINISTIC LATTICE APPROACH FOR BESSY III*

B. Kuske[†], P. Goslawski, Helmholtz-Zentrum Berlin, Berlin, Germany

Abstract

Since 2021, HZB pursues the design of a 2.5 GeV storage ring as a successor of BESSY II in Berlin. The user's demand for diffraction-limited radiation at 1 keV corresponds to an emittance of 100 pm, making an MBA lattice indispensable. The envisaged location limits the circumference to ≈ 350 m. MBA lattices are composed of smaller substructures that can be analyzed and optimized separately, before combining them into one super period. The prerequisite for this approach is a clear idea of the goal parameters and their prioritization, as the design process is dominated by permanent decisions between different options. The resulting generic baseline lattice for BESSY III is a simple structure with few non-linear elements, already fulfilling all goal parameters and showing a very compatible non-linear behavior. This is our starting point for further optimizations including swarm or MOGA approaches.

INTRODUCTION

Multi-bend achromat lattices utilize many bending magnets with low deflection angles to reduce the emittance. Usually, these bends are placed at the center of repetitive unit cells, UCs. Multi-bend achromat lattices were pioneered by MAX LAB, Sweden. MAX IV, [1], was successfully commissioned in 2016. Sirius in Brazil followed in 2021, [2]. The ESRF, France, followed with the hybrid MBA in 2021, [3]. Nowadays, practically every new machine design or upgrade utilizes this type of lattice.

In 2014, A. Streun, PSI, added the concept of reverse bends (RB) to the MBA unit cell, UC, [4]. RBs are focusing quadrupoles placed off-axis to achieve negative bending. They detach the dispersion- and beta-function matching and significantly reduce the emittance.

In 2017, J. Bengtsson contributed the Higher-Order-Achromat approach to MBA-lattices [5, 6], where the linear lattice is constructed such, that all 1st and 2nd order resonance driving terms are suppressed by phase cancellation.

HZB now proposes a deterministic lattice design approach based on both, RB and HOA. The repetitive structure of MBA lattices is exploited to optimize small substructures, the UC, the dispersion suppression cell (DSC), and the straight section separately before they are composed into one generic super period. An important goal is to minimize non-linear effects by the set-up of the linear lattice structure. This approach leads to lattices close to the achievable optimum under the given boundary conditions, including fundamental decisions on a promising sextupole scheme. Opposed to generic optimizations this approach leads to

a clear understanding of the parameter space and optional trade-offs.

An indispensable prerequisite of this approach is a clear definition of the design goals and their priorities. For BESSY III [7], these are listed in Tables 1 and 2.

Table 1: BESSY III Goal Parameters

Parameter	Value
Energy	2.5 GeV
Super Periods	16
Circumference	≈ 350 m
Emittance	100 pm
Momentum Compaction Factor, α_c	$> 1e-4$
Momentum Acceptance	$> 3\%$

Table 2: Design Priorities

Goal	Reason
1 MBA lattice	emittance
1 realization of HOA	non-linear behaviour
1 usage of reverse bends	emittance, circumference
2 low sextupole strength	non-linear behaviour
2 short circumference	site, costs
3 DSC as close as possible to half UC	non-linear behaviour

CONSTRUCTION OF THE UC

The half UC minimally consists of a central, main bend, MB, the reverse bend, RB, the defocusing quadrupole, QD, and 2 sextupoles, SF and SD. Initially, all drifts are 0.1 m.

HOA Condition for UC

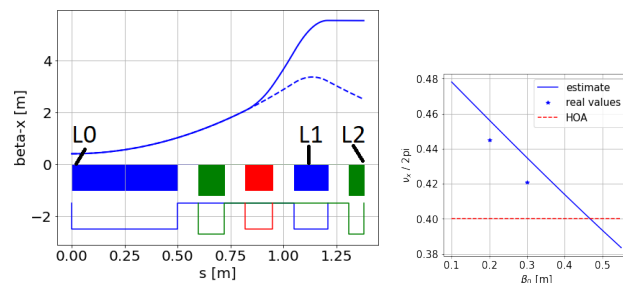


Figure 1: Left: β_x in half UC, regular (line) and for QD=0 (dashed line); magnet color code: MB: blue; RB: purple; QD: red, SF, SD: green. Right: ν_x , analytic estimate (blue line), exact phase advance (stars), and option for HOA (red).

* Work supported by German Bundesministerium für Bildung und Forschung, Land Berlin, and grants of Helmholtz Association
[†] Bettina.Kuske@helmholtz-berlin.de

DESIGN OF A 166.6 MHz HOM-DAMPED COPPER CAVITY FOR THE SOUTHERN ADVANCED PHOTON SOURCE*

Junyu zhu^{†,1}, Xiao Li¹, Jiebing Yu¹, Zhijun Lu¹,

Institute of High Energy Physics, Chinese Academy of Sciences, Beijing, China

¹also at Spallation Neutron Source Science Center, Dongguan, China

Abstract

The Southern Advanced Photon Source (SAPS) aims to achieve ultra-low emittances and is expected to adopt low-frequency cavities (< 200 MHz) to accommodate on-axis injection. This paper focuses on the design of a 166.6 MHz HOM-damped normal conducting (NC) cavity for the SAPS. We propose a novel approach to achieve efficient HOM damping by optimizing the lowest frequency HOM and implementing a beam-line absorber in a coaxial resonant NC cavity. Notably, unlike beam-line absorbers for conventional NC cavities, the presence of a large beam tube in a coaxial resonant cavity does not affect the accelerating performance. This enables effective HOM damping while maintaining a high shunt impedance in a NC cavity. The numerical simulation results show that a compact copper cavity with effective HOM damping and excellent RF properties has been achieved.

INTRODUCTION

The Southern Advanced Photon Source (SAPS), planned for construction in the southern region of China, aims to become an advanced fourth-generation light source in the world. Its main parameters are listed in Table 1 [1-2]. The recent lattice design of SAPS has successfully achieved a natural emittance of 32.5 pm, with an effective DA of 5 mm (horizontal) and 4 mm (vertical). Such a small DA is not enough for traditional off-axis injection schemes, which typically requires a DA of the order of 10 mm [3]. The on-axis longitudinal accumulation scheme is attractive due to its less demanding dynamic aperture requirement and the exempt from full-charge bunch delivery. However, a lower frequency RF system is required for a large separation between RF buckets since the state-of-art kicker has a total width of a few nanoseconds. In addition, lower frequency RF systems also have the advantages of low cost for RF power amplifiers and large acceptance, and have been used in many facilities, such as ILSF [4], MAX IV [5], Solaris [6], etc. Considering the technology readiness of 500 MHz HOM damped cavities and the fast kicker, a frequency of 166.6 MHz can be chosen for the fundamental cavity and 500 MHz for the third harmonic cavity.

Both normal conducting (NC) and superconducting (SC) options have been considered for the fundamental cavities during the design phase. The main parameters of these options are listed in Table 2. Due to the large RF power requirement and relatively small voltage requirement of SAPS, the number of cavities in the two schemes is very

close. However, the NC option offers cost savings of at least 40% in construction expenses and requires less space in the straight section, which is valuable for synchrotron light sources. Compared with the SC option, the NC case can save at least 40% of the construction expenses and need less space of straight section, which is very precious for the synchrotron light sources. Furthermore, the NC scheme can enhance system stability by adding an additional cavity and can continue to operate even if one set of RF systems fails, although this is expensive for the SC option. Therefore, we decided to develop a HOM damped 166.6 MHz compact NC cavity for the SAPS, although the 166.6 MHz SC cavity has successfully developed in our institute [7].

Table 1: Main Parameters of SAPS

Parameter	Value
Beam energy (E_0)	3.5 GeV
Circumference	810 m
Natural emittance ($\epsilon_{\text{natural}}$)	32.5 pm-rad
Energy loss per turn	0.898 MeV
Synchrotron tune (Q_s)	0.709E-03
Betatron tunes ν_x/ν_y	81.23/ 64.18
Momentum compaction (α_p)	1.37E-05
Damping time (x/y/z)	18.1/28.1/19.3ms

Table 2: NC and SC Options for the 166.6 MHz RF System

Parameter	NC	SC
Frequency	166.6 MHz	
Total RF power	778 kW	
Total RF voltage	2.0 MV	
Number of cavities	5	4
Cavity voltage/MV	0.4	0.5
Cavity length/m	~ 1.0	3.0
Total cavity wall loss/kW	110	~0.4
Total RF power/kW	906	778
Total AC power/MW	1.776	1.756

RF CAVITY DESIGN

Due to the low RF frequency, the implementation of cylindrical or spherical shapes for the cavity geometry would lead to an overly large design. Therefore, a quarter-wave cavity was chosen for the 166.6 MHz NC cavity. In an ideal quarter-wave cavity, the resonant frequencies of eigenmodes induced by a coaxial structure are $f_n =$

* This work was supported by the funds of National Natural Science Foundation of China (Fund No: 12205168),

[†] zhuji@ihep.ac.cn.

THE CRYOGENIC UNDULATOR UPGRADE PROGRAMME AT DIAMOND LIGHT SOURCE

Z. Patel*, W. Cheng, A. George, S. Hale, M. Marziani, A. Ramezani Moghaddam, M. Reeves,
G. Sharma, S. Tripathi, Diamond Light Source Ltd., UK

Abstract

Diamond Light Source has installed four 2 m long, 17.6 mm period Cryogenic Permanent Magnet Undulators (CPMUs) as upgrades for crystallography beamlines since 2020, with two more planned within the next year. The CPMUs provide 2 - 3 times more brightness and 2 - 4 times more flux than the pure permanent magnet (PPM) devices they are replacing. They have been designed, built, and measured in-house. All four have a 4 mm minimum operating gap and are almost identical in their construction: the main difference being an increase in the number of in-vacuum magnet beam support points from four to five, between CPMU-1 and CPMUs 2 - 4, to better facilitate shimming, particularly at cold temperatures. The ability to shim at cryogenic temperatures necessitated the development of an in-vacuum measurement system. The details of the measurement system will be presented alongside the mechanical and cryogenic design of the undulators, including issues with the magnet foils, and the shimming procedures and tools used to reach the tight magnetic specifications at room temperature and at 77 K.

INTRODUCTION

Diamond Light Source has 24 straight sections, all of which are filled. With the exception of creating new straight sections, as with the installation of a DDBA cell [1], or replacing a sextupole magnet with a short wiggler [2], upgrading of existing insertion devices is the next major step in improving the existing machine for the beamlines.

CPMUs have become an attractive prospect as insertion devices since the manufacture of praseodymium material magnets. The remanence of PrFeB and PrNdFeB magnets increases when cooled to the cryogenic temperature of liquid nitrogen (77 K), unlike NdFeB magnets which undergo spin reorientation at 150 K [3]. Therefore, cryogenic cooling allows for a shorter period device while achieving the same, or stronger, magnetic field. An increase in the number of magnetic periods of an insertion device over the same length results in an increase in the radiation flux and brightness for the beamlines. Four in-house designed, built, and measured CPMUs have been installed at Diamond Light Source over the three years 2020 - 2022, with one new CPMU planned for installation this year, and two to be re-worked to overcome an issue with the magnet beam foil discussed later in this paper.

* zena.patel@diamond.ac.uk

MAGNETIC AND MECHANICAL DESIGN

The magnetic design was developed to increase the brightness and flux of several of the Diamond crystallography beamlines (I03, I04, I11, I24, and VMXm). The design was modelled in Radia [4] using PrNdFeB magnets and vanadium permendur pole pieces, the details of which can be found in [5]. A 17.6 mm period was used for all CPMUs, chosen to cover a suitable x-ray energy range (5 - 30 keV) for the beamlines using the existing Diamond ring and the proposed Diamond-II ring.

The mechanical structure is based on the Diamond third-generation in-vacuum undulator (IVU) structure [6], shown in Fig. 1. Two out-of-vacuum beams move vertically along the two main columns of the structure by way of slides on linear guide rails. Two in-vacuum magnet girders, populated with magnets and poles, are attached to the beams by columns. A 100 μm CuNi foil is placed over the magnets and poles and attached by spring tensioners at the ends of the girders in order to reduce the wakefields produced by the electron beam as it traverses the undulator [7].

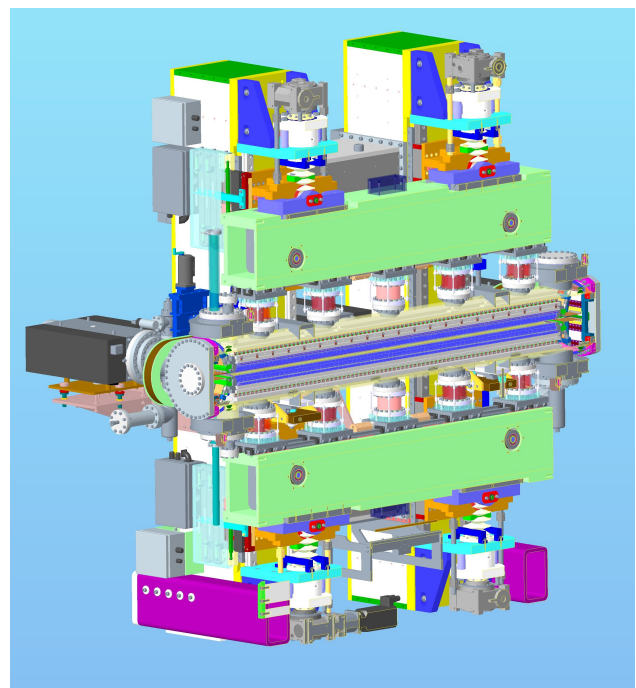


Figure 1: Model of CPMU-3 with the vacuum chamber cut away. The beams are light green with the bellows of the columns shown in red.

Cooling pipes are welded to the magnet beams in order to cool the magnets using a recirculating LN₂ cryocooler, supplied by FMB Oxford. The CPMUs typically reach 77 K

LASER INTERFEROMETER FOR HALL PROBE ALIGNMENT AND MEASUREMENT OF UNDULATOR*

Saif Mohd Khan^{†,1}, Mona Gehlot², Shreya Mishra³, Ganeswar Mishra¹

¹School of Physics, Devi Ahilya Vishwa Vidyalaya (DAVV), Indore, India

²Deutsches Elektronen-Synchrotron DESY, Hamburg, Germany

³Institute of Engineering and Technology (IET), DAVV, Indore, India

Abstract

In the Hall probe Magnetic measurement method the field mapping is done along the length of the undulator. The field integral and phase error computed from the field mapping works as the figure of merit of the undulator. In this paper, we discuss the working of a laser interferometer for precise Hall probe alignment. A new user friendly software based on MATLAB has been developed. The phase error and magnetic field integrals are calculated for both taper and untaper U50 undulator of the Laser and Insertion Device Application (LIDA) Laboratory.

INTRODUCTION

The Hall probe method is widely used measurement system for field integral and phase error calculations of undulators. In this method a Hall probe is moved on a moving sledge and the field is mapped along the undulator length. The measurement accuracy of the filed mapping gives precision in the field integral computation. For this purpose a position sensitive detection system is often used to calibrate the z-position of the Hall probe on the translation sledge [1, 2]. In this paper, we introduce additional laser interferometer system and compare the two methods.

LASER INTERFEROMETER ALIGNMENT AND MEASUREMENT

The experimental setup consists of a Hall probe sledge mounted on a motorized z-linear translation stage with a length of 2000 mm. The z-linear translation stage is driven by a stepper motor controlled by a single-axis motion controller. The controller operates using specialized software that enables the recording of multiple Teslometer channels at once. It is programmable to control the speed and direction of the sledge's movement, as well as the delay time and step length for measurements, which can be defined by the user. The control software allows the linear translation stage to move in both forward and reverse directions within a distance range of 2 μm to 2000 mm. The permissible speed of movement can reach up to 20 mm/s, and the system can be set to capture data with a delay time between 0 ms and 9999 ms for each measurement. To ensure accurate measurements of the magnetic field, it is crucial to maintain precise alignment of the Hall probe with the undulator axis. Any deviation from the desired position can introduce errors in the recorded data.

* Work supported by SERB, Govt. of India, Grant- CRG/2022/001007
[†] saiffukhan@gmail.com

To verify the results of PSD, The Wollaston prism based laser interferometer is also implemented on the linear translation stage. The setup employs a laser as the primary light source. The light emitted by laser is directed towards a beam splitter. The transmitted light from the beam splitter is then passed through a polarizer. The polarized light emerging from the polarizer enters a Wollaston prism, a birefringent optical element. The Wollaston prism divides the incident light into two distinct rays based on their polarization characteristics: the ordinary ray (o-ray) and the extraordinary ray (e-ray). The retro reflector consists of two mirrors, both equipped with mounts on rotational stages featuring angular adjustment capabilities. These adjustments allow precise control over the tilt angles of the mirrors. By carefully adjusting the tilt angles of the mirrors in the retro reflector setup, the two reflected light rays combine at the Wollaston prism, resulting in constructive or destructive interference. The recombined light rays at the Wollaston prism pass through the polarizer and beam splitter once again facilitating the observation of the interference fringe pattern. The movement of the Wollaston Prism in vertical direction leads to shift in the interference pattern which is used to measure the misalignment of the Hall probe sledge on the linear translation stage. Laser interferometer assembly with Hall probe system shown in Fig. 1.

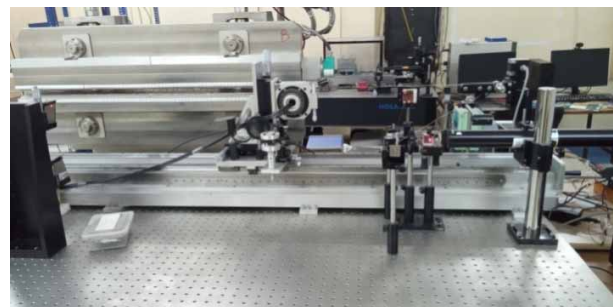


Figure 1: Laser Interferometer system on Hall probe bench.

RESULTS AND DISCUSSION

Throughout the entire length of the undulator, we carefully monitored the motion of the Hall probe with help of PSD. Our observations revealed that the Hall probe remained consistently positioned along the axis of the undulator, with a tolerance within the range of $\pm 30 \mu\text{m}$ along the vertical direction presented in Fig. 2. The calibration curve of the laser interferometer was constructed as shown in Fig. 3 to facilitate the determination of transverse offset.

PULSED WIRE MEASUREMENT OF 20 mm PERIOD HYBRID UNDULATOR*

Saif Mohd Khan^{1,†}, Ganeswar Mishra¹, Mona Gehlot²

¹Laser & Insertion Device Application Laboratory (LIDA),
 Devi Ahilya VishwaVidyalaya, Indore, India

²Deutsches Elektronen-Synchrotron DESY, Hamburg, Germany

Abstract

We investigate pulsed wire measurements of field integrals and phase error of a 20 mm-period, 500 mm-long undulator and discuss variation in performance with Hall probe data without any dispersion correction algorithm.

INTRODUCTION

The Pulsed wire method is alternate to Hall probe method and is preferred in in-vacuum, out-vacuum undulators with limited access. The pulsed wire technique finds potential applications in in-vacuum undulators and cryogenic undulators. The pulsed wire method is faster and suitable in detecting magnet position errors and replacing it. The pulsed wire technique with orthogonal pair of sensors can be utilized as similar to Hall probes with multi axis Hall sensors. Nevertheless, although the pulsed wire method proposed three decades back in 1988 and successfully improved over the years, the method needs to be carefully calibrated for wave dispersion & accurate pulse widths, sensor sensitivity and more importantly the tension in the wire in order that the method emerges as individual precision measurement system independent of the Hall probe method. The wire sag arises due to catenary weight of the wire and poses a serious threat for measurement of long undulators. The second important issue of concern is the dispersion associated with finite rigidity of the wire.

PULSED WIRE MEASUREMENT SYSTEM

The Hall probe and Pulsed wire magnetic bench have been described in Ref. [1]. A motorized linear translation stage with a Hall probe measures the magnetic field profile. The undulator length is 500 mm with 20 mm period length. The accuracy of the Hall probe position during the motion along the undulator length is measured by a position sensitive measuring detector system. The pulsar in the pulsed wire bench is a 50V-12A High Current Voltage Source (HCVS). Two CuBe wires of different diameters are used for the experiment. The 250 μm wire is used with a current of 5A in the wire. The 125 μm wire is used with 1.32 A for the experiment. A current probe measures the current in the wire. We use Tektronix make, Model No A622 AC/DC current probe for the measurement. The total wire length is 1660 mm and passes through the 500 mm length undulator on axis. The pulley end is 660 mm away from the undulator end. The fixed end is 500 mm away from the other undulator end. The wire

length in the arrangement is kept at 3.32 times the length of the undulator. The transverse wire displacement propagates along the wire as a wave longitudinally along both the directions and is detected by a laser-photodiode sensor located at the ends of the undulator. The wire displacement at the sensor for the first field integral is given by:

$$x(0, t) = -\frac{i_0 \Delta t_{short}}{2v\mu} I_1, \text{ where } \Delta t_{short} < \lambda_u / 2v \quad (1)$$

and i_0 is the amplitude (A) of the current pulse, v is the velocity of the wave (m/s) in the wire, Δt is the pulse width (s), μ (kg/m) is the mass per unit length of the wire. Equation (1) is evaluated by looking at the wire displacement with a current of short duration applied to the wire. The wire displacement at the sensor for the second field integral is given by for a longer pulse:

$$X(0, t) = -\frac{i_0}{2v^2\mu} I_2, \text{ where } \Delta t > N\lambda_u / v \quad (2)$$

FIELD INTEGRAL MEASUREMENT

The first and second field integrals of U20 are measured by Hall probe [2]. The second field integral centroid is displaced from the axis by 500 Gcm². From the peak field data, first field integral (rms) is 732 Gcm and the second field integral (rms) reads 553 Gcm².

We choose tension at a preselect sag for the measurement. The second field integral from the pulsed wire data is captured at a tension of 22.9N as shown in Fig. 1. The sag with the 250 μm wire is 52 μm. The pulsed wire integral data is stretched beyond the Hall probe data implying that the pulsed wire is tension under-compensated. The tension is gradually increased. We define the tension compensated length as the difference in length of the und-

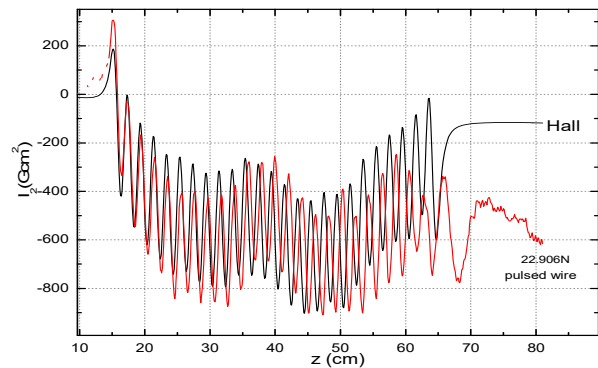


Figure 1: Second field integral at a wire tension.

LARMOR RADIUS EFFECT ON IFEL ACCELERATOR WITH STAGGERED UNDULATOR

Roma Khullar, Government Holkar Science College, Indore, Madhya Pradesh, India
 Saif Mohd Khan, G. Mishra, Deviahilya Vishwavidyalaya, Indore, Madhya Pradesh, India

Abstract

In this paper, the theory of inverse free electron (IFEL) accelerator using staggered undulator has been discussed. The important contribution of staggered undulator parameter and the finite Larmor radius effect on energy saturation, saturation length and accelerating gradient of the IFEL accelerator are included in the analysis. Considering the synchrotron radiation losses, the IFEL accelerator equations are derived.

INTRODUCTION

The inverse free electron laser (IFEL) accelerator is the most advance laser based accelerator scheme [1-6]. It has been demonstrated that the accelerating gradient is significantly larger than what we achieve with conventional IF accelerator [7-9]. In the IFEL accelerator the energy transfer is from the laser beam to electrons. In an IFEL relativistic particles are moving through an undulator magnetic field with an electromagnetic wave propagating parallel to the beam. The undulator magnets produces a wiggling motion in a direction parallel to the electric vector of the laser. Hence energy is transferred from wave to the particle, if the resonance condition $\lambda = \frac{\lambda_u}{2\gamma^2}(1+K^2)$ satisfies where λ is the laser wavelength, λ_u is undulator wavelength and

$K = \frac{eB_0\lambda_u}{2\pi mc^2}$ is undulator parameter. B_0 is the undulator magnetic field amplitude, ' m ' is the mass of particle, ' c ' speed of light. As the particle gain energy, the resonance condition of the free electron laser cannot be maintained for a long distance. The resonance condition can be maintained in two ways, firstly by changing the undulator period and secondly by changing the magnetic field of the undulator. The spectral properties of undulator radiation and the free electron laser gain in staggered undulator with the finite Larmor radius effect of electron are shown [10].

In this paper, we analyse the effect of Larmor radius on Inverse free electron laser accelerator with staggered undulator. We have obtained accelerator equation for inverse free electron laser accelerator. Synchrotron radiation losses are also included in the analysis. We have analysed the effect of Larmor radius on maximum energy gained by the electron and saturation length of the accelerator. Result and discussion of the analysis are given in the last section.

IFEL ACCELERATOR EQUATIONS

The motion and the energy change of relativistic electron in the presence of staggered array undulator and uniform magnetic field produced by a solenoid is calculated. The equation describing the motion of the electrons in the IFEL can be derived from the Lorentz equation of motion,

$$\frac{d\vec{\beta}}{dt} = \frac{e}{\gamma m_e c} [\vec{E}_L + \vec{\beta} \times (\vec{B}_L + \vec{B}_s)] \quad (1)$$

where B_L is the magnetic field of the laser and B_s is the magnetic field of the staggered undulator. e , m_e are the particle charge and mass respectively, c is the speed of light, $\gamma = (1 - \beta^2)^{-1/2}$ and $\beta = v/c$. We consider the magnetic field of a staggered array undulator with an axial magnetic field produced by a solenoid as

$$\vec{B}_s = [0, B_u (\sin \pi f / \pi f) \sin k_u z, B_0] \quad (2)$$

where λ_u is the undulator period with $k_u = 2\pi / \lambda_u$, $\omega_u = ck_u$, $f = \alpha / \lambda_u$, $\alpha = \lambda_u - d$ where ' d ' is the width of the rectangular pole and ' α ' is the pole to pole gap. The undulator field strength is derived from a solenoid and reads

$$B_u = 2B_0 / \sinh(\pi g / \lambda_u)$$

where ' B_0 ' is the axial field strength derived from the solenoid and ' g ' is the undulator gap. The electromagnetic wave propagating along the undulator is described by,

$$\begin{aligned} \vec{E}_L &= [E_0 \sin \psi, E_0 \cos \psi, 0] \\ \vec{B}_L &= [E_0 \cos \psi, E_0 \sin \psi, 0] \end{aligned} \quad (3)$$

where $\psi = n(kz - \omega t)$ and $k = 2\pi / \lambda$, λ is wavelength of the laser. Using Eq. (1-3) for a staggered array undulator with an axial magnetic field, the electron velocity is given by,

$$\beta_x = \frac{\tilde{K}}{\gamma} \cos(\omega_u t) - \frac{K_L}{\gamma} \cos \psi + \beta_{\perp} \cos(\omega_u t) \quad (4a)$$

$$\beta_y = \beta_{\perp} \sin(\omega_u t) \quad (4b)$$

where the undulator and electromagnetic wave parameter is defined through

$$K = \frac{eB_u \lambda_u}{2\pi m_e c^2}, K_L = \frac{eE_L \lambda}{2\pi m_e c^2}, \tilde{K} = K \sin(\pi f) / \pi f$$

A BULK SUPERCONDUCTOR AND ITS APPLICATION TO INSERTION DEVICES*

T. Kii[†], Institute of Advanced Energy, Kyoto University, Uji, Japan

Abstract

High-field short-period undulator will be one of the key technologies for the future light sources. Various approaches have been continued under the limitation of materials for permanent/superconducting magnets. The use of bulk superconductors is attractive because of their high current density in the presence of a high magnetic field. The critical current density for rare-earth barium copper oxide (REBCO) bulk superconductors exceeds 10 kA/mm² even at 10 K in a field range below about 3 T, and exceeds 20 kA/mm² at 4.2 K.

In order to utilize the relatively high current density in the bulk REBCO and to generate periodic magnetic field we proposed a staggered array bulk superconductor undulator. Recently, we have developed the third undulator prototype consisting of a 6 T solenoid and a 6 period bulk REBCO array, and successfully demonstrated periodic field amplitude of 2.22 T for period length of 10 mm and undulator gap of 4.0 mm at 7 K.

INTRODUCTION

Periodic alternating magnetic fields can be used in magnetic levitation systems, linear motors, undulators/wigglers in accelerators, and low-dimensional electron, spin systems for spin-state control in fundamental physics, etc.

Periodic magnetic fields can be generated relatively easily with strong neodymium permanent magnets. Stronger magnetic fields can be obtained by using commercially available superconducting wires. The critical density of commercially available superconducting wire is on the order of several kA/mm² at 4.2 K, and the strength of the periodic magnetic field is limited by this practical critical current density.

In order to generate stronger periodic magnetic field, we have to handle much higher current density than the practical SC wires. Focusing on the core of the superconducting wire, the critical current density is more than an order of magnitude higher than the effective engineering current density. For example, the engineering current density of NbTi and Nb₃Sn superconducting wires is limited to the order of a few kA/mm² due to the sheath required for wire fabrication, but the core parts have a critical current density of about 10 kA/mm². In the case of rare-earth barium copper oxide (REBCO) coated superconducting tapes, the critical current density of the superconducting thin-film layer can reach a few hundred kA/mm², but the thickness of the superconducting material layer is only a few micrometers and constitutes only a few percent of the total volume of the wire, resulting in an effective critical current density of the order of 1 kA/mm² as well as NbTi/Nb₃Sn.

On the other hand, the critical current density of bulk superconductors, which are formed from only superconductor materials in a bulk form, is lower than the superconducting part of wires and tapes, but the current density of the material is equal to the engineering current density. Critical current densities exceeding 10 kA/mm² at 4 K self-field have been achieved in the best performing rare-earth cuprate superconducting system. Therefore, the use of bulk superconductors potentially makes it possible to control magnetic fields using the superconducting current with current density that is one order of magnitude higher than that of commercial superconducting wires.

Therefore, we proposed [1] and demonstrated [2-4] a staggered array bulk superconducting undulator with periodically arranged bulk superconductors (Bulk HTS SAU), focusing on the high magnetic performance of rare earth cuprate superconductors. Recently, PSI started development for SwissFEL and Swiss Light Source 2.0 (SLS2.0) storage ring [5, 6].

In this study, a 6 T solenoid and a gadolinium barium cuprate (GdBaCuO) superconductor were used to generate and control periodic magnetic fields that significantly exceed the limits of permanent magnets and practical commercial wires.

BULK HTS SAU

The structural schematic drawing of a Bulk HTS SAU and the mechanism of periodic magnetic field generation are shown in Fig. 1.

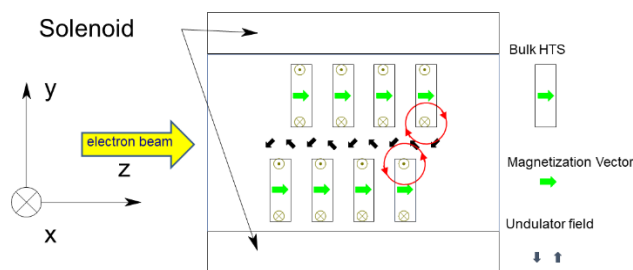


Figure 1: A schematic cross sectional view of a Bulk HTS SAU. When the magnetic field is changed by an external solenoid, a shielding current is induced inside the bulk HTS to cancel out the magnetic field change. The induced current produces a periodic alternating magnetic field along the z-axis.

When a magnetic field change is applied to the superconductor array installed in the solenoid, a shielding current is induced in each superconductor to cancel the magnetic field change. As a result, the large supercurrents, whose directions are different and having half a period offset from each other generate a strong periodic alternating magnetic field on the central axis.

* Work supported by KAKENHI 17H01127, JP22H03870

[†] kii@iae.kyoto-u.ac.jp

BI-PERIODIC UNDULATOR: INNOVATIVE INSERTION DEVICE FOR SOLEIL II

Angela Potet*, Frédéric Blache, Pascale Brunelle, Marie-Emmanuelle Couprie, Carlos De Oliveira, Arnaud Mary, Thibaut Mutin, Amor Nadji, Keihan Tavakoli, Olivier Marcouillé
 Synchrotron SOLEIL, France

Abstract

SOLEIL II project aims at optimizing the production of photons by a modification of the present facility. The storage ring will be redesigned to reduce electron beam emittance and as a consequence increase photon beam brightness. The number of magnetic elements will be increased and the space reserved for insertion devices will be decreased by 30%. Among solutions of undulators fitting in a smaller space while maintaining the full spectral domain, the innovative and compact Bi-Periodic undulator allowing the use of two selectable magnetic periodicities by superimposition of magnets. The magnetic period can be switched from one value to its triple value by mechanical shift of magnetic arrays. A magnetic design has been performed and the construction of a prototype, including magnetic measurements and corrections, is under progress. The magnetic fields, the radiation produced and the electron beam dynamics will be considered to have a complete knowledge on this undulator.

INTRODUCTION

SOLEIL II [1] will lead to increase photon beam brightness. The storage ring presently composed of 16 cells and 3 straight section types will be redesigned to reduce electron beam emittance from 3.9 nm.rad to below 100 pm.rad. To achieve this reduction, the number of magnetic elements along the storage ring will be enlarged considerably. The consequence will be a reduction of the straight sections length reserved for the insertion devices. In present medium straight sections of 7 meters, the wide ranges of photons are obtained thanks to the longitudinal juxtaposition of two undulators with different magnetic periods. For the future ring, as straight section length is reduced to 4.2 or 3.7 meters, it will be impossible to iterate the same configuration to maintain the full spectral domain. Alternatives to combine several magnetic periods on a smaller space exist such as a dual undulator with lateral shifting of two undulators [2], revolvers [3] with several independent magnetic structures of different periods arranged radially around the axis and a variable period helical undulator with tunable polarization [4] allows to modify the direction of the magnetization of the magnets by simple rotation of magnets. SOLEIL considers for its Upgrade DUAL, APPLE X [5] and BiPeriodic undulators. The Bi-Periodic solution is presented in this paper. This undulator is a device allowing the use of two selectable magnetic periodicities by superimposition of magnets. This technique permits to save half the longitudinal

space previously required for SOLEIL I. The purpose of this study is to demonstrate the feasibility of this system through simulations, construction of a prototype and tests on the present ring to validate its operation.

PRINCIPLE OF OPERATION

The Bi-Periodic undulator (Patent pending [6]) has a special arrangement of magnets allowing to switch from a magnetic period to its triple value by a longitudinal shift. It is based on the vertical superimposition of two magnetic systems in the Halbach configuration [7]. A system of magnets with a periodicity λ_0 is equipped vertically with another array of magnets with triple periodicity $3\lambda_0$. This special arrangement of magnets enables to obtain two operating modes presented in Fig. 1. To alternate between the two periods, a phase shift system with a value of $3\lambda_0/2$ enables to obtain on the beam axis the cancellation of the vertical magnetic field of one period (red arrows) and the maximum value of the vertical magnetic field for the other period (green arrows).

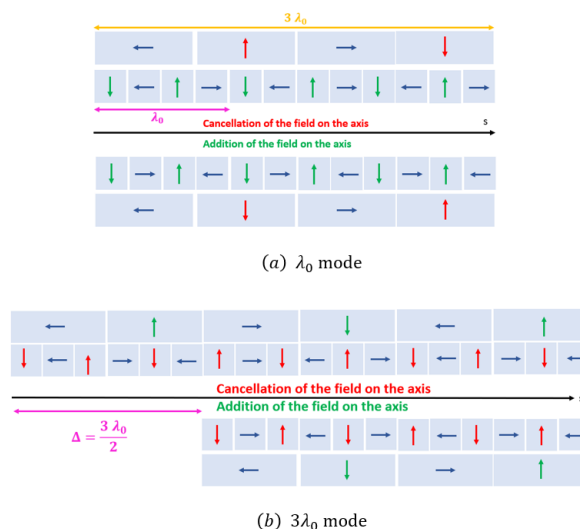


Figure 1: Configuration of magnet magnetization.

BI-PERIODIC PROTOTYPE DESIGN

The choice to make a design with a $\lambda_0 = 50$ mm period and its triple period of 150 mm was made to correspond to the needs of a potential beamline. NdFeB magnets were considered with a remanence of $B_r = 1.37$ T and a special trapezoidal geometry to facilitate the maintenance of the magnets on their supports.

* angela.potet@synchrotron-soleil.fr

THE COXINEL SEEDED FREE ELECTRON LASER DRIVEN BY THE LASER PLASMA ACCELERATOR AT HZDR

M. E. Couprie[†], M. Labat, T. André, A. Berlioux, P. Berteaud, F. Blache, F. Bouvet, F. Briquez, C. de Oliveira, J. P. Duval, Y. Dietrich, M. El Ajjouri, C. Herbeaux, N. Hubert, C. Kitégi, S. Lê, B. Leluan, A. Loulergue, F. Marteau, M. H. N'guyen, D. Oumbarek-Espinos¹, D. Pereira, J. P. Ricaud, P. Rommeluère, M. Sebdaoui, K. Tavakoli, M. Valléau, M. Vandenberghe, J. Vétéran, Synchrotron SOLEIL, Saint-Aubin, France,
A. Ghaith, A. Irman, S. Bock, Y. Y. Chang, A. Debus, C. Eisenmann, R. Gebhardt, S. Grams, U. Helbig, M. Kuntzsch, M. La Berge, R. Pausch, T. Püschel, S. Schöbel, K. Steiniger, P. Ufer, U. Schramm, Helmholtz-Zentrum Dresden – Rossendorf (HZDR), Dresden, Germany.
S. Corde, J. Gautier, J. P. Goddet, I. Andriyash, O. Kononenko, G. Lambert, V. Malka², P. Rousseau, A. Tafzi, C. Thauray, Laboratoire d'Optique appliquée (LOA), ENSTA Paris, CNRS, Ecole Polytechnique, Institut Polytechnique de Paris, Palaiseau, France
E. Roussel, Univ. Lille, CNRS, UMR 8523-PhLAM, Lille, France

¹ present address: Institute of Scientific and Industrial Research, Osaka University, Ibaraki, Japan

² Present address: Department of Physics of Complex Systems, Weizmann Institute of Science, Rehovot, Israel

Abstract

Laser Plasma Accelerators know a tremendous development these recent years. Being able to reach up to ~100 GV/m, they open new perspectives for compact accelerators. Their performance can be qualified by a Free Electron Laser (FEL) application. We report here on the COXINEL (COherent X-ray source INferred from Electrons accelerated by lasers) seeded FEL in the UV using high-quality electron beam generated by the 150 TW DRACO laser. We present the COXINEL line developed at Synchrotron SOLEIL (France), the first results when installed at LOA and the seeded FEL achieved at HZDR.

INTRODUCTION

The FEL [1] following the laser invention [2, 3] was developed from infra-red [4], visible [5], UV-VUV [6, 7] in oscillator and coherent harmonic generation, to X-rays in the Self-Amplified Spontaneous Emission (SASE) after demonstrations at long wavelengths [8, 9], thanks to the high-quality electron beams provided by state-of-the-art photo-injectors and accelerators. Longitudinal coherence is improved with external seeding [10] and self-seeding [11]. In the Laser Plasma Acceleration (LPA) concept [12], following the laser discovery, an ultrashort and intense laser focused in a gas cell/jet excites a plasma oscillation, leads to a strong longitudinal accelerating field. High power lasers using chirped pulse amplification [13] boosted experimental demonstrations with hundred MeV range beams with few percent energy spread [14-16]. It opened the hope for driving FELs with LPA [17, 18] considering the use of a 5 fs- 1 PW laser leading to electron beams with 1.74 GeV, 0.1 % energy spread, 10 μ rad divergence, 20 μ m beam size, 1 nC charge and 150 kA peak current. LPA now reaches ~100 GV/m accelerating field with up to 8 GeV energies [19], 0.4%–1.2% energy spread [20], nC charge [21,

22], few fs bunch duration [23], and low emittance (~mm·mrad) [24]. These features, even though not simultaneously achieved, get closer to the FEL application requirements. Indeed, the first LPA based FEL has been demonstrated at SIOM with state-of-the-art LPA performance at 27 nm in the SASE regime [25]. The second LPA driven FEL has been achieved on COXINEL at HZDR in the seeded configuration at 267 nm [26], enabling for an improved longitudinal coherence.

COXINEL LINE

The COXINEL line was designed in 2010 considering a 200 MeV electron beam with a 1 mrad RMS divergence, 1 μ m RMS beam size, 3.3 fs RMS bunch length, 34 pC charge, 1 % energy spread, 1 mm·mrad normalised emittance. The divergence is handled via a strong transverse focusing [27, 28] at the gas jet exit to prevent chromatic emittance growth [29]. The large energy spread is mitigated by a magnetic chicane, reducing the slice one by its decompression factor while elongating the bunch and reducing the peak current accordingly. Thanks to this energy/position correlation introduced in the chicane, the electron beam transverse focusing and the light progress along the undulator can be synchronized (chromatic matching) [28]. Modelling include electron beam transport with collective effects (space charge, coherent synchrotron radiation) [30], FEL sensitivity to parameters [31], FEL radiation. The chicane induced energy chirp coupled with undulator dispersion leads to a red-shifted FEL [33], and interference fringes between the seed and the FEL appear.

The COXINEL equipment have been prepared. The magnetic elements include the QUAPEVA permanent magnet quadrupoles for the initial strong focusing, with gradients up to 200 T/m and 50 % variability [33-35], four chicane electromagnetic dipoles for the slice energy spread reduction and the seed mirror insertion, an electromagnetic

[†] couprie@synchrotron-soleil.fr

DEVELOPMENT OF LASER-DRIVEN PLASMA ACCELERATOR BASED UNDULATOR RADIATION SOURCE AT ELI-BEAMLINES

A. Molodozhentsev[†], J. T. Green, A. Mondal, S. Maity, S. Niekrasz, E. Vishnyakov,
A. Jancarek, P. Zimmermann
Extreme Light Infrastructure ERIC, ELI-Beamlines, Dolni Brezany, Czech Republic

Abstract

A compact undulator radiation source based on a laser-driven plasma accelerator (LPA) is currently being commissioned at ELI-Beamlines (ELI-ERIC, Czech Republic). An intermediate goal of this activity is to deliver a stable and repeatable incoherent photon beam with a wavelength of about 4 nm to a user station. As a result of this development, the electron beam parameters will be improved, with the aim of producing a coherent photon beam, utilising a dedicated FEL undulator. An overview of the current status of the project (LUIS) is presented in this report, including the high-power high-repetition rate laser, the compact electron beam accelerator based on the laser-plasma interaction, and the electron and photon beamlines with relevant diagnostics. The challenges and future developments of the LUIS project, aimed at LPA-based EUV-FEL, will also be discussed.

INTRODUCTION

The scientific success and tremendous demand from the photon beam user community stimulate intensive research to find competitive approaches which would lead to a significant size and cost reduction of the instruments for both incoherent and coherent photon beams.

Constantly developing Laser Wakefield Acceleration (LWFA) techniques make it a very attractive candidate for novel, compact undulator radiation sources, especially in the light of recent progress in the laser technology [1], acceleration gain [2] and breakthroughs in electron beam quality improvement [3]. With the electron beam properties, obtained experimentally by different teams as the result of the laser-plasma interaction in the compact laser-plasma accelerator (LPA), a generation of the incoherent photon radiation in a compact undulator has already been demonstrated [4-6].

Nowadays main effort is concentrated on the improvement of the LPA-based electron beam quality to be able to use such a beam to generate a coherent undulator photon radiation utilizing the so-called Self-Amplified Spontaneous Emission (SASE) regime [7] of a Free Electron Laser (FEL). The novel LPA-based source of incoherent and coherent photon radiation has attracted interest for applications in medicine [8] and industry [9].

A compact LPA-based undulator radiation source (LUIS) is currently under development at ELI-ERIC in the Czech Republic. After the commissioning, it will bring to the user community a high repetition rate (50-100 Hz) of soft X-ray radiation aiming for high-temporal-resolution

pump-probe experiments, combined with XANES spectroscopy and high-resolution microscopy.

The main goal of this development is to improve the quality of the LPA-based electron beam to make this beam usable for not only for the incoherent regime but also for the coherent one in the extreme ultra-violet range of the radiation wavelength (for the fundamental harmonic). It will open the way to prepare the user-oriented compact LPA-based FEL, based on the 100 TW-class laser system with a repetition rate up to 100 Hz.

DEVELOPMENT AT ELI-BEAMLINES (ELI-ERIC)

The Extreme Light Infrastructure (ELI-ERIC) is the world's largest and most advanced high-power laser infrastructure and a global technology and innovation leader in high-power, high-intensity and short-pulsed laser systems. ELI-beamlines, as a part of ELI-ERIC, locates near Prague (Czech Republic). ELI-beamlines is a unique infrastructure in the field of photonic-based user-oriented research and the first large-scale facility in this worldwide domain. The specific nature of the ELI-beamlines user facility is its multi-disciplinary features, which open extremely wide opportunities for the user community to develop new secondary radiation and particle sources, creating new paths of applied and fundamental research, pushing the boundaries of science and technology.

Laser Development at ELI-beamlines

New LUIS-dedicated high-repetition high-power laser system is under development at ELI-ERIC (L2-DUHA laser) [10], based on the OPCPA technology, will deliver two pulses: the main laser pulse with energy of up to 5 J, 25 fs pulse duration and the wavelength of 820 nm, as well as the auxiliary laser pulse with the energy of a few mJ, 30 fs pulse duration and the wavelength of around 2.2 μm . The main laser pulse will be focused in the prefilled gas-cell (or preformed plasma channel) to produce a high-quality high-energy electron bunch. The auxiliary laser pulse will be used for the pump-probe experiments.

At the moment the LUIS technology is integrated with the L3-HALPS laser. This laser system currently operated at a 3.3 Hz repetition rate and provides a pulse with a central wavelength of 820 nm, 30 fs pulse duration and a pulse energy of up to 13 J with a possible upgrade up to 30 J. In the case of the L3-LUIS operation, the maximum pulse energy of the cropped laser beam is limited by 1.5 J (before the L3 upgrade) or 3.5 J after upgrade.

[†] Alexander.Molodozhentsev@eli-beams.eu

NOVEL X-RAY BEAM POSITION MONITOR FOR COHERENT SOFT X-RAY BEAMLINES*

B. Podobedov^{1,†}, D.M. Bacescu¹, D. Donetski², C. Eng¹, S.L. Hulbert¹, K. Kucharczyk², J. Liu²,
 R. Lutchman², C. Mazzoli¹, C.S. Nelson¹, J. Zhao²

¹Brookhaven National Laboratory, Upton, NY, USA

²Stony Brook University, Stony Brook, NY, USA

Abstract

A novel soft X-ray BPM (sXBPM) for high-power white beams of synchrotron undulator radiation is being developed through a joint effort of BNL/NSLS-II and Stony Brook University. In our approach, custom-made multi-pixel GaAs detector arrays are placed into the outer portions of the X-ray beam, and the beam position is inferred from the pixel photocurrents. Our goal is to achieve micron-scale positional resolution ~ 30 μ m away from the source, without interfering with user experiments, especially the most sensitive ones exploiting coherent properties of the beam. To this end, an elaborate mechanical system has been designed, fabricated, and installed in the 23-ID canted undulator beamline first optical enclosure (FOE), which allows positioning of the detectors with micron-scale accuracy, and provisions for possible intercepts of kW-level beam in abnormal conditions. Separately, GaAs detectors with specially tailored spectral response have been designed, fabricated, and tested in the soft and hard X-ray regions at two NSLS-II beamlines. This paper gives an overview of the sXBPM system and presents the first preliminary results from the high-power white X-ray beam.

INTRODUCTION

Non-invasive soft X-ray BPMs (sXBPMs) do not exist yet but are greatly desired for coherent soft X-ray beamlines. We are working to develop such sXBPM for high-power, white X-ray beams. In our approach [1], multi-pixel GaAs detector arrays are placed into the outer portions of X-ray beam, away from the undulator central cone. Beam position, together with other information, is inferred from the pixel photocurrents, see Fig. 1.

Potential advantages of this approach include much higher sensitivity of GaAs compared to metal blades used in conventional photoemission type XBPM designs for hard X-rays [2, 3]. Also, with pixelated detectors, we expect better positional resolution, spatial feature resolution, smaller systematic errors due to undulator gap changes (and phase changes for EPUs), and the ability to discriminate stray light from bending magnets and other sources. The last two are long-standing challenges for the conventional hard X-ray XBPMs (e.g., [4]).

The main challenges with our approach are that the device must have adequate responsivity in soft X-ray; it must withstand high power, potentially leading to elevated diode junction temperature and high pixel photocurrents, and it must reliably operate in UHV.

The first goal of our R&D program to investigate this approach includes the design, fabrication, and demonstration of suitable performance of the detector arrays. The second goal is to design, fabricate, and install the sXBPM into the 23-ID FOE, where movable sXBPM detectors intercept the outer portions of white X-ray beam (Fig. 1) from two identical APPLE-II undulators (EPU49, $L=2$ m each, 2.5 m center-to-center spacing), nominally canted at 0.16 mrad. Each undulator serves as a primary radiation source for one of the two soft X-ray beamlines, CSX or IOS. Our final goal is to demonstrate micron-scale positional resolution of the sXBPM at the sampling rate of 10 Hz or higher for the undulator fundamental harmonic (E_1) tuned in the range of $E_1=250-2000$ eV covering the operating energy range of the beamlines.

Figure 1 shows the maximum expected power density at the sXBPM location from a single (downstream) undulator tuned to $K=3.458$ ($E_1=250$ eV) in linear horizontal polarization. Due to the FOE mask (fixed water-cooled aperture) ~ 1 m upstream of the sXBPM, the photons outside a $\sim 5 \times 10$ mm² rectangle (shown in dash) are not accessible for detection. During user operations, the beam from the other undulator, independently tuned in the range of $E_1=250-2000$ eV, is also present. In this (canted) configuration the two beams are displaced horizontally at the sXBPM location by about ± 2 mm with respect to the center of the mask. The photon beam can be further clipped by front-end (FE) slits, located in the ring tunnel ~ 7 m upstream of the sXBPM.

To install the sXBPM into an operating beamline our design must guarantee no interference with beamline operations under all possible scenarios. Therefore, the detectors are placed on movable blades, which can be completely removed (parked in the FOE mask shade) or positioned to intercept any desired fraction of the beam.

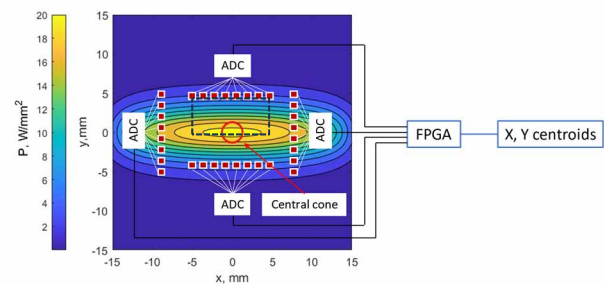


Figure 1: sXBPM concept (detector pixels shown overlaid on the X-ray power density distribution 26 m away from a single EPU in the non-canted configuration).

[†] boris@bnl.gov

RADIATION PROTECTION ISSUES IN UNDULATOR UPGRADES FOR THE EUROPEAN XFEL*

A. Potter^{†,1}, A. Wolski¹, Department of Physics, University of Liverpool, Liverpool, UK
S. Liu, W. Decking, A. Leuschner
Deutsches Elektronen-Synchrotron - DESY, Hamburg, Germany
S. Casalbuoni, S. Karabekyan, H. Sinn, F. Wolff-Fabris
European XFEL GmbH, Schenefeld, Germany
F. Jackson¹, ASTeC, STFC Daresbury Laboratory, Daresbury, Warrington, UK
¹also at the Cockcroft Institute, Daresbury, Warrington, UK

Abstract

European XFEL is the first free electron laser operating at MHz repetition rate with electron beam energy up to 17.5 GeV. The high repetition rate together with the high electron beam energy provides unique opportunities for users in different domains. To further extend the operation schemes, some upgrades have already been implemented and several more are planned. The advanced operation schemes may require devices inserted into the beam (e.g. slotted foil) or narrow vacuum chambers (e.g. corrugated structure, Apple-X undulator, superconducting undulator), and due to the high beam power, there are concerns about increased radiation loads. Therefore, simulations and measurements have been carried out to study the radiation dose rates that may be generated. We give an overview of the simulations and measurements for the case of the Apple-X undulators, and briefly consider the implications for other schemes.

INTRODUCTION

The SASE3 beamline [1] at the European XFEL (EuXFEL) delivers FEL beam in the photon energy range 0.25–3 keV. Photon pulses are generated by an electron beam with energy up to 17.5 GeV in a planar undulator, consisting of 21 modules each of length 5 m. To allow control of the polarisation of the X-ray beam, during the winter 2021/22 shutdown an Apple-X undulator (consisting of four modules each of length 1.98 m) was installed in the beamline following the planar undulator [2]. First lasing with the Apple-X undulator in place was achieved in early April 2022 [3]. However, after a short period of operation, faults began to occur with the linear and rotary encoders and cam movers used in the control of the magnet arrays in the Apple-X undulator. It was suspected that the damage was caused by spontaneous synchrotron radiation from the SASE3 planar undulator, and to prevent further damage the Apple-X undulators were removed in the summer shutdown 2022, and the new (narrower aperture) vacuum chamber in the Apple-X section was replaced by the original vacuum chamber. Simulation and experimental studies were begun to understand the cause of the radiation damage, and to plan potential mitigations to

allow reinstallation of the Apple-X: in this paper, we summarise the studies and outline the results. Other upgrades of EuXFEL, planned or in progress, also raise concerns regarding the effects of increased radiation loads on components in the machine, and we conclude this paper by considering briefly the lessons and implications of the Apple-X studies for these upgrades.

SYNCHROTRON RADIATION MODEL

The study reported here aimed to develop an understanding, through simulations and measurements, of the radiation loads on the Apple-X undulators in EuXFEL (in particular, the loads on the damaged encoders) arising from spontaneous synchrotron radiation from the SASE3 planar undulator. Note that it is assumed that FEL radiation from the undulator can be cleanly extracted along the beamline, and is therefore not included in this study: where we refer to synchrotron radiation in the present paper, it should be understood that (unless stated otherwise) the term refers only to spontaneous radiation. Following construction of a radiation model, the simulations can be developed to investigate possibilities for additional protection, allowing to reinstall the Apple-X undulators. As a first step, a model for the distribution of synchrotron radiation photons was constructed: this distribution was then tracked through a model of the machine (including detailed representations of relevant apertures and components) to the Apple-X undulators using a suitable simulation code, which can be used to estimate the radiation dose rates. We used analytical formulae verified with SPECTRA [4] for generating the photon distribution, and BDSIM [5] for the tracking simulations and radiation dose rate calculations.

For tracking photons in BDSIM, the initial distribution (at the mid-point of an undulator module) is modelled as a set of macroparticles over a 200×200 uniform grid of points in the transverse angular space, up to 0.5 mrad. The initial transverse spatial coordinates were assumed to be negligible, since the beam size towards the end of the undulator is dominated by the initial divergence. The electron beam emittance and energy spread are also neglected. Each macroparticle contains a number of photons with a range of energies: the number density and energy spectrum were calculated analytically as a function of angle using standard

* Work supported by the Science and Technology Facilities Council UK by a grant to the Cockcroft Institute, U.K.

[†] sgapotte@liverpool.ac.uk

HOW CAN MACHINE LEARNING HELP FUTURE LIGHT SOURCES?

A. Santamaria Garcia*, C. Xu, L. Scomparin, E. Bründermann, M. Caselle, G. De Carne, A.-S. Müller, Karlsruhe Institute of Technology (KIT), Karlsruhe, Germany

Abstract

Machine learning (ML) is one of the key technologies that can considerably extend and advance the capabilities of particle accelerators and needs to be included in their future design. Future light sources aim to reach unprecedented beam brightness and radiation coherence, which require challenging beam sizes and accelerating gradients. The sensitive designs and complex operation modes that arise from such demands will impact the beam availability and flexibility for the users, and can render future accelerators inefficient. ML brings a paradigm shift that can re-define how accelerators are operated. In this contribution we introduce the vision of ML-driven facilities for future accelerators, address some challenges of future light sources, and show an example of how such methods can be used to control beam instabilities.

INTRODUCTION

Frontier Accelerators

Both the photon science and high energy physics research communities generally aim at increasing the performance of accelerators, reduce their cost, and make them more power efficient. These goals are even more relevant for frontier particle accelerators, driven by ambitious research programs that require demanding beam parameters, often outpacing the progress of traditional accelerator technologies [1–3]. The current cost of frontier accelerators is estimated at more than 1 billion dollars, where larger facilities can cost up to 10 times more [4]. This cost is directly related to the technology these accelerators are based on, and can be reduced with advancements in such technology. Given the size, cost, and technological advancements required, frontier accelerators are one of the most challenging scientific endeavors.

The Potential of Machine Learning for Particle Accelerators

The potential of ML methods in accelerators was already identified back in 2018 [5], and their popularity has been rapidly increasing since then, as shown in Fig. 1.

This is due not only to the general rise in popularity of artificial intelligence (AI), but thanks to the continuous development of easily accessible ML software libraries and recent advances of ML methods, applied to a variety of fields. While interesting improvements have already been observed in existing accelerator facilities, particularly in tuning and optimization tasks [6, 7], a promising avenue for ML methods in accelerators is their potential to help overcome the challenges of frontier accelerators [8], which could become a liability in their development if unaddressed (e.g., technical impossibilities, insufficient beam availability, inefficient

* andrea.santamaria@kit.edu

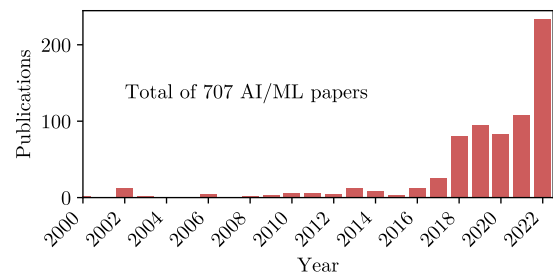


Figure 1: Number of publications with the words "machine learning" or "artificial intelligence" in the abstract, scraped from the JACoW database.

design). Some of the challenges that can be approached with ML are listed in Fig. 2, for different frontier accelerator design trends.

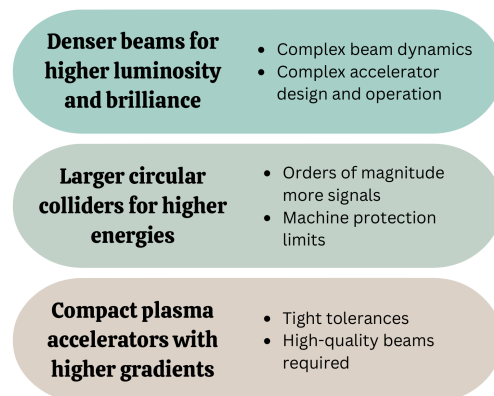


Figure 2: Some trends and related challenges of frontier accelerators.

ML methods can yield fast predictions at a reduced computational cost compared to analytical or classical numerical methods, can take into account the non-linear correlations in the data, and can adapt the predictions to the drifts in the machine state. These capabilities are highly desirable in accelerators since they open the door to a very robust and tailored online detection, prediction, optimization, and control. They can also help design future accelerators by alleviating the computational cost of numerical simulations and guiding the search for optimal parameters in a high-dimensional parameter space. Table 1 summarizes some applications of ML in current accelerators, split by the type of task. There are also numerous applications in particle physics that are not covered in this publication [9, 10].

Looking ahead into the future we can imagine a completely autonomous accelerator [11] where the operation is user-centric and guided by the changing demands of more complex and maybe ML-driven experiments. Such an accelerator would be energy responsible, with an automated

A COMPACT INVERSE COMPTON SCATTERING SOURCE BASED ON X-BAND TECHNOLOGY AND CAVITY-ENHANCED HIGH AVERAGE POWER ULTRAFast LASERS

A. Latina*, V. Muşat, R. Corsini, L. A. Dyks, E. Granados, A. Grudiev, S. Stapnes,
P. Wang, W. Wuensch, CERN, Geneva, Switzerland
E. Cormier, G. Santarelli, LP2N, Talence, France

Abstract

A high-pulse-current photoinjector followed by a short high-gradient X-band linac and a Fabry-Pérot enhancement cavity are considered as a driver for a compact Inverse Compton Scattering (ICS) source. Using a high-power ultra-short pulse laser operating in burst mode in a Fabry-Pérot enhancement cavity, we show that outcoming photons with a total flux over 1×10^{13} ph/s and energies in the MeV range are achievable. The resulting high-intensity and high-energy photons allow various applications, including cancer therapy, tomography, and nuclear material detection. A preliminary conceptual design of such a compact ICS source and simulations of the expected performance are presented.

INTRODUCTION

In recent years, research and development of normal-conductive X-band accelerator technologies have seen tremendous progress in the context of the next generation of electron-positron linear colliders, where very high gradients are required to achieve the multi-TeV beam energy target for particle physics. The CLIC Study at CERN is the most notable example, where multi-bunch beams and accelerating gradients three to five times greater than those in currently operating linacs have been demonstrated in prototype accelerator structures [1].

During the last years, alongside X-band developments, laser technology has also undergone significant advancements, with high-power lasers becoming more readily available on the market. At the same time, to generate high-intensity photons, Fabry-Pérot enhancement cavities (FPCs) are becoming widely adopted in inverse Compton scattering sources, as reported in [2, 3].

There has been recent consideration for operating FPCs in pulsed (or burst) mode. FPCs operated in burst mode can achieve effective gains 2 to 3 orders of magnitude larger than in continuous mode, which is the commonly used operation mode in storage-ring-based sources. The operation of FPCs in burst mode is particularly well-suited for inverse Compton scattering sources based on X-band linacs as they have a lower repetition rate than storage rings or energy-recovery linacs [4] and allow for multi-bunch acceleration.

This paper presents the conceptual design of an ICS source based on X-band acceleration and external optical cavity enhancement in an optimised FPC operated in burst mode. By accelerating electrons to 240 MeV energy in less than 10 m,

our proposed ICS source could generate gamma photons with energies up to 2 MeV and unprecedented flux and brilliance values. High-quality gamma rays in the MeV energy range can have a wide range of applications in various fields, including material science [5], medicine [6], nuclear physics research [7], homeland security by nuclear resonance fluorescence inspection [8, 9], and nondestructive testing of industrial materials [10]. We named this apparatus HPCI-ICS, which stands for “High Pulse Current Injector driven Inverse Compton Scattering” source.

FACILITY DESCRIPTION

The High-Pulse-Current Injector consists of an S-band photoinjector operating at 3 GHz followed by a high-gradient X-band linac at 12 GHz and a short final focus preparing the beam for the interaction. The main parameters of the facility have been optimised along three axes: (1) ensure high RF power efficiency, (2) maintain beam stability in the linac by reducing the disruptive effects of wakefields, and (3) maximise the photon flux at the IP.

The result is a 12 m long setup that accelerates trains of 1000 electron bunches, each with 100 pC bunch charge, up to 240 MeV with a repetition rate of 100 Hz. These bunches are then collided with a laser beam stored in a burst-mode FPC. Table 1 summarises the main parameters of the facility. A short description of each subsystem is provided in the following sections.

Injector

The S-band photoinjector is similar to that of the CLEAR test facility at CERN [11]. The electrons are released from a photocathode due to the photoelectric effect induced by a UV laser. The single-bunch charge extracted from the cathode is 100 pC. A Cs₂Te cathode was selected due to the small spot size and the limited power required on the laser, thanks to the high quantum efficiency of this semiconductor. The photocathode is located at the centre of the half-cell of a 2.5-cell standing-wave electron gun with a cathode peak gradient of 90 MV/m, immersed in a solenoid field. The total length of the injector is 1.3 m, which accounts for diagnostics and trajectory correctors. Table 2 summarises the main parameters of the injector.

Linac

The X-band linac starts 1.3 m downstream of the cathode and operates at a repetition rate of 100 Hz with an average gradient of 35 MV/m. The linac consists of three X-band

* andrea.latina@cern.ch

RESEARCH ON BUNCH-BY-BUNCH POLARIZATION SWITCH MECHANISMS OF HIGH-REPETITION-RATE X-RAY FELs

Z. F. Gao, T. Liu, Shanghai Advanced Research Institute, Shanghai, China

Abstract

X-ray free electron laser (FEL) is one of the latest generation of high-quality accelerator-based light sources in the world. With the continuous development and improvement of magnetic dichroism, in order to meet the needs of various users, many mainstream X-ray FEL facilities in the world have been equipped with elliptically polarized undulators (EPUs) to realize polarization control. These schemes cannot switch the FEL polarization at a high speed, so it is difficult to meet the needs of high-frequency hard X-ray FEL facilities. This study aims to generate FEL radiation with different polarization states pulse by pulse on the first superconducting hard X-ray FEL facility under construction in China (SHINE), whose repetition rate will be up to 1 MHz. A new scheme is proposed combining a bunch-by-bunch phase shifter and several EPUs. Based on the parameters of FEL-II, the simulation results show that it is possible to produce X-ray pulses with higher than 85% circular polarization under SASE mode.

INTRODUCTION

Nowadays, several XFEL facilities around the world exploit circular polarization by employing Apple-type or Delta undulators as afterburner, such as Linac Coherent Light Source (LCLS), European XFEL, etc. [1, 2]. It's easy to reach as high as over 90% polarization degree for these EPU afterburner, but can hardly switch the polarization state at a high repetition rate, e.g more than 1 kHz. Another way to generate circularly polarized X-ray FEL is proposed by K.-J. Kim by using crossed-planar undulators (CPUs) as shown in Fig. 1 [3, 4]. In this case, the FEL polarization is significantly determined by the phase difference between horizontal and vertical radiation, which contributes to the possibility of fast arbitrary polarization switching. However, the circular polarization degree of the CPU radiation is theoretically limited to under 80% under SASE mode, much lower than EPU afterburner [5].

The scheme is based on the interference of horizontal and vertical radiation from two planar undulators in a crossed configuration. The CPUs serve as the afterburner, and a special bunch-by-bunch phase shifter is designed to change the phase difference rapidly. There will be 4 Apple-type undulators on FEL-II, 2 for horizontal radiation and 2 for vertical radiation, but only part of them will work meanwhile at a certain wavelength so as to reach a higher polarization degree. The phase shifter will be set between the horizontal undulators and vertical ones. It's also possible to make those Apple-type undulators generate left-handed and right-handed radiation, finally obtaining linear polarized radiation with different polarization directions.

BUNCH-BY-BUNCH PHASE SHIFTER

The bunch-by-bunch phase shifter consists of 4 kickers as shown in Fig. 2, with similar structure to normal phase shifters, usually called a chicane. The main parameters of the kickers are shown in Table 1, and the frequency and amplitude are adjustable continuously. It's apparently more difficult for kickers to achieve strong magnetic fields than normal dipoles, so the length of such a phase shifter is also much larger. In order to reduce the possible influence on the bunched electron beam, the whole length is limited under 2.5 m. The kickers operate on the 1 MHz continuous-wave (CW) electron beam, deflecting half of the bunches while allowing the rest of the beams to pass smoothly through the original trajectory. On the one hand, the parameters of the kickers make sure that the path length difference will offer enough phase difference (more than π) during the whole wavelength range. On the other hand, based on the existing conditions, these demands are not too high to be reached.

Table 1: Kicker Parameters

Parameter	Value	Unit
Beam energy	8	GeV
Max frequency	500	kHz
Working mode	bunch by bunch	
Effective length	300	mm
Deflection angle	25 -60	μ rad

SASE FEL WITH THE PHASE SHIFTER

SASE starts from electron density shot noise and produces X-ray pulses with spiky temporal and spectrum profile, which leads to poor polarization purity [6, 7]. It can be improved by working under self-seeding mode, HGHG mode, or EEHG mode instead. Up to now, since seeded FEL is still much more complicated and difficult than SASE FEL in terms of high repetition, it's essential to generate FEL pulses with high polarization degree under SASE mode. Slight reverse tapering is used in the scheme to preserve the electron beam micro-bunching. Fewer planar undulators are on work than usual to prevent saturation, thus reducing the impact of phase difference.

As a numerical example, the three-dimensional FEL simulation is conducted by Genesis 1.3 using parameters of SHINE [8]. The main parameters of SHINE are listed in Table 2. The electron beams are chosen to be Gaussian profile and the radiation field file is obtained 100 m downstream of the last EPU.